A Comprehensive Statistically-Based Method to Interpret Real-Time Flowing Measurements

Annual Report

Period Start	August 2004
Period End	August 2005

By

Pinan Dawkrajai, Keita Yoshioka, Analis A. Romero,
Ding Zhu, A. D. Hill and Larry W. Lake
Oct 2005

DOE Award Number; DE-FC26-03NT15402

The University of Texas at Austin
Texas A&M University

Disclaimer

Abstract

This project is motivated by the increasing use of distributed temperature sensors for real-time monitoring of complex wells (horizontal, multilateral and multi-branching wells) to infer the profiles of oil, gas, and water entry. Measured information can be used to interpret flow profiles along the wellbore including junction and build section.

In this second project year, we have completed a forward model to predict temperature and pressure profiles in complex wells. As a comprehensive temperature model, we have developed an analytical reservoir flow model which takes into account Joule-Thomson effects in the near well vicinity and multiphase non-isothermal producing wellbore model, and couples those models accounting mass and heat transfer between them. For further inferences such as water coning or gas evaporation, we will need a numerical non-isothermal reservoir simulator, and unlike existing (thermal recovery, geothermal) simulators, it should capture subtle temperature change occurring in a normal production.

We will show the results from the analytical coupled model (analytical reservoir solution coupled with numerical multi-segment well model) to infer the anomalous temperature or pressure profiles under various conditions, and the preliminary results from the numerical coupled reservoir model which solves full matrix including wellbore grids.

We applied Ramey's model[1] to the build section and used an enthalpy balance to infer the temperature profile at the junction. The multilateral wellbore temperature model was applied to a wide range of cases varying fluid thermal properties, absolute values of temperature and pressure, geothermal gradients, flow rates from each lateral, and the trajectories of each build section.

Table of Contents

Lists of Graphical Materials

Table

Figure

1 INTRODUCTION

Interpretation of temperature has been done successfully in vertical wells to identify water or gas entries location, detect casing leaks, and evaluate cement placement. Recent works[2-4] show the usefulness of temperature logs in horizontal wells to locate different types of fluid entries. The unwanted fluid is located by means of an intelligent well technology. Downhole temperature measurements have been improved in terms of resolution, accuracy and reliability. Current fiber optic measurements can provide a near-continuous profile of distributed temperature with resolution less than 0.1 ^{o}C, over a distance of several kilometers, with a spatial resolution of one meter, and with a measurement time of typically a few minutes.

Modeling the temperature behavior in horizontal wells is challenging task because of, for example, the complexity of the geometry and the almost invariant formation temperature. To translate the causes of temperature profiles that are measured, the model is necessary to take into account all subtle thermal energy effects including Joule-Thomson expansion, viscous dissipation heating, and thermal conduction. Our previous work divided the problem into three parts, reservoir, wellbore, build section/junction. The result showed that reservoir temperature profile would deviate from geothermal by a few degrees and the temperature or pressure along the wellbore could vary sometimes significantly from the boundary conditions. To be more realistic, interaction between reservoir and wellbore is considered in this project.

In this period, we have parametrically studied temperature logs for numerous cases to infer the characteristics or limitations for an inversion problem. Detailed results are given in the following sections.

2 EXECUTIVE SUMMARY

We have been developing new methods to interpret measurements in complex wells. Use of distributed temperature sensors is becoming increasingly common for monitoring producing sections of horizontal wells. This information can potentially be inverted to infer the types and amounts of fluid entering at numerous locations along the wellborn, can identify production problems (excessive water or gas influx), and decide if reservoir stimulation is needed in a particular horizontal section.

The inferences described above require a model to translate temperature information into flow information. The objectives of this project are two parts. The first goal is to develop a comprehensive prediction model of temperature and pressure behavior in horizontal laterals, build sections, junctions and entire complex well systems. The second one is to interpret the results from the forward model and apply the inversion method to actual field data.

This report first presents a simple and comprehensive model for predicting the temperature profile in a horizontal well during normal production (steady state flow). Prediction of the wellbore temperature profile requires modeling of all thermal effects occurring in the reservoir and in the wellbore itself. For the reservoir temperature model, we couple mass and energy balances of fluid flow in a permeable media in a rectangular homogeneous reservoir with no flow boundaries at the top and bottom of reservoir. There are two flow regions (radial and linear) considered in the reservoir, and the equation is analytically solved in one dimension. This analytical solution is then coupled with a wellbore temperature model using a multi-segment technique to obtain the fluid temperature profile along the wellbore. The wellbore model presented in this paper accounts for Joule-Thomson effects, and convective and conductive heat transfer from the formation. It can model both compressible and incompressible single/multi phase flow in a wellbore with an arbitrary inclination.

The primary results of the model are estimates of the extent of temperature change during flow. Results show that temperature changes on the order of a few degrees are possible and temperature changes of this magnitude are certainly detectable with current technology. A second result is a demonstration of the inference of a single phase and multiphase flow profiles from a synthetic case. Sensitivity studies with the model illustrate the flow conditions that cause measurable temperature changes or anomalies that could be recognized in an analysis of distributed temperature measurements.

As a second, we present the ongoing numerical model of non-isothermal horizontal well reservoir. This numerical model no more consider reservoir segments independently. This could simulate 3-D or multiphase effects in the reservoir. The objectives of this numerical model are to test the validity of the simple analytical model, infer its limit, and analyze physically complicated situation such as water coning. The preliminarily results of single phase flow from this numerical model are shown later in

this report. It verifies the analytical model and shows a little discrepancy in flow rate but almost matches pressure and temperature under some conditions. This indicates that there is little difference between analytical coupled model and numerical model for single phase flow in sense of temperature/pressure estimation.

Finally, we show a temperature estimation model for build sections and junctions. The model predicts the temperature profiles in the build sections connecting the laterals to one another or to a main wellbore, accounting for the changing well angle relative to the geothermal temperature profile. In addition, energy balance equations applied at each junction predict the effect of mixing on the temperature above each junction. The sensitivity studies in build section and junction are shown in the report.

3 WELLBORE MODEL

Unlike the reservoir with vertical production/injection wells, horizontal/multi-lateral wells needs more careful treatment in pressure or temperature profile estimations. Because of the length of the well that is exploiting the reservoir, the pressure and temperature inside wellbore has to be considered as varying values with their position instead of unified values.

Also, we need to be aware that mass or heat transfer between wellbore and reservoir will be a function of the wellbore pressure, temperature and the reservoir condition. For instance, when we have higher pressure drop inside the wellbore, the more inflow comes from the formation and a similar interaction will happen to heat transfer.

3.1 Derivation of working equations for single phase flow

First we consider the physical wellbore model as shown in Fig. 3.1 that receives mass and heat from the formation (in radial direction) and fluid flows in axial direction. Then we account the net input and output of intensive properties such as mass, moment and total energy using shell balance.

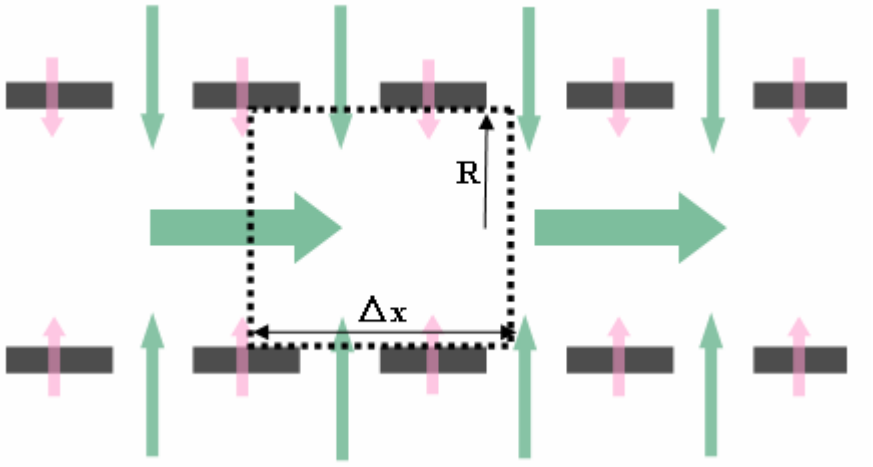

Fig. 3.1 Wellbore segment.

The completion types may be open hole or slotted liner etc. We introduce the pipe opened ratio defined as;

$$\gamma = \frac{\text{Opened area of pipe}}{\text{Surface are of pipe}} \tag{3.1}$$

Here we consider opened area of pipe for a certain length so the pipe opened ratio is a function of position. Then we can express the surface area of a volume element as $2\pi R\gamma\Delta x$ and convective properties from formation, for example transferred mass, can be written as $2\pi R\gamma\Delta xM$. The pipe opened ratio will be the perforation density for perforated wells and is the porosity for openhole completed wells.

3.1.1 Mass balance equation

Considering steady state mass balance, we have

$$0 = \rho v_I 2\pi R\gamma\Delta x + (\rho v)_x \pi R^2 - (\rho v)_{x+\Delta x} \pi R^2 \tag{3.2}$$

Dividing by $\pi R^2 \Delta x$ yields

$$0 = \frac{2\gamma}{R}\rho_I v_I + \frac{(\rho v)_x - (\rho v)_{x+\Delta x}}{\Delta x} \tag{3.3}$$

Taking $\Delta x \to 0$ gives

$$\frac{d(\rho v)}{dx} = \frac{2\gamma}{R}\rho_I v_I \tag{3.4}$$

where subscript I means inflow properties. ρ is density and v is velocity.

3.1.2 Momentum balance equation

Combined momentum is defined as[4]

$$\mathbf{\Phi} = \rho \mathbf{v}\mathbf{v} + p\boldsymbol{\delta} - \boldsymbol{\tau} \tag{3.5}$$

where $\boldsymbol{\delta}$ is Kronecker delta. $\boldsymbol{\tau}$ is shear stress tensor and p is pressure. The momentum flux from formation is given as

$$\Phi_{rx}\big|_{r=R} 2\pi R(1-\gamma)\Delta x = \left(\rho v_r v_x - \tau_{rx}\right)\big|_{r=R} 2\pi R(1-\gamma)\Delta x \tag{3.6}$$

Since there is no slip at the wall ($v_x\big|_{r=R} = 0$), the momentum flux becomes

$$\Phi_{rx}\big|_{r=R} 2\pi R(1-\gamma)\Delta x = -\tau_{rx} 2\pi R(1-\gamma)\Delta x \tag{3.7}$$

Wall stress shear is defined as

$$-\tau_{rx}(1-\gamma) = -\frac{\rho f v_x^2}{2} \equiv -\tau_{w,I} \tag{3.8}$$

where f is a fanning friction factor. The momentum flux at $x = x$ is

$$\Phi_{xx}\big|_x = \left(\rho v_x v_x + p - \tau_{xx}\right)\big|_x \pi R^2 \tag{3.9}$$

Neglecting viscous shear yields

$$\Phi_{xx}\big|_x = \left(\rho v_x v_x + p\right)\big|_x \pi R^2 \tag{3.10}$$

The momentum flux at $x = x + \Delta x$ is obtained similarly. The momentum equation is given as

$$0 = -2\pi R\Delta x\tau_{w,I} + \pi R^2\left[\left(\rho v_x v_x + p\right)_x - \left(\rho v_x v_x + p\right)_{x+\Delta x}\right] - \rho\pi R^2 g\sin\theta \tag{3.11}$$

dividing by $\pi R^2\Delta x$ yields

$$0 = -\tau_{w,I}\frac{2}{R} + \frac{\left(\rho v_x v_x + p\right)_x - \left(\rho v_x v_x + p\right)_{x+\Delta x}}{\Delta x} - \rho g\sin\theta \tag{3.12}$$

Taking $\Delta x \to 0,\ \Delta t \to 0$

$$0 = -\tau_{w,I}\frac{2}{R} - \frac{d\left(\rho v_x v_x + p\right)}{dx} - \rho g\sin\theta \tag{3.13}$$

Henceforth we denote v_x as v. Solving for pressure gradient term gives

$$\frac{dp}{dx} = -\tau_{w,I}\frac{2}{R} - \frac{d\rho v^2}{dx} - \rho g\sin\theta \tag{3.14}$$

After substitution of wall shear stress and mass balance, we obtain

$$\frac{dp}{dx} = -\frac{\rho v^2 f}{R} - \left(\frac{2}{R}\rho_I v_I v + \rho v\frac{dv}{dx}\right) - \rho g\sin\theta \tag{3.15}$$

Correlation of the friction factor[6] is derived for pipe surface area $2\pi R(1-\gamma)\Delta x$. The friction factor is a function of Reynolds number, wall Reynolds number and pipe roughness. For laminar flow, it is given as

$$f = f_o\left(1 + 0.04304\left(N_{\mathrm{Re},w}\right)^{0.6142}\right) \tag{3.16}$$

where f_o is a friction factor without wall flux and is given as

$$\left(f_0\right) = \frac{16}{N_{\mathrm{Re}}} \tag{3.17}$$

When flow is turbulence, it is given as followings;
For openhole,

$$f = f_o\left(1 - 29.03\left(\frac{N_{\mathrm{Re},w}}{N_{\mathrm{Re}}}\right)^{0.8003}\right) \tag{3.18}$$

For perforated,

$$f = f_o\left(1 - 0.0153\left(N_{\mathrm{Re},w}\right)^{0.3978}\right) \tag{3.19}$$

The friction factor without wall flux is available in several published correlations, for example, Chen's equation is given by

$$f_0 = \left[-4\log\left\{ \frac{\varepsilon}{3.7065} - \frac{5.0452}{N_{\mathrm{Re}}} \log\left[\frac{\varepsilon^{1.1098}}{2.8257} + \left(\frac{7.149}{N_{\mathrm{Re}}} \right)^{0.8981} \right] \right\} \right]^{-2} \tag{3.20}$$

3.1.3 Energy balance equation

We neglect viscous shear stress and heat conduction in flowing direction (axial direction). Total energy is defined as[5]

$$\mathbf{e} = \left(\frac{1}{2}\rho v^2 + \rho\hat{H} \right)\mathbf{v} + \left[\boldsymbol{\tau} \cdot \mathbf{v} \right] + \mathbf{q} \tag{3.21}$$

where $\hat{H}$ is an enthalpy and $\mathbf{q}$ is a heat flux. Without viscous shear, it becomes

$$\mathbf{e} = \left(\frac{1}{2}\rho v^2 + \rho\hat{H} \right)\mathbf{v} + \mathbf{q} \tag{3.22}$$

Then, the total energy in at $r = R$

$$\begin{aligned} e_r\big|_R 2\pi R\Delta x &= \left[\left[\left(\frac{1}{2}\rho v^2 + \rho\hat{H} \right) v_r \right]_R + q_r\big|_R \right] 2\pi R \\ &= \left[\left[\left(\frac{1}{2}\rho v^2 + \rho\hat{H} \right) v_r \right]_R + q_r\big|_R \right] 2\pi R\gamma + \left[\left[\left(\frac{1}{2}\rho v^2 + \rho\hat{H} \right) v_r \right]_R + q_r\big|_R \right] 2\pi R(1-\gamma) \end{aligned} \tag{3.23}$$

It was split into two parts; one is the energy through the pipe material and the other is through opened area. Since the pipe is impermeable, the energy transport from formation can be viewed as Fig. 3.2.

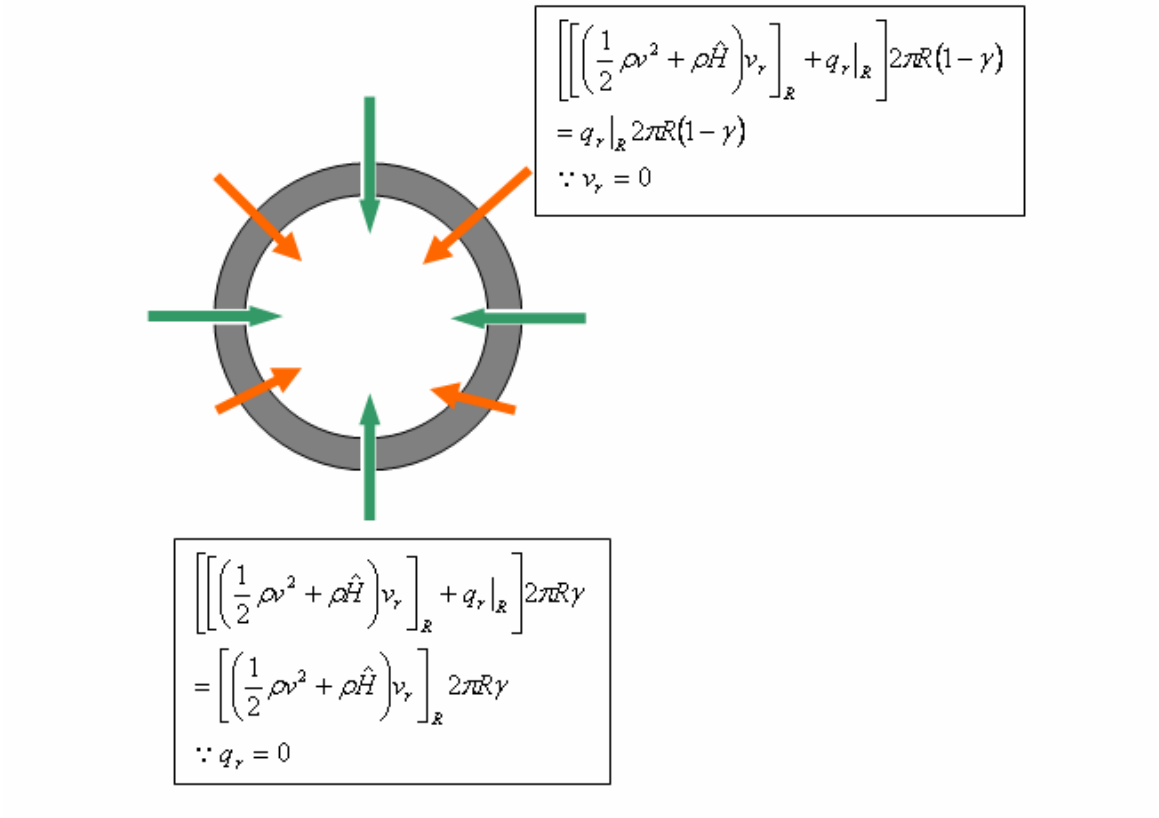

Fig. 3.2 Energy transport through porous pipe.

Then, we have

$$e_r|_R\,2\pi R\Delta x=\left[\left[\left(\frac{1}{2}\rho v^2+\rho\hat{H}\right)v_r\right]_R\right]2\pi R\gamma+\left[q_r|_R\right]2\pi R(1-\gamma) \tag{3.24}$$

Also, in x-direction

$$e_x=\left(\frac{1}{2}\rho v^2+\rho\hat{H}\right)v_x \tag{3.25}$$

Equating net input gives

$$0=e_r|_R\,2\pi R\Delta x+e_x|_x\,\pi R^2-e_x|_{x+\Delta x}\,\pi R^2+\rho vg\sin\theta\pi R^2\Delta x \tag{3.26}$$

Dividing by $2\pi R\Delta x$ and taking $\Delta x\to 0$ yield

$$0=e_r|_R\,\frac{2}{R}-\frac{\partial e_x}{\partial x}+\rho vg\sin\theta \tag{3.27}$$

Substituting Eqs. 3.24 and 3.25 into Eq. 3.27 yields

$$0 = -\frac{d}{dx}\left(\left(\frac{1}{2}\rho v^2 + \rho\hat{H}\right)v\right) + \frac{2}{R}\left[\left(\frac{1}{2}\rho_I {v_I}^2 + \rho_I \hat{H}_I\right)v_I\gamma + q_I(1-\gamma)\right] + \rho v g\sin\theta \tag{3.28}$$

where

$$\frac{d}{dx}\left(\frac{1}{2}\rho v^3\right) = \frac{1}{2}v^2\frac{d(\rho v)}{dx} + \rho v\frac{d}{dx}\left(\frac{1}{2}v^2\right) \tag{3.29}$$

From mass balance (Eq. 3.4)

$$\frac{1}{2}v^2\frac{d(\rho v)}{dx} + \rho v\frac{d}{dx}\left(\frac{1}{2}v^2\right) = \frac{1}{2}v^2\frac{2}{R}\gamma\rho_I v_I + \rho v^2\frac{dv}{dx} = \frac{1}{R}\gamma\rho_I v_I v^2 + \rho v^2\frac{dv}{dx} \tag{3.30}$$

Similarly,

$$\frac{d\left(\rho\hat{H}v\right)}{dx} = \rho v\frac{d\hat{H}}{dx} + \hat{H}\frac{d(\rho v)}{dx} = \rho v\frac{d\hat{H}}{dx} + \hat{H}\frac{2}{R}\gamma\rho_I v_I \tag{3.31}$$

Substitution yields

$$\begin{aligned} &-\frac{1}{R}\gamma\rho_I v_I v^2 - \rho v^2\frac{dv}{dx} - \rho v\frac{d\hat{H}}{dx} - \hat{H}\frac{2}{R}\gamma\rho_I v_I + \frac{1}{R}\gamma\rho_I v_I^3 \\ &\qquad + \frac{2}{R}\gamma\left(\rho_I\hat{H}_I\right)v_I + \frac{2}{R}q_I(1-\gamma) - \rho v g\sin\theta \\ &= \frac{\gamma\rho_I v_I}{R}\left(v_I^2 - v^2\right) - \rho v^2\frac{dv}{dx} - \rho v\frac{d\hat{H}}{dx} \\ &\qquad + \frac{2}{R}\gamma\rho_I v_I\left(\hat{H}_I - \hat{H}\right) + \frac{2}{R}q_I(1-\gamma) - \rho v g\sin\theta = 0 \end{aligned} \tag{3.32}$$

An enthalpy is a function of temperature and pressure and can be expressed as

$$d\hat{H} = C_p dT + \frac{1}{\rho}(1-\beta T)dp \tag{3.33}$$

Where C_p is a heat capacity and β is an isobaric thermal expansion defined as

$$\beta = -\frac{1}{\rho}\left(\frac{\partial\rho}{\partial T}\right)_P = \frac{1}{\hat{V}}\left(\frac{\partial\hat{V}}{\partial T}\right)_p \tag{3.34}$$

Let the pressure at the boundary, p_I, be same as the pressure of wellbore p. Then, the enthalpy difference term between inflow and wellbore becomes

$$\hat{H}_I - \hat{H} = C_p(T_I - T) + \frac{1}{\rho}(1-\beta T_I)(p_I - p) = C_p(T_I - T) \tag{3.35}$$

Therefore, we have

$$-\rho v C_p \frac{dT}{dx} - v(1-\beta T)\frac{dp}{dx} - \rho v^2 \frac{dv}{dx} + \gamma \frac{\rho_I v_I}{R}\left(v_I^2 - v^2\right) + \frac{2}{R}\gamma \rho_I v_I C_p (T_I - T) + \frac{2}{R} q_I (1-\gamma) - \rho v g \sin\theta = 0 \tag{3.36}$$

Solving for temperature gradient

$$\frac{dT}{dx} = -\frac{(1-\beta T)}{\rho C_P}\frac{dp}{dx} - \frac{v}{C_P}\frac{dv}{dx} + \frac{\gamma}{RC_P}\frac{\rho_I v_I}{\rho v}\left(v_I^2 - v^2\right) + \frac{2\gamma}{R}\frac{\rho_I v_I}{\rho v}(T_I - T) + \frac{2(1-\gamma)}{R\rho v C_P} q_I - \frac{1}{C_P} g \sin\theta \tag{3.37}$$

Joule – Thomson coefficient is defined as

$$\frac{\beta T - 1}{\rho C_P} = K_{JT} \tag{3.38}$$

Let the heat flux from the formation be

$$q_I = U(T_I - T) \tag{3.39}$$

where U is an overall heat transfer coefficient. The details about the overall heat transfer coefficient are discussed in Appendix A. Substituting Eqs. 3.38 and 3.39 into Eq. 3.37 gives

$$\frac{dT}{dx} = K_{JT}\frac{dp}{dx} - \frac{v}{C_P}\frac{dv}{dx} + \frac{\gamma}{RC_P}\frac{\rho_I v_I}{\rho v}\left(v_I^2 - v^2\right) + \frac{2}{R\rho v}\left(\gamma \rho_I v_I + \frac{1-\gamma}{C_P} U\right)(T_I - T) - \frac{1}{C_P} g \sin\theta \tag{3.40}$$

3.2 Studies from single phase model

We have derived the working equations for a single phase flow. Before going through multiphase flow equations, we evaluate how much the kinetic energy terms affect on temperature solution. The numerical solution procedures will be addressed later in this report.

The energy balance derived in the previous section is

$$\frac{dT}{dx} = K_{JT}\frac{dp}{dx} - \frac{v}{C_P}\frac{dv}{dx} + \frac{1}{RC_P}\frac{\rho_I v_I}{\rho v}\left(v_I^2 - v^2\right) + \frac{2}{R\rho v}\left(\rho_I v_I + \frac{1}{C_P} U\right)(T_I - T) - \frac{1}{C_P} g \sin\theta \tag{3.40}$$

The terms $-\frac{v}{C_P}\frac{dv}{dx}$ and $\frac{1}{RC_P}\frac{\rho_I v_I}{\rho v}\left(v_I^2 - v^2\right)$ are from kinetic energy terms. $-\frac{v}{C_P}\frac{dv}{dx}$ is a kinetic energy change because of axial velocity gradient. We call this term axial kinetic energy (AKE) and $\frac{1}{RC_P}\frac{\rho_I v_I}{\rho v}\left(v_I^2 - v^2\right)$ represents kinetic energy change caused by inflow. We call this term inflow kinetic energy (IKE). Following figures show with/without either AKE or IKE.

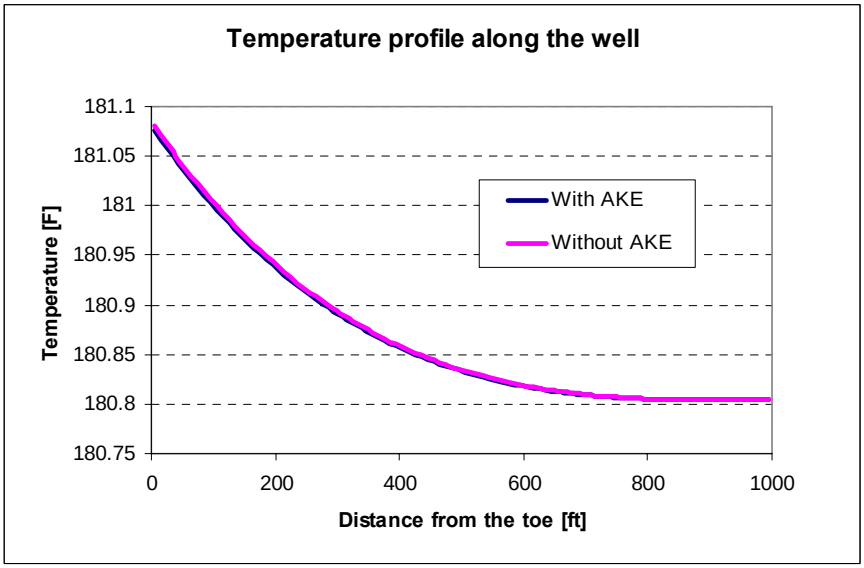

Fig. 3.3 Temperature profile with/without AKE.

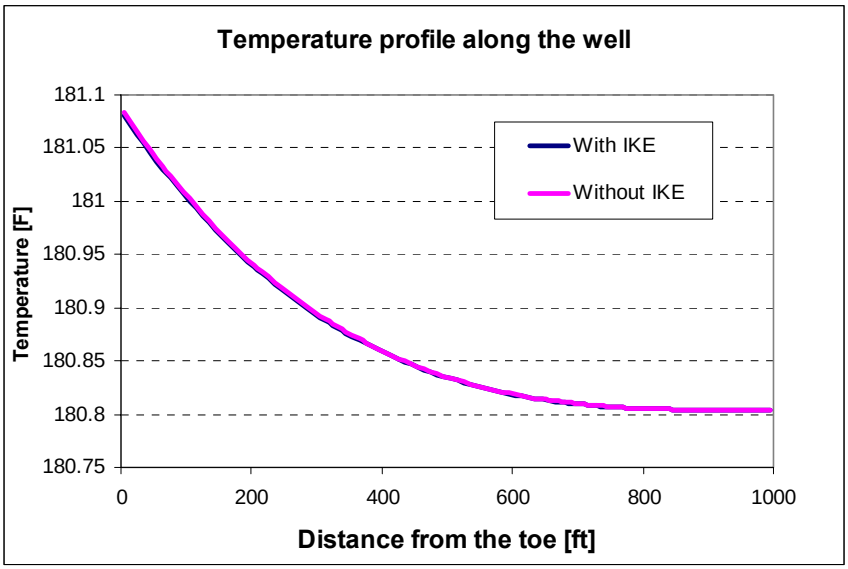

Fig. 3.3 Temperature profile with/without IKE.

From above results we can conclude that kinetic energy doesn't affect the computed temperature very much. We neglect kinetic energy change in further discussions. Neglecting kinetic energy, the energy balance becomes

$$\frac{dT}{dx} = K_{JT}\frac{dp}{dx} + \frac{2}{R\rho v}\left(\rho_I v_I + \frac{1}{C_P}U\right)(T_I - T) - \frac{1}{C_P}g\sin\theta \tag{3.41}$$

or

$$\frac{dT}{dx} = K_{JT}\frac{dp}{dx} + \frac{2}{R}\frac{U_I}{\rho v C_P}(T_I - T) - \frac{1}{C_P}g\sin\theta \tag{3.42}$$

where

$$U_I = \rho_I v_I C_P + U \tag{3.43}$$

This U_I is the combined (conduction and convection) overall heat transfer coefficient.

3.3 Working equations for multiphase flow

Using a similar shell balance to the single phase flow, equations for multiphase flow can be developed. We assume homogeneous flow for oil-water two phase flow and consider slip velocity fro gas-liquid flow (drift-flux model[7, 8]).

Mass balance for phase i (= oil, water, or gas) is given as

$$\frac{d(\rho_i v_i y_i)}{dx} = \frac{2\gamma y_{i,I}}{R}\rho_i v_{i,I} \tag{3.44}$$

where y_i is a volume fraction of phase i. We don't consider mass transfer between phases.

Energy balance for phase i, without kinetic energy is

$$\rho_i v_i y_i C_{p,i} \frac{dT_i}{dx} = \rho_i v_i y_i C_{p,i} K_{JT,i} \frac{dp_i}{dx} + \frac{2}{R} \rho_{i,I} v_{i,I} \gamma y_{i,I} C_{p,i} \left(T_{i,I} - T_i\right) + \frac{2}{R} q_{i,I} (1-\gamma) + \rho_i y_i v_i g \sin\theta \tag{3.45}$$

Summation of the equation for the three phases gives

$$\sum_i \rho_i v_i y_i C_{p,i} \frac{dT_i}{dx} = \sum_i \rho_i v_i y_i C_{p,i} K_{JT,i} \frac{dp_i}{dx} + \frac{2}{R} \sum_i \rho_{i,I} v_{i,I} \gamma y_{i,I} C_{p,i} \left(T_{i,I} - T_i\right) + \frac{2}{R} \sum_i q_{i,I} (1-\gamma) + \sum_i \rho_i y_i v_i g \sin\theta \tag{3.46}$$

Assuming that the pressures are same in each phase,

$$\sum_i \rho_i v_i y_i C_{p,i} \frac{dT_i}{dx} = \frac{dp}{dx} \sum_i \rho_i v_i y_i C_{p,i} K_{JT,i} + \frac{2}{R} \sum_i \rho_{i,I} v_{i,I} \gamma y_{i,I} C_{p,i} \left(T_{i,I} - T_i\right) + \frac{2}{R} \sum_i q_{i,I} (1-\gamma) + \sum_i \rho_i y_i v_i g \sin\theta \tag{3.47}$$

We also assume the temperatures are same in each phase

$$\frac{dT}{dx} \sum_i \rho_i v_i y_i C_{p,i} = \frac{dp}{dx} \sum_i \rho_i v_i y_i C_{p,i} K_{JT,i} + \frac{2}{R} \sum_i \rho_{i,I} v_{i,I} \gamma y_{i,I} C_{p,i} \left(T_{i,I} - T\right) + \frac{2}{R} (1-\gamma) U_T \left(T_{i,I} - T\right) + (\rho v)_T g \sin\theta \tag{3.48}$$

Finally,

$$\frac{dT}{dx} = \frac{dp}{dx} \frac{\sum_i \rho_i v_i y_i C_{p,i} K_{JT,i}}{\sum_i \rho_i v_i y_i C_{p,i}} + \frac{2}{R} \frac{\sum_i \rho_{i,I} v_{i,I} \gamma y_{i,I} C_{p,i} \left(T_{i,I} - T\right)}{\sum_i \rho_i v_i y_i C_{p,i}} + \frac{2}{R} \frac{(1-\gamma) U_T}{\sum_i \rho_i v_i y_i C_{p,i}} \left(T_{i,I} - T\right) + \frac{(\rho v)_T}{\sum_i \rho_i v_i y_i C_{p,i}} g \sin\theta \tag{3.49}$$

Total (mixing) properties can be factorized as

$$(\rho v)_T = \sum_i \rho_i v_i y_i \tag{3.50}$$

$$\left(\rho v C_p\right)_T = \sum_i \rho_i v_i y_i C_{p,i} \tag{3.51}$$

$$\left(\rho v C_p K_{JT}\right)_T = \sum_i \rho_i v_i y_i C_{p,i} K_{JT,i} \tag{3.52}$$

In any one segment, there is only a single phase entry in to the wellbore or inflow has a single value of temperature. Then, we have

$$T_{i,I} = T_I \qquad \text{for} \quad i = o, w, g \tag{3.53}$$

Finally,

$$\begin{aligned}\frac{dT}{dx} &= \frac{2}{R}\left[\gamma \frac{\left(\rho v C_p\right)_{T,I}}{\left(\rho v C_p\right)_T} + (1-\gamma)\frac{U_T}{\left(\rho v C_p\right)_T}\right](T_I - T) \\ &\qquad + \frac{\left(\rho v C_p K_{JT}\right)_T}{\left(\rho v C_p\right)_T}\frac{dp}{dx} + \frac{(\rho v)_T}{\left(\rho v C_p\right)_T} g \sin\theta \\ &= \frac{U_{T,I}}{\left(\rho v C_p\right)_T}(T_I - T) + \frac{\left(\rho v C_p K_{JT}\right)_T}{\left(\rho v C_p\right)_T}\frac{dp}{dx} + \frac{(\rho v)_T}{\left(\rho v C_p\right)_T} g \sin\theta\end{aligned} \tag{3.54}$$

3.4 The momentum balance equation for multiphase flow

When estimating the pressure profile along the well, we can apply the homogeneous, drift-flux, or mechanistic models to the multiphase flow. If we choose the drift-flux, we would need the slip-velocity to estimate holdup, or flow regime must be known for mechanistic model. In this study we use homogeneous model for oil-water two phase flow and drift-flux model for liquid-gas multiphase flow. It is an open issue that which model is the best estimator for pressure profile. We will not go through comparison issue in this study.

3.4.1 Oil- water two phase flow

For oil-water two phase flow, a homogeneous model is used for pressure equation which is given with mixture properties as

$$\frac{dp}{dx} = -\frac{\rho_m v_m{}^2 f_m}{R} - \frac{d\left(\alpha \rho_m v_m{}^2\right)}{dx} - \rho_m g \sin\theta \tag{3.55}$$

The mixture density is given as

$$\rho_m = \frac{M_T}{V_T} = \frac{M_o + M_w}{V_T} = \frac{M_o}{V_o}\frac{V_o}{V_T} + \frac{M_w}{V_w}\frac{V_w}{V_T} = \rho_o y_o + \rho_w y_w \tag{3.56}$$

$$\rho_{m,I} = \rho_{o,I} y_{o,I} + \rho_{w,I} y_{w,I} \tag{3.57}$$

Since we consider homogeneous flow (no slip velocity between phases), holdup is simply

$$y_w = \frac{v_{sw}}{v_{sw} + v_{so}} \tag{3.58}$$

where v_{sw} and v_{so} represent superficial velocity of water and oil. Mixture velocity is weighted by mass

$$\rho_m v_m = \rho_o v_{so} + \rho_w v_{sw} \tag{3.59}$$

$$v_m = \frac{\rho_o}{\rho_m} v_{so} + \frac{\rho_w}{\rho_m} v_{sw} \tag{3.60}$$

$$v_{m,I} = \frac{\rho_{o,I}}{\rho_{m,I}} v_{so,I} + \frac{\rho_{w,I}}{\rho_{m,I}} v_{sw,I} \tag{3.61}$$

Mixture viscosity[9] that includes phase inversion that is given by

$$\mu_m = \mu_c \left(1 - y_d\right)^{-2.5} \tag{3.62}$$

The inversion point[10] is

$$y_{inv} = \left[1 + \left(\frac{\mu_c}{\mu_d}\right)^{1/6} \left(\frac{\rho_c}{\rho_d}\right)^{5/6}\right]^{-1} \tag{3.63}$$

Where subscript c means continuous phase and d means dispersed phase. Then Reynolds number for mixture will be

$$N_{\mathrm{Re}} = \frac{\rho_m v_m D}{\mu_m} \tag{3.64}$$

The wall Reynolds number is defined as

$$N_{\mathrm{Re},w} = \frac{\rho_{m,I} v_{m,I} D}{\mu_{m,I}} \tag{3.65}$$

3.4.2 Liquid--gas two phase flow

For oil-gas two phase flow, homogeneous with slip velocity model[7] (drift-flux model) is used for pressure drop calculation. It consists of frictional, gravitational and accelerational pressure drops. It can be expressed as,

$$\frac{dp}{dx} = \left(\frac{dp}{dx}\right)_f + \left(\frac{dp}{dx}\right)_g + \left(\frac{dp}{dx}\right)_a \tag{3.67}$$

Pressure gradient because of the wall friction is given by

$$\left(\frac{dp}{dx}\right)_f = -\frac{2\tau_w}{R} = -\frac{f_m \rho_m v_m^{\,2}}{R} \tag{3.68}$$

where

$$\rho_m = \rho_l y_l + \rho_g y_g \tag{3.69}$$

$$v_m = \frac{\rho_l}{\rho_m} v_{sl} + \frac{\rho_g}{\rho_m} v_{sg} \tag{3.70}$$

$$N_{\mathrm{Re}} = \frac{\rho_m v_m D}{\mu_m} \tag{3.71}$$

$$N_{\mathrm{Re},w} = \frac{\rho_{m,I} v_{m,I} D}{\mu_{m,I}} \tag{3.72}$$

Pressure gradient because of gravity is

$$\left(\frac{dp}{dx}\right)_g = -\rho_m g \sin\theta \tag{3.73}$$

Pressure gradient because of acceleration can be divided to the one caused by a fluid expansion, and a wall influx such as

$$\left(\frac{dp}{dx}\right)_a = \left(\frac{dp}{dx}\right)_{aE} + \left(\frac{dp}{dx}\right)_{aW} \tag{3.74}$$

From Duns and Ros[11], the pressure gradient because of fluid expansion can be evaluated as

$$\left(\frac{dp}{dx}\right)_{aE} = -\left(\rho_l v_{sl} + \rho_g v_{sg}\right)\frac{dv_{sg}}{dx} \tag{3.75}$$

Assuming the gas expansion to be isothermal, such that pv_{sg} is constant,

$$v_{sg}\frac{dp}{dx} + p\frac{dv_{sg}}{dx} = 0 \tag{.3.76}$$

$$\therefore \frac{dv_{sg}}{dx} = -\frac{v_{sg}}{p}\frac{dp}{dx} \tag{3.77}$$

Substituting Eq. 3.77 into Eq. 3.75 gives,

$$\begin{aligned}\left(\frac{dp}{dx}\right)_{aE} &= \left(\rho_l v_{sl} + \rho_g v_{sg}\right)\frac{v_{sg}}{p}\frac{dp}{dx} \\ &= \left(\rho_l v_{sl} + \rho_g v_{sg}\right)\frac{v_{sg}}{p}\left[\left(\frac{dp}{dx}\right)_f + \left(\frac{dp}{dx}\right)_g + \left(\frac{dp}{dx}\right)_{aW} + \left(\frac{dp}{dx}\right)_{aE}\right]\end{aligned} \tag{3.78}$$

Therefore,

$$\left(\frac{dp}{dx}\right)_{aE}\left[1-\left(\rho_l v_{sl}+\rho_g v_{sg}\right)\frac{v_{sg}}{p}\right]=\left(\rho_l v_{sl}+\rho_g v_{sg}\right)\frac{v_{sg}}{p}\left[\left(\frac{dp}{dx}\right)_f+\left(\frac{dp}{dx}\right)_g+\left(\frac{dp}{dx}\right)_{aW}\right] \quad (3.79)$$

Then, we obtain

$$\left(\frac{dp}{dx}\right)_{aE}=\frac{\alpha\left[\left(\frac{dp}{dx}\right)_f+\left(\frac{dp}{dx}\right)_g+\left(\frac{dp}{dx}\right)_{aW}\right]}{1-\alpha} \quad (3.80)$$

where

$$\alpha=\left(\rho_l v_{sl}+\rho_g v_{sg}\right)\frac{v_{sg}}{p} \quad (3.81)$$

The acceleration pressure drop because of wall friction can be evaluated as

$$\left(\frac{dp}{dx}\right)_{aW}=\varpi\left(\frac{dp}{dx}\right)_{aW1}+\left(1-\varpi\right)\left(\frac{dp}{dx}\right)_{aW2} \quad (3.82)$$

where

$$\left(\frac{dp}{dx}\right)_{aW1}=-\frac{1}{A}\left[\left(v_{sl}+v_{sg}\right)\left(\rho_l w_{l,I}+\rho_g w_{g,I}\right)+\left(\rho_l v_l+\rho_g v_g\right)\left(w_{l,I}+w_{g,I}\right)\right] \quad (3.83)$$

$$\left(\frac{dp}{dx}\right)_{aW2}=-\frac{2}{A\rho_m}\left(\rho_l v_{sl}+\rho_g v_{sg}\right)\left(\rho_l w_{l,I}+\rho_g w_{g,I}\right) \quad (3.84)$$

From experimental data, $\varpi=0.8$ is suggested[7]. The pressure gradient is then given

$$\frac{dp}{dx}=-\frac{f_m\rho_m {v_m}^2}{R}-\rho_m g\sin\theta+\frac{\alpha\left[\left(\frac{dp}{dx}\right)_f+\left(\frac{dp}{dx}\right)_g+\left(\frac{dp}{dx}\right)_{aW}\right]}{1-\alpha}+\varpi\left(\frac{dp}{dx}\right)_{aW1}+\left(1-\varpi\right)\left(\frac{dp}{dx}\right)_{aW2} \quad (3.85)$$

Rearranging gives

$$\frac{dp}{dx}=\frac{1}{1-\alpha}\left[-\frac{f_m\rho_m {v_m}^2}{R}-\rho_m g\sin\theta+\varpi\left(\frac{dp}{dx}\right)_{aW1}+\left(1-\varpi\right)\left(\frac{dp}{dx}\right)_{aW2}\right] \quad (3.86)$$

The holdup is needed to obtain velocities of liquid and gas and mixture properties. The estimation of the holdup is shown in the next section.

3.4.3 Holdup estimation

Considering drift-flux model[8], gas phase velocity is given as

$$v_g = C_0(v_{sl} + v_{sg}) + u_0 m(\theta) \tag{3.87}$$

where C_0 and u_0 are the slip parameters

$$C_0 = \frac{A}{1+(A-1)\eta^2} \tag{3.88}$$

where

$$\eta = \frac{\lambda - B}{1 - B} \tag{3.89}$$

$$\lambda = \max\left(y_g, F_v \frac{y_g |v_{sl} + v_{sg}|}{v_{sg}} \right) \tag{3.90}$$

And the drift-flux is

$$u_0 = \frac{(1 - y_g C_0) C_0 K(y_g) v_c}{y_g C_0 \sqrt{\frac{\rho_g}{\rho_l}} + 1 - y_g C_0} \tag{3.91}$$

where

$$v_c = \left[\frac{\sigma_{gl} g(\rho_l - \rho_g)}{\rho_l^2} \right] \tag{3.92}$$

$$K(y_g) = 1.53 / C_0 \qquad \text{when} \qquad y_g \le a_1 \tag{3.93}$$

$$K(y_g) = K_u(\hat{D}) \qquad \text{for} \quad y_g \ge a_2 \tag{3.94}$$

$$\hat{D} = \left[\frac{g(\rho_l - \rho_g)}{\sigma_{gl}} \right]^{0.5} D \tag{3.95}$$

K_u is the 'critical Kutateladze number whose value is selected according to the table below.

Table 3.1 Kutateladze number.

$\hat{D}$	K_u
$\leq$ 2	0
4	1.0
10	2.1
14	2.5
20	2.8
28	3.0
≥ 50	3.2

If α_g is between a_1 and a_2, gives linear interpolated value. A, B, F_v are determined to fit the experimental data then $A = 1.0$ was obtained. This means B and F_v don't appear in the slip parameters. Then, we have

$$C_0 = 1 \tag{3.96}$$

$$u_0 = \frac{(1-y_g)K(y_g)v_c}{y_g\sqrt{\frac{\rho_g}{\rho_l}} + 1 - y_g} \tag{3.97}$$

$$m(\theta) = 1.85(\sin\theta)^{0.21}(1+\cos\theta)^{0.95} \tag{3.98}$$

Also,

$$a_1 = 0.06 \tag{3.99}$$

$$a_2 = 0.21 \tag{3.100}$$

The gas holdup estimation is

$$y_g = \frac{v_{sg}}{C_0(v_{sl}+v_{sg})+u_0} = \frac{v_{sg}}{(v_{sl}+v_{sg})+u_0(y_g)} \tag{3.101}$$

As can be seen, holdup is then estimated implicitly.

3.4.4 Three-phase flow

For three-phase, liquid phase will be considered as oil-water homogeneous flow. Then, the mixture properties of liquid (oil and water) will be calculated as followings;

Oil mass balance is given as

$$\frac{d(\rho_o v_o y_o)}{dx} = \frac{2\gamma y_{o,I}}{R}\rho_{o,I} v_{o,I}$$
$$= \frac{d(\rho_o v_{so})}{dx} = \frac{2}{R}\gamma\rho_{o,I} v_{so,I} \tag{3.102}$$

Water mass balance is given as

$$\frac{d(\rho_w v_w y_w)}{dx} = \frac{2\gamma y_{w,I}}{R}\rho_{w,I} v_{w,I}$$
$$= \frac{d(\rho_w v_{sw})}{dx} = \frac{2}{R}\gamma\rho_{w,I} v_{sw,I} \tag{3.103}$$

where

$$y_w = y_l F_w = y_l \frac{v_{sw}}{v_{sw} + v_{so}} \tag{3.104}$$

The mass of the liquid mixture is

$$M_l = M_o + M_w \tag{3.105}$$

Then, the density of the liquid mixture is

$$\rho_l = \frac{M_l}{V_l} = \frac{1}{V_l}(M_o + M_w) = \frac{V_o}{V_l}\frac{M_o}{V_o} + \frac{V_w}{V_l}\frac{M_w}{V_w}$$
$$= \frac{V_o}{V_l}\rho_o + \frac{V_w}{V_l}\rho_w = F_o\rho_o + F_w\rho_w \tag{3.106}$$

Therefore, the mass balance equation is

$$\frac{d(\rho_l v_{sl})}{dx} = \frac{d(\rho_o v_{so})}{dx} + \frac{d(\rho_l v_{sw})}{dx} = \frac{2}{R}\gamma\rho_{o,I} v_{so,I} + \frac{2}{R}\gamma\rho_{w,I} v_{sw,I} = \frac{2}{R}\gamma\rho_{l,I} v_{sl,I} \tag{3.107}$$

where

$$\rho_l v_{sl} = \rho_o v_{so} + \rho_w v_{sw} \tag{3.108}$$

Superficial velocity of liquid is

$$v_{sl} = \frac{\rho_o v_{so} + \rho_w v_{sw}}{\rho_l} = \frac{\rho_o v_{so} + \rho_w v_{sw}}{\rho_o F_o + \rho_w F_w}$$
$$= \frac{\rho_o v_{so} + \rho_w v_{sw}}{\rho_o \dfrac{v_{so}}{v_{so} + v_{sw}} + \rho_w \dfrac{v_{sw}}{v_{so} + v_{sw}}} = \frac{(v_{so} + v_{sw})(\rho_o v_{so} + \rho_w v_{sw})}{\rho_o v_{so} + \rho_w v_{sw}} = v_{so} + v_{sw} \tag{3.109}$$

$$\therefore v_{sl,I} = v_{so,I} + v_{sw,I} \tag{3.110}$$

3.5 Flow regime transition

Even though we use the drift-flux model, which doesn't account for flow regime, for liquid-gas two-phase pressure gradient calculation, the overall heat transfer coefficient depends on the flow regime. Therefore, we need to know flow regime before solving the energy equation from superficial liquid and gas velocities. A flow transition model for liquid-gas flow with radial influx was developed by Ouyang et. Al[12]. They defined four kinds of flow regime as most of previous studies did. We first check for the existence of bubble flow then check for stratified flow and annular flow. If none of them existed, the flow regime would be intermittent (slug) flow.

3.5.1 Bubble flow transition

If superficial liquid velocity is

$$v_{sl} \geq 0.92 v_{sg} \tag{3.111}$$

and droplet size is

$$d_{-} < d < d_{+} \tag{3.112}$$

flow regime would be dispersed bubble flow. Parameters are defined as

$$d_{\pm} = \frac{1}{2}\left(A \pm \sqrt{A^2 + 4B}\right) \tag{3.113}$$

$$A = \frac{3\rho_l f \left(v_{sl} + v_{sg}\right)^2}{2\left(\rho_l - \rho_g\right) g \cos\theta} \tag{3.114}$$

$$B = \frac{6\mu_l \left(v_{sl,I} + v_{sg,I}\right) C_{id}}{\left(\rho_l - \rho_g\right) g \cos\theta} \frac{2\lambda + 3}{\lambda + 1} \tag{3.115}$$

where f is a friction factor. Since liquid flow is dominant in bubble flow, it can be estimated as

$$f \approx F\left(\frac{\rho_l \left(v_{sg} + v_{sl}\right) D}{\mu_l}, \frac{\varepsilon}{D}\right) \tag{3.116}$$

And the other parameters are given by,

$$\lambda = \frac{\mu_l}{\mu_g} \tag{3.117}$$

$$C_{id} = 0.8 \tag{3.118}$$

Stable droplet size can be calculated as

$$d = 1.14\left(\frac{\sigma}{\rho_l}\right)^{0.6}\eta^{-0.4} \tag{3.119}$$

and

$$\eta = \frac{8f\left(v_{sg}+v_{sl}\right)^3}{D} \tag{3.120}$$

3.5.2 Stratified flow transition

Stratified flow occurs if the gas velocity doesn't satisfy that Kelvin-Holmholtz instability which is given by

$$v_g > \left(1-h_l/D\right)\left[\frac{A_g}{2\sqrt{h_l\left(D-h_l\right)}}\left\{\frac{\rho_l g\cos\theta}{\rho_g}+\frac{\left(v_{sl,I}+v_{sg,I}\right)\left|v_{sl,I}+v_{sg,I}\right|}{2\left(D-h_l\right)}\right\}\right]^{0.5} \tag{3.121}$$

Liquid height must be determined by the following equation

$$X^2F_2 - F_1 - 4Y_{ST} - 4I_{ST} = 0 \tag{3.122}$$

where

$$X^2 = \frac{f_{sl}v_{sl}{}^2\rho_l}{f_{sg}v_{sg}{}^2\rho_g} = \frac{-\left(dp/dx\right)_{sl}}{-\left(dp/dx\right)_{sg}} \tag{3.123}$$

$$Y_{ST} = \frac{\left(\rho_l-\rho_g\right)g\sin\theta}{\left(dp/dx\right)_{sg}} \tag{3.124}$$

Following variables implicitly contain liquid height;

$$F_1 = \left(\frac{f_{wg}}{f_{sg}}\right)\left(\frac{v_g}{v_{sg}}\right)^2\left[\frac{DS_g}{A_g}+\frac{f_{i,ST}}{f_{wg}}\frac{v_{i,ST}\left|v_{i,ST}\right|DS_{i,ST}}{v_g{}^2}\left(\frac{1}{A_l}+\frac{1}{A_g}\right)\right] \tag{3.125}$$

$$F_2 = \left(\frac{f_{wl}}{f_{sl}}\right)\left(\frac{v_l}{v_{sl}}\right)^2\frac{DS_l}{A_l} \tag{3.126}$$

$$I_{ST} = \frac{2\left[\frac{\rho_l v_l w_{l,I}}{A_l} - \frac{\rho_g v_g w_{g,I}}{A_g}\right]}{\left(\frac{dp}{dx}\right)_{sg}} \tag{3.127}$$

where

$$v_{i,ST} = v_g - v_l \tag{3.128}$$

$$f_{i,ST} = \left(0.004 + 0.5\times 10^{-6}\left(N_{\mathrm{Re}}\right)_{sl}\right)\left(F_r\right)_l^{1.335}\left(\frac{\rho_l g D}{\rho_g v_g{}^2}\right) \tag{3.129}$$

$$\left(N_{\mathrm{Re}}\right)_{sl} = \frac{\rho_l v_{sl} D}{\mu_l} \tag{3.130}$$

$$\left(F_r\right)_l = \frac{v_l}{\sqrt{g h_l}} \tag{3.131}$$

Liquid film height h_l, which corresponds to X and Y will be determined iteratively by Eq. 3.122 with h_l dependent variables F_1, F_2, I_{ST}.

3.5.3 Annular flow transition

If holdup is

$$y_l \le 0.24 \tag{3.132}$$

then annular-mist flow exists. The liquid holdup can be estimated by liquid film thickness δ_l as

$$y_l = 1 - \left(1 - 2\delta_{lD}\right)^2 \frac{v_{sg}}{v_{sg} + F_e v_{sl}} \tag{3.133}$$

where

$$\delta_{lD} = \frac{\delta_l}{D} \tag{3.134}$$

The volume fraction of the liquid phase entrained in the gas core F_e is

$$F_e = \frac{0.735\left(\frac{\mu_l{}^2 v_{sg}{}^2 \rho_g}{\sigma^2 \rho_l}\right)^{0.074}\left(\frac{v_{sg}}{v_{sl}}\right)^{0.2}}{1+0.735\left(\frac{\mu_l{}^2 v_{sg}{}^2 \rho_g}{\sigma^2 \rho_l}\right)^{0.074}\left(\frac{v_{sg}}{v_{sl}}\right)^{0.2}} \tag{3.135}$$

The liquid film thickness is given by solving

$$X^2 F_4 - F_3 - 4Y_{AN} - 4I_{AN} = 0 \tag{3.136}$$

The Lockhart-Martinell parameter X^2 is given in previous section. The liquid film thickness dependent variables are given as

$$Y_{AN} = \frac{(\rho_l - \rho_c) g \sin\theta}{\left(dp/dx\right)_{sg}} \tag{3.137}$$

$$F_3 = \frac{f_{i,AN}}{f_{sg}}\frac{\rho_c}{\rho_g}\left(\frac{v_c}{v_{sg}}\right)^2 DS_{i,AN}\left(\frac{1}{A_l}+\frac{1}{A_c}\right) \tag{3.138}$$

$$F_4 = \left(\frac{f_{wl}}{f_{sl}}\right)\left(\frac{v_f}{v_{sl}}\right)^2 \frac{DS_l}{A_l} \tag{3.139}$$

$$I_{AN} = \frac{\left\{\frac{2\rho_l}{A_l} v_f \left[w_{l,I} - \frac{F_e}{1-F_e} w_{g,I}\right] - \frac{2\rho_c}{A_c}\frac{v_c w_{g,I}}{1-F_e}\right\}}{\left(\frac{dp}{dx}\right)_{sg}} \tag{3.140}$$

where

$$\rho_c = \rho_g (1 - y_{cl}) + \rho_l y_{cl} \tag{3.141}$$

$$v_{i,AN} = v_c - v_f \tag{3.142}$$

$$f_{i,AN} = 0.24\, f_c \left(N_{\mathrm{Re}}\right)_f{}^{0.305}\left(\frac{\sigma}{\rho_c v_c{}^2 D_c}\right) \tag{3.143}$$

f_c is a fanning friction factor based on the gas core Reynolds number, and D_c is the gas core hydraulic diameter.

4 RESERVOIR MODEL

The working equations for wellbore flow have been derived. Our previous study[13] showed the temperature and pressure behavior of the wellbore, supposing the inflow temperature is equal to geothermal temperature. For vertical well production, inflow temperature can be considered as geothermal temperature since there is a significant difference between inflowing fluid temperatures from different depths. However some studies[14] pointed out the importance of Joule-Thomson effect near wellbore vicinity. We will show that inflow temperature can deviate from geothermal temperature on the order of a few degrees. This amount of change, of course, should not be overlooked especially for horizontal or near horizontal well production.

For reservoir flow, fluid temperature is obtained by coupling mass and energy balances along with Darcy's Law. A new analytical temperature model has been developed to apply for the single phase flow of oil, water or gas. It is certainly appropriate for modeling primary production. For wellbore flow, the mass and momentum balances are coupled with energy balance. The numerical wellbore model is applicable two or three phase flow.

To enable to detect small temperature changes, the models account for subtle thermal energy including Joule-Thomson expansion, viscous dissipative heating, and thermal conduction. Heat conduction both in wellbore and reservoir flows provide a tight linkage between wellbore and reservoir, which means that while wellbore is receiving fluid and flowing along the wellbore, fluid can loss or gain energy through the pipe wall by mean of heat conduction. The mass and energy balances mentioned are general and applicable to any types of flow. They will be discussed and formulated to fit the scope of this study.

4.1 Mass balance

A starting point for studying fluid flow is the mass balance. It is the conservation of mass per unit area (perpendicular to the velocity vector) per unit time. By understanding the mechanisms of mass flow, we can infer velocity and pressure distribution of fluid in space. The velocity and pressure distribution will then be used in the energy equation. Lake[15] formulated a mass balance that can apply directly to fluid flow in permeable media. It is simplified here for single phase and steady state flow condition.

$$\vec{\nabla} \cdot (\rho \vec{\mathbf{u}}) = 0 \tag{4.1}$$

where the auxiliary relation $\vec{\mathbf{u}} = -\frac{\vec{\vec{\mathbf{k}}}}{\mu} \cdot (\vec{\nabla} p + \rho \vec{\mathbf{g}})$ derived from Darcy's law.

4.2 Energy balance

Flow in permeable media is not an isothermal process because there is a temperature change resulting from fluid expansion and viscous dissipation heating. One of the interests of this study is to use the energy balance for prediction of temperature profiles. For single phase, we can start from the thermal energy balance at steady state condition as the following form,

$$\vec{\nabla}\cdot(\rho\hat{U}\vec{\mathbf{v}}) + p\vec{\nabla}\cdot\vec{\mathbf{v}} - \vec{\nabla}\cdot K_T\vec{\nabla}T - (-\vec{\vec{\boldsymbol{\tau}}}:\vec{\nabla}\vec{\mathbf{v}}) = 0 \tag{4.2}$$

where $\vec{\mathbf{v}}$ is interstitial velocity $(\vec{\mathbf{v}} = \frac{\vec{\mathbf{u}}}{\phi})$, $\vec{\mathbf{u}}$ is the Darcy velocity. To express the thermal energy balance in terms of extensive properties (p, T etc.), we can substitute the definition of enthalpy which is $\hat{H} = \hat{U} + p\hat{V}$ or $\hat{U} = \hat{H} - \frac{p}{\rho}$ into the equation. The equation becomes,

$$\vec{\nabla}\cdot(\rho\vec{\mathbf{v}}\hat{H}) - \vec{\nabla}\cdot(p\vec{\mathbf{v}}) + p\vec{\nabla}\cdot\vec{\mathbf{v}} - \vec{\nabla}\cdot K_T\vec{\nabla}T - (-\vec{\vec{\boldsymbol{\tau}}}:\vec{\nabla}\vec{\mathbf{v}}) = 0 \tag{4.3}$$

Expanding the first term following the definition of the enthalpy,

$$\begin{aligned}&\rho\vec{\mathbf{v}}\cdot\vec{\nabla}\hat{H} - \vec{\nabla}\cdot(p\vec{\mathbf{v}}) + p\vec{\nabla}\cdot\vec{\mathbf{v}} - \vec{\nabla}\cdot K_T\vec{\nabla}T - (-\vec{\vec{\boldsymbol{\tau}}}:\vec{\nabla}\vec{\mathbf{v}})\\ &= \rho\vec{\mathbf{v}}\cdot\left\{\left[\frac{1}{\rho} - \frac{\beta T}{\rho}\right]\vec{\nabla}p + C_p\vec{\nabla}T\right\} - \vec{\nabla}\cdot(p\vec{\mathbf{v}}) + p\vec{\nabla}\cdot\vec{\mathbf{v}} - \vec{\nabla}\cdot K_T\vec{\nabla}T - (-\vec{\vec{\boldsymbol{\tau}}}:\vec{\nabla}\vec{\mathbf{v}})\end{aligned} \tag{4.4}$$

Rearranging Eq. 4.4,

$$\rho C_p\vec{\mathbf{v}}\cdot\vec{\nabla}T - \beta T\vec{\mathbf{v}}\cdot\vec{\nabla}p - \vec{\nabla}\cdot K_T\vec{\nabla}T - (-\vec{\vec{\boldsymbol{\tau}}}:\vec{\nabla}\vec{\mathbf{v}}) = 0 \tag{4.5}$$

where β is thermal expansion coefficient. The $\left(-\tau:\vec{\nabla}\cdot\vec{\mathbf{v}}\right)$ term is the viscous dissipation heating that describes the degradation of mechanical energy into thermal energy. It is always positive number (heating) for Newtonian fluid, and commonly substituted by $\left(-\vec{\mathbf{u}}\cdot\vec{\nabla}p\right)$ in flow through porous media[16, 17]. In permeable media, the interstitial velocity, $\vec{\mathbf{v}}$, is replaced by Darcy velocity, $\frac{\vec{\mathbf{u}}}{\phi}$. And, the heat conduction coefficient is the effective heat conduction coefficient, K_T, which combines both fluid and matrix. Then, the equation becomes,

$$\rho C_p\vec{\mathbf{u}}\cdot\vec{\nabla}T - \beta T\vec{\mathbf{u}}\cdot\vec{\nabla}p - \vec{\nabla}\cdot\vec{\vec{\mathbf{K}}}_T\vec{\nabla}T + \vec{\mathbf{u}}\cdot\vec{\nabla}p = 0 \tag{4.6}$$

The first term is thermal energy transported by convection. The second term is thermal energy (cooling) because of fluid expansion. The third term is thermal energy by heat conduction, and the last term represents the viscous dissipation heating.

If we were to use the energy Eq. 4.6 to describe the Joule-Thomson experiment, which is a steady state isenthalpic process with no heat conduction, we would arrive at

$\rho C_p \vec{\mathbf{u}} \cdot \vec{\nabla} T + \vec{\mathbf{u}} \cdot \vec{\nabla} p - \beta T \vec{\mathbf{u}} \cdot \vec{\nabla} p = 0$, which can be integrated as $\Delta T = \left(\frac{\beta T - 1}{\rho C_p} \right) \Delta p$. The term $\frac{\beta T - 1}{\rho C_p}$ is a Joule-Thomson coefficient, K_{JT}. This is a well-known relationship that describes the change in temperature of a fluid upon expansion in a steady state flow with neither heat nor work done on the system. An example of this kind of process is a flow through an expansion valve.

5 COUPLED MODEL

Here we present equations that describe the coupling between the reservoir and wellbore. The reservoir energy balance can be solved analytically with some simplifications and assumptions, and it can be coupled with multiphase wellbore model by dividing reservoir into a series of single phase producing segments (multi-segment technique). The computational time of this coupling model is fast because we only need so many grids as the number of wellbore segments.

Analytical coupling model assumes no interaction between reservoir segments i.e. no mass and heat transfer between reservoir segments. As long as reservoir inflow follows 1-D linear flow and 1-D radial flow paths or wellbore passes through the single fluid production zones, this model should give reasonable profiles of temperature and pressure. To rigorously analyze non-isothermal horizontal well flow, the number of grids must be extended to the reservoir. First we show the results from analytical coupling model which provide various features on temperature or pressure profiles with various production conditions. As a second, we show the numerical coupling model.

5.1 Analytical coupled model

We consider a horizontal well fully penetrated through a box-shaped homogeneous reservoir as shown in Fig. 5.1.

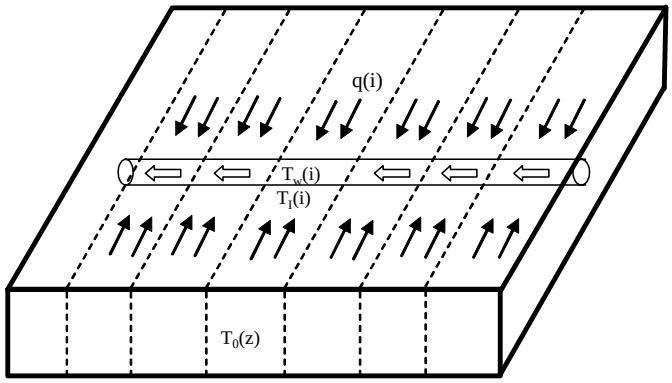

Fig. 5.1 Physical condition of coupled model.

With no-flow lateral boundaries, flow in the reservoir is only in the y and z directions; flow in the horizontal wellbore is in the x-direction. The assumptions for this coupled model are the following:

(1) Steady-state flow: For continuous well flow, changes in the well rate are much slower than the response time of any sensor; hence, we can neglect time derivatives in our treatment. We use the steady-state model of Furui et al.[18] to describe the pressure profile in the reservoir.

(2) Isolated reservoir segments: Each segment of the reservoir is idealized to be isolated from each other. There is no flow in the x-direction within the reservoir.
(3) Single-phase reservoir flow: Each reservoir segment produces a single-phase fluid. Multiphase flow occurs only in the wellbore as a result of the combination of single phase flows of different phases from the reservoir segments.

5.1.1 Analytical solution to the reservoir equation

Furui et al.[18] model considers linear flow becomes radial flow at $y_t = h/2$ as shown in Fig. 5.2.

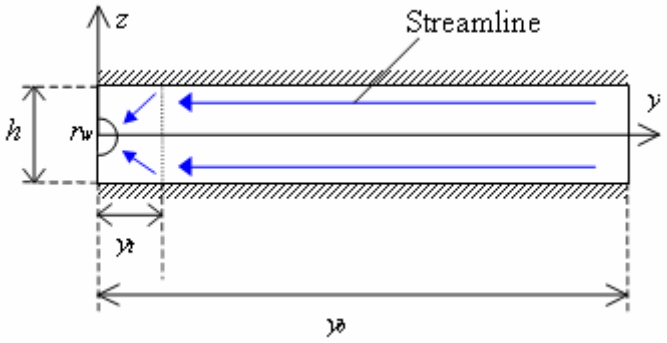

Fig. 5.2 Streamline path in the reservoir.

For linear flow Eq. 4.6 can be solved analytically in 1-D to yield

$$T = L_1 e^{m_+ y} + L_2 e^{m_- y} + \frac{1}{\beta} \tag{5.1}$$

The radial flow solution is

$$T = R_1 r^{n_+} + R_2 r^{n_-} + \frac{1}{\beta} \tag{5.2}$$

The solution procedure is presented and all parameters are defined in Appendix B. The temperature profiles perpendicular to the wellbore of fluid flowing into a wellbore for various inflow rates, permeabilities and fluid types are shown in followings. The input parameters used are in Table 5.1.

Table 5.1 Default properties for inflow temperature.

	Oil	Water	Gas
Viscosity (cp)	0.6	0.5	0.017
Heat capacity (Btu/lb ^{o}F)	0.528	1.002	0.587
Density (lb/ft^3)	43	63.027	13
Thermal expansion (1/^{o}F)	0.000632	0.000311	0.00297
Permability (md)	50		
Total thermal conductivity (Btu/hr ft ^{o}F)	2	2.5	1.3
Reservoir length (ft)	1000		
Reservoir width (ft)	3000		
Reservoir height (ft)	50		
T at outer boundary (^{o}F)	180		
Geothermal gradient (^{o}F/ft)	0.01		

Figure 5.3 shows how the temperature in the reservoir varies with different oil flow rates. As flow rate increases, the temperature change increases because larger frictional pressure drop leads to a greater Joule-Thomson effect. Figure 5.4 shows the effect of permeability on temperature distribution with a fixed flow rate. The inflow temperature decreases as permeability increases because less pressure drop caused by higher permeability leads to a smaller Joule-Thomson effect. Figure 5.5 presents the reservoir temperature profiles with different fluids. It is obvious that the temperature of gas is substantially lower than the geothermal temperature because of Joule-Thomson cooling. The temperature of water is slightly lower than for oil because water has a greater heat capacity.

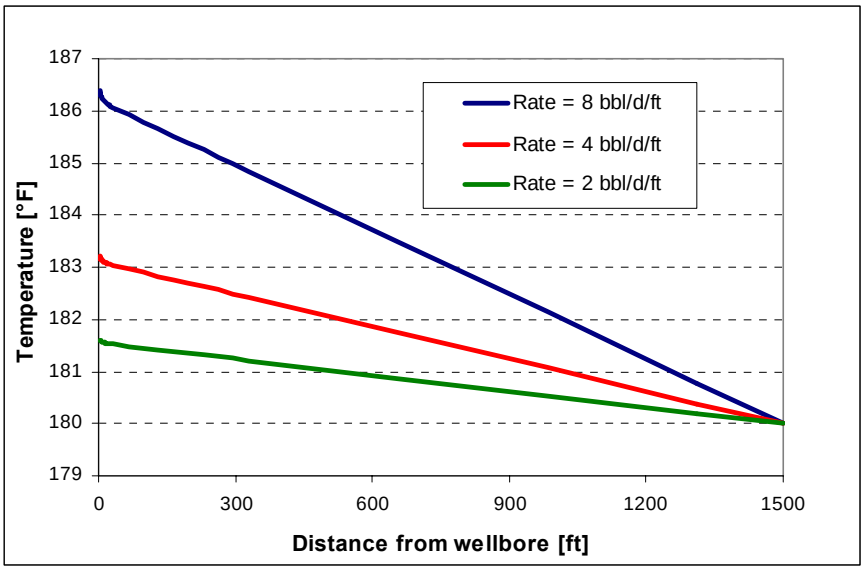

Fig. 5.3 Temperature profiles for different inflow rates.

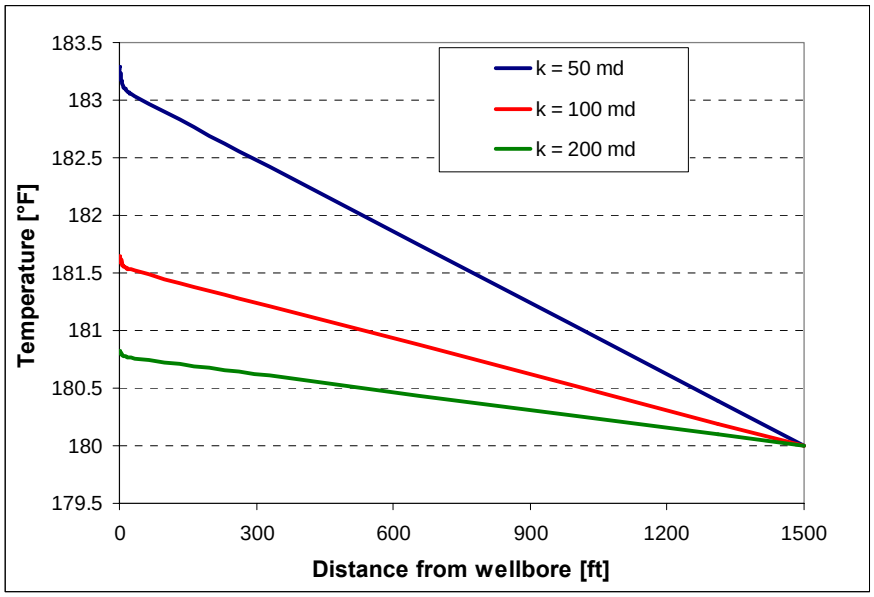

Fig. 5.4 Temperature profiles for different permeabilities.

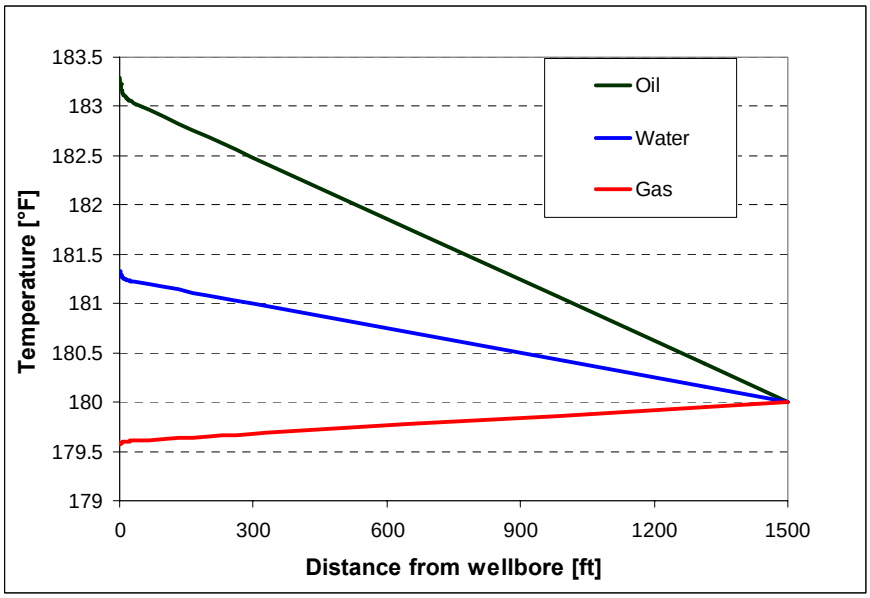

Fig. 5.5 Temperature profiles for different fluids.

The reservoir temperature is influenced by the wellbore temperature and its heat transfer. Figure 5.6 shows how inflow temperature differs near the wellbore with different overall heat transfer coefficient keeping wellbore temperature 180 ^{o}F. Zero heat transfer means that there is no heat communication between formation and wellbore,

in other words, the wellbore is perfectly insulated. On the other hand, as heat transfer coefficient approaches infinity, both temperatures become identical (Fig. 5.7).

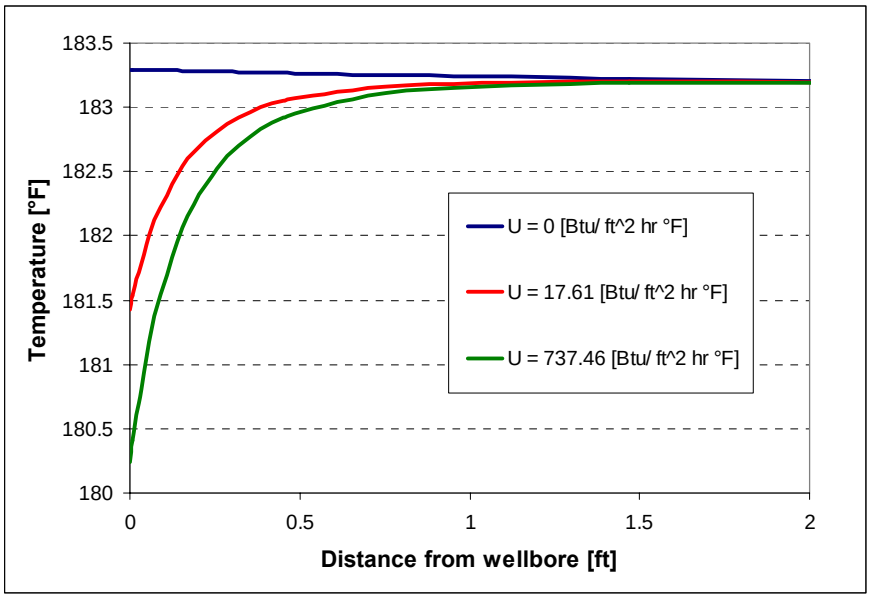

Fig. 5.6 Inflow temperatures with different overall heat transfer coefficient in near wellbore region. Tw=180 ^{o}F

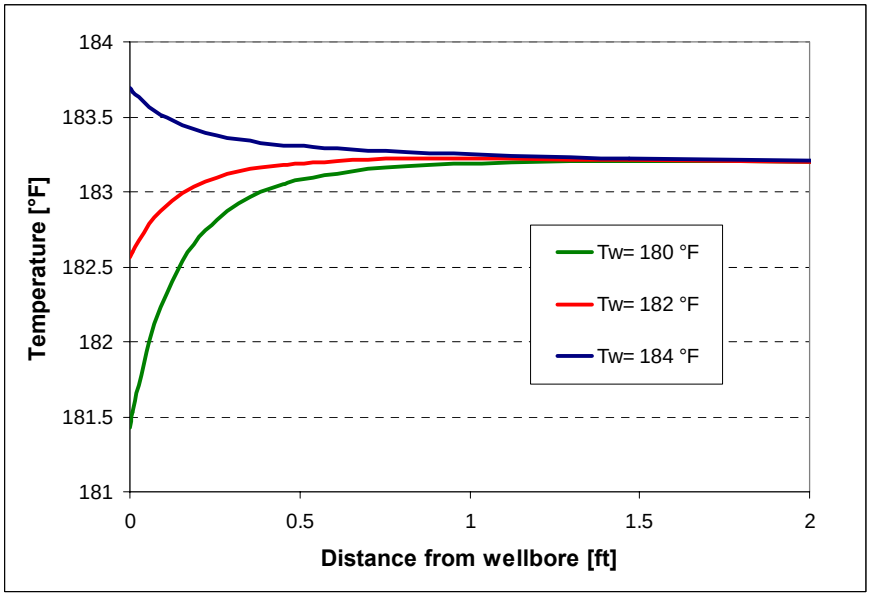

Fig. 5.7 Inflow temperatures with varying wellbore temperature in near wellbore region. U=17.61 Btu/ft^2 hr ^{o}F

5.1.2 Solution procedure of the coupled equations

The coupled equations can be solved numerically. The working equations can be discretized by finite difference method. In matrix forms, they are written as

$$\mathbf{A}\cdot\mathbf{v}=\mathbf{B} \tag{5.3}$$

$$\mathbf{C}\cdot\mathbf{p}=\mathbf{D} \tag{5.4}$$

$$\mathbf{E}\cdot\mathbf{T}=\mathbf{F} \tag{5.5}$$

where **A**, **B, C, D, E** and **F** are the coefficient matrices. For example, single phase energy balance equation can be discretized as

$$T_j + E_j T_{j-1} = F_j \tag{5.6}$$

where

$$E_j = -\left[1+\frac{2U_{I,j}\Delta x}{R\rho_j C_{p,j} v_j}\right]^{-1} \tag{5.7}$$

$$F_j = \Delta x\left[\frac{2U_{I,j}}{R\rho_j C_{p,j} v_j}\left(T_I\right)_j + K_{JT,j}\left(\frac{dp}{dx}\right)_j - \frac{g\sin\theta_j}{C_{p,j}}\right]E_j \tag{5.8}$$

The fluid physical properties are a function of pressure and temperature so is inflow temperature. Also, friction factor and heat transfer coefficient are velocity dependent. Therefore, the coefficients will be written as

$$E_j = E_j\left(v_j, p_j, T_j\right) \tag{5.9}$$

$$F_i = F_j\left(v_j, p_j, T_j, T_{I,j}\right) \tag{5.10}$$

As shown in Appendix A, $T_{I,j}$ is a function of wellbore temperature, overall heat transfer coefficient and reservoir and fluid properties. Therefore, we can rewritten F_i as $F_j\left(v_j, p_j, T_j\right)$ and obtain

$$\mathbf{E}(\mathbf{v},\mathbf{p},\mathbf{T})\cdot\mathbf{T}=\mathbf{F}(\mathbf{v},\mathbf{p},\mathbf{T}) \tag{5.11}$$

The solution can be found iteratively. For example, when velocity and pressure profile ($\mathbf{v}^n, \mathbf{p}^n$) are known, the temperature profile can be obtained as follows;
Solve

$$\mathbf{E}\left(\mathbf{v}^n, \mathbf{p}^n, \mathbf{T}^l\right)\cdot\mathbf{T}=\mathbf{F}\left(\mathbf{v}^n, \mathbf{p}^n, \mathbf{T}^l\right) \tag{5.12}$$

for **T** . Then **T** will be updated as

$$\mathbf{T}^{l+1} = \kappa\left(\mathbf{T} - \mathbf{T}^{l}\right) + \mathbf{T}^{l} \tag{5.13}$$

where κ is a relaxation factor that takes value between 0 and 1. This process will be repeated until we have

$$\frac{(\mathbf{T}^{l} - \mathbf{T})^{T}(\mathbf{T}^{l} - \mathbf{T})}{(\mathbf{T}^{l})^{T}(\mathbf{T}^{l})} < \varepsilon_{tol}^{\ 2} \tag{5.14}$$

where ε_{tol} is a pre-assigned tolerance. Schematic solution procedure is shown in Fig. 5.8.

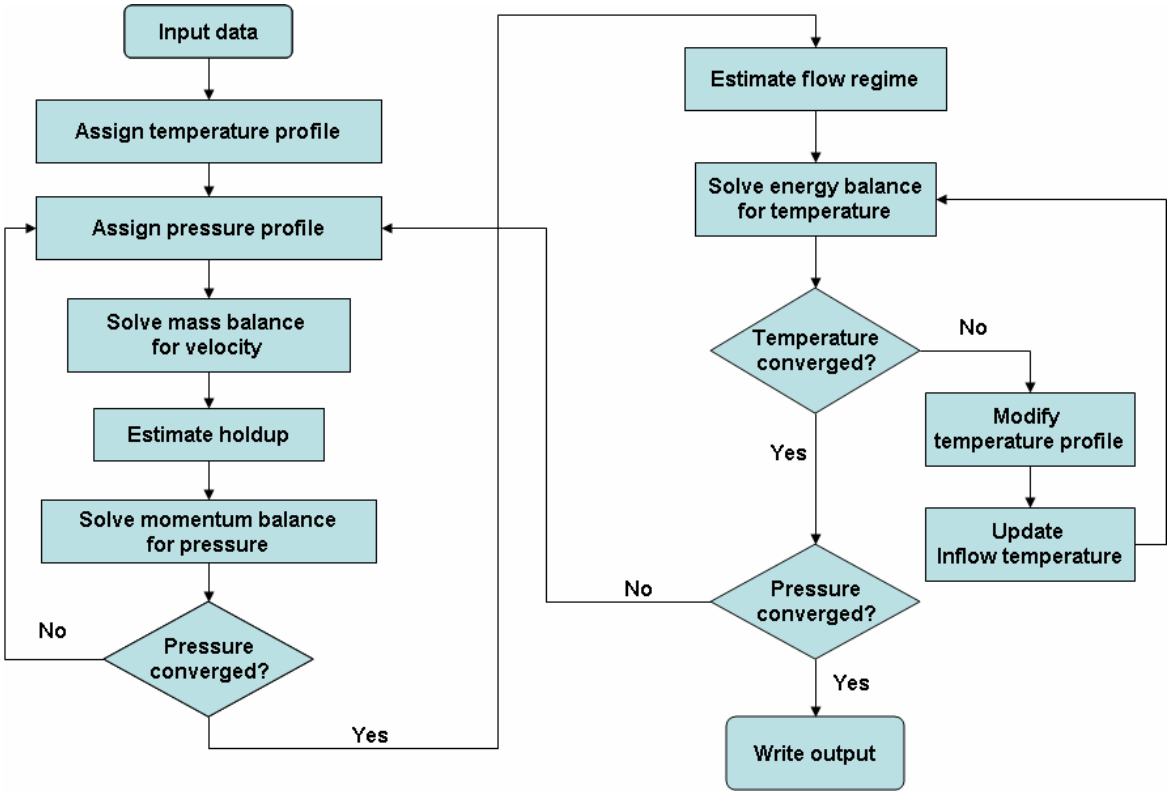

Fig. 5.8 Schematic solution procedure.

5.1.3 Example studies from analytical coupled model

This section shows examples using the coupled model. We are interested in determining the conditions for which measurable temperature changes occur along a horizontal wellbore, so we focus on how much temperature change is possible under

specified conditions. We also looked for conditions that caused anomalies in the pressure or temperature profiles caused by the inflow of different fluids.

We consider two kinds of wells; one with a small diameter and the other large, and both are completed as cased, perforated wells. The details are shown in Table 5.2. Oil, gas and water are the produced fluids. The average reservoir pressure is 4000 psia, except for the single-phase gas reservoir for which it is 2000 psia. The physical fluid properties are estimated based on pressure and temperature along the wellbore, and Table 5.3 using accepted correlations[19].

Table 5.2 Well properties.

	Small	Large
ID (in)	2.602	4
OD (in)	3.5	4.5
Diameter with cement (in)	5	6
K_c (Btu/hr ft ^oF)	6.933	
K_{cem} (Btu/hr ft ^oF)	4.021	
Relative roughness	0.01	
Total length (ft)	2000	
Pipe opened ratio (%)	2	

Table 5.3 Fluid properties.

K_o (Btu/hr ft ^oF)	0.0797
K_g (Btu/hr ft ^oF)	0.0116
Salinity of water (%)	5
Specific gravity of gas	0.75
Oil API	45.176
Disolved GOR (SCF/STB)	800
Surface tension (dyne/cm)	10

Possible temperature changes in single-phase production

To evaluate the temperature changes possible along the wellbore in a single phase production system, we studied two extreme cases; small and large production scenarios with small or large well diameter. These cases should bracket the possible temperature changes in actual wells.

Figure 5.9 displays the flow rate profile and pressure change from the toe pressure for flow through a small diameter well. With a total flow rate of about 5300 b/d, the total pressure drop in the 2000 ft. long wellbore is only about 50 psi; at a very high rate of almost 20,000 b/d, the wellbore pressure drop is over 600 psi. The corresponding

temperature change profiles, the temperature at any location along the well minus the temperature at the toe along the wellbore, are shown in Fig. 5.10. For the small flow rate case, the temperature changes only 0.5 ^{o}F from the toe to the heel of the well. In the large production rate case, the temperature deviation is substantial (6.4 ^{o}F). This case, a high flow rate in a small diameter well, illustrates the largest temperature change that can be expected in a horizontal single-phase oil production well.

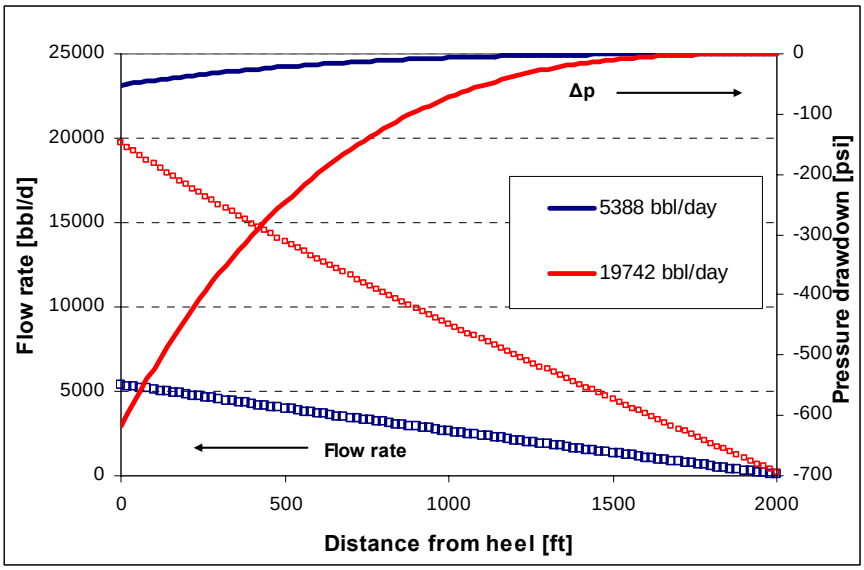

Fig. 5.9 Flow rate and pressure profiles (oil, small).

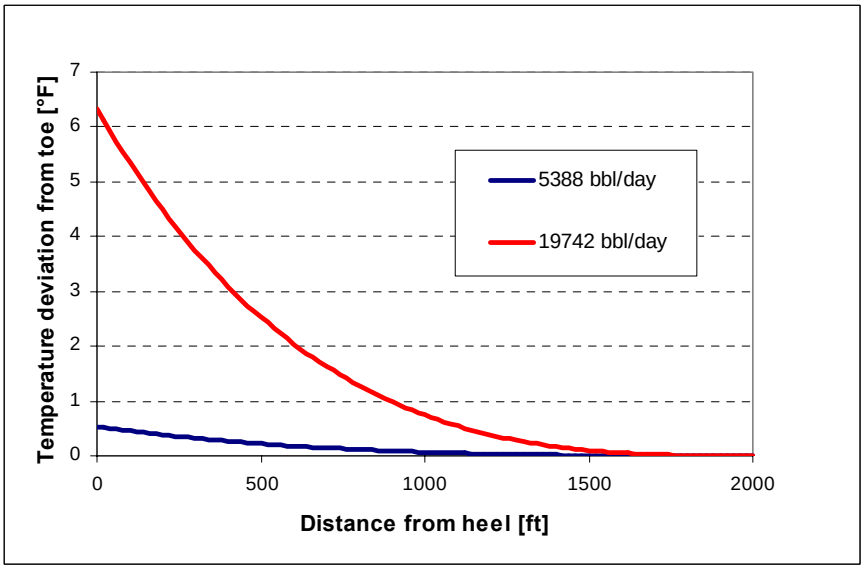

Fig. 5.10 Temperature deviations (oil, small).

Table 5.4 summarizes results from several other cases. The profiles for each are similar to those shown in Figs. 5.9 and 5.10. In these calculations the temperature changes for low production rates with the larger diameter wellbore for both oil (maximum change of 0.06 ^{o}F) and gas production (0.02 ^{o}F) cases were small. However, if the production rate is large, the temperature change would be measurable. Even though the pressure change along a well producing gas is small, the temperature change of gas is more sensitive to the production rate.

Table 5.4 Summary of wellbore results.

Fluid	Rate	Diameter	ΔP_{total}	ΔT_{total}
oil	Low (5399 STB/day)	*Small*	51.5	0.5
oil	High (19742 STB/day)	*Small*	617.8	6.3
oil	Low (5164 STB/day)	*Large*	5.8	0.06
oil	High (19875 STB/day)	*Large*	81.7	0.8
gas	Low (3596 MSCF/day)	*Small*	6.3	0.2
gas	High (9986 MSCF/day)	*Small*	52.9	2.3
gas	Low (3579 MSCF/day)	*Large*	0.7	0.02
gas	High (9904 MSCF/day)	*Large*	6.2	0.3

Pressure and temperature profiles with various well trajectories

Horizontal wells are rarely perfectly horizontal, with varying inclination angles along the well trajectory. Deviations of the well trajectory may alter the temperature and pressure distributions along the wellbore from the profiles of a perfectly horizontal wellbore.

The geothermal temperature of the formation monotonically increases with depth, so that in an upwards flow, the wellbore fluids will encounter cooler formation temperatures as they move up the wellbore, while with a downwards trajectory, the wellbore stream will contact warmer surroundings. To study these effects, we considered the upward and downward well trajectories shown in Figs. 5.10 and 5.11. These results are compared with the horizontal small-diameter case that has a uniform inflow (5 bbl/day/ft for oil, 25 MCF/day/ft for gas).

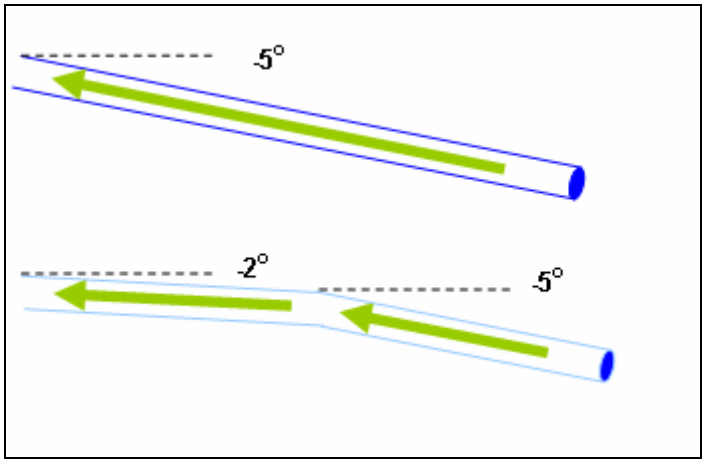

Fig. 5.11 Wellbore trajectories for upward case.

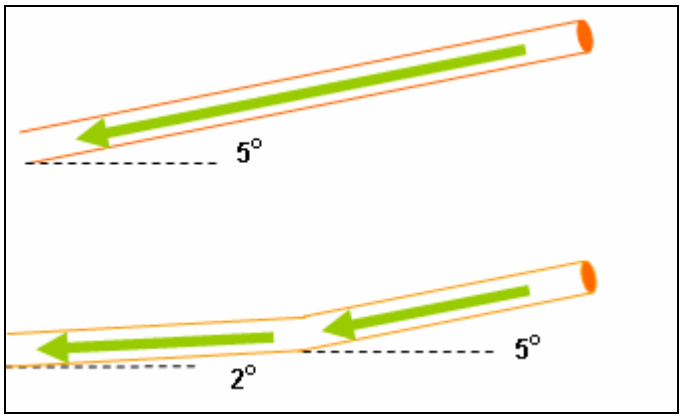

Fig. 5.12 Wellbore trajectories for downward case.

For oil flow, the pressure loss will be larger in upward flow compared to horizontal flow because of the decreasing hydrostatic pressure drop. Figure 5.12 shows the pressure change from the toe pressure (wellbore Δp) for upward trajectories, at a uniform angle ($+5^o$) and at varying inclinations ($+5^o$ to $+2^o$). Since upward with $+5^o$ case results in a larger elevation change, the pressure drop is higher and formation temperature will be cooler because of the geothermal temperature effect. Figure 5.13 plots the temperature deviations from the toe temperature. Both plots show more cooling than in the horizontal case but there is little difference between the two inclination cases. There are two factors that affect the temperature profile in this process; one is a pressure dependence of the Joule-Thomson coefficient and the other is a cooler surrounding temperature. At lower pressures, the Joule-Thomson coefficient of a liquid is larger. The first factor tends to increase the temperature when the wellbore pressure becomes low (high pressure drop in the wellbore) and the other factor tends to

decrease it. Therefore, uniform angle case ($+5^o$) experiences higher pressure drop and cooler surrounding temperature, but has a larger Joule-Thomson coefficient.

Similar but opposite effects can be observed in downwards flows. Compared to the horizontal case the downward wellbore pressure drop is less (Fig. 5.14) and the temperature increase is smaller (Fig 5.15). Again there is very little difference between the -5^o inclination and -5^o to -2^o inclinations. However, we clearly see the difference between the horizontal and $\pm 5^o$ inclinations. With $\pm 5^o$ inclinations, geothermal gradient effects are more significant than Joule-Thomson effects.

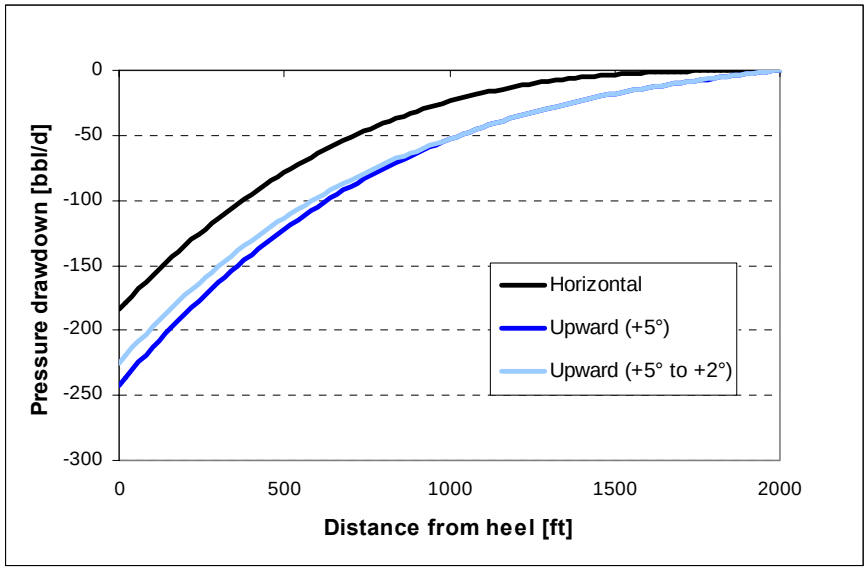

Fig. 5.13 Wellbore pressure drops (oil, upward).

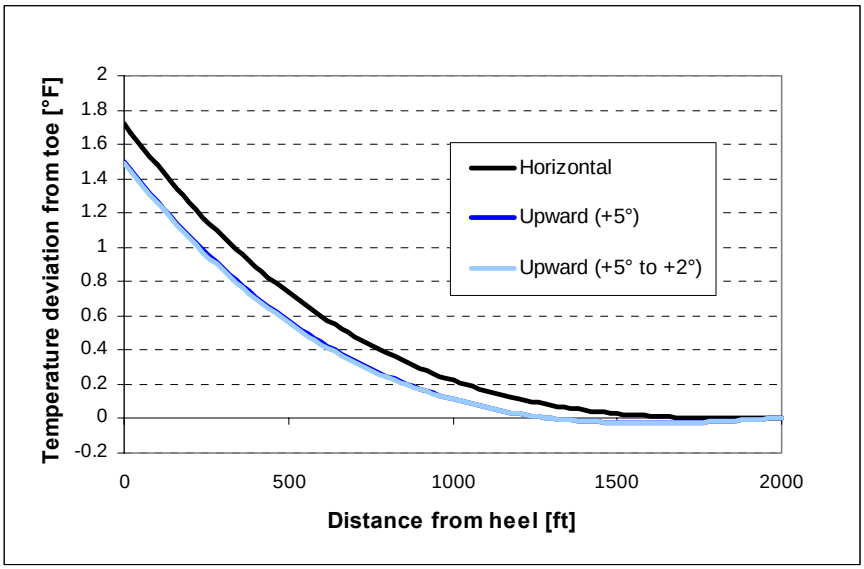

Fig. 5.14 Temperature deviations (oil, upward).

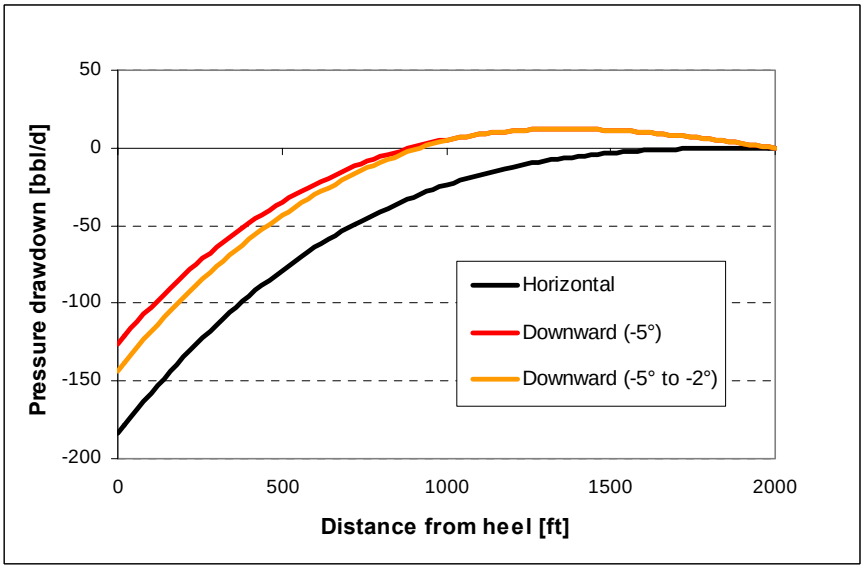

Fig. 5.15 Wellbore pressure drops (oil, downward).

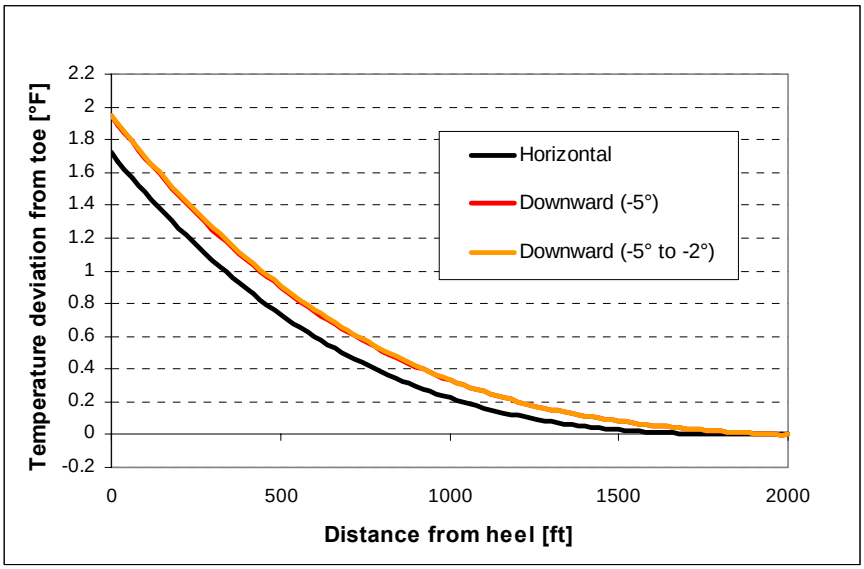

Fig. 5.16 Temperature deviations (oil, downward).

Next, we present the gas production cases. Figure 5.16 shows wellbore pressure drop for two kinds of upward trajectories. The more upward the inclination, the more the pressure drops. Since the Joule-Thomson coefficient of gas will be smaller at lower pressures, higher pressure drops causes more Joule-Thomson cooling. Therefore, upward gas flow is cooled by both the temperature change in the formation and pressure drop. Temperature deviations are shown in Fig. 5.17. The temperature change is significant even though the wellbore pressure drop is small. Similarly, downward examples are shown in Fig. 5.18 and Fig. 5.19. We can find where the well changes inclination from the temperature profile.

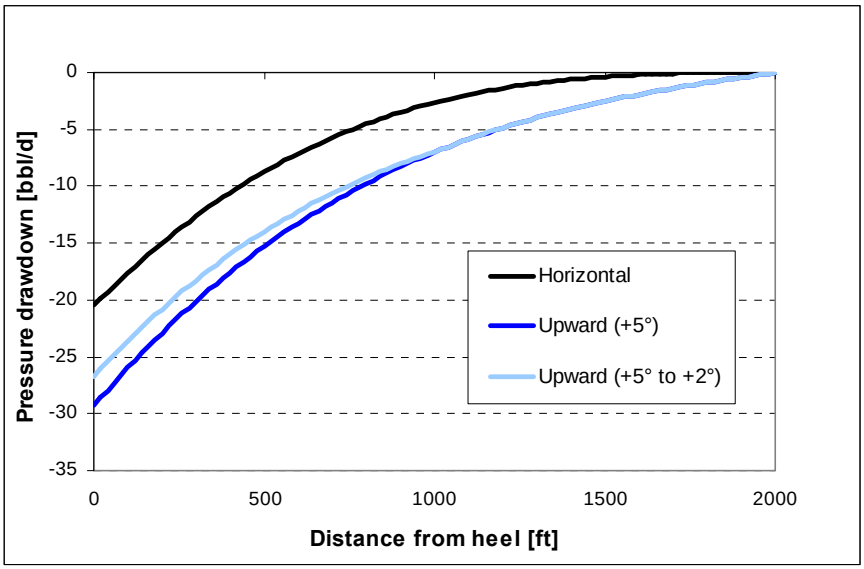

Fig. 5.17 Wellbore pressure drops (gas, upward).

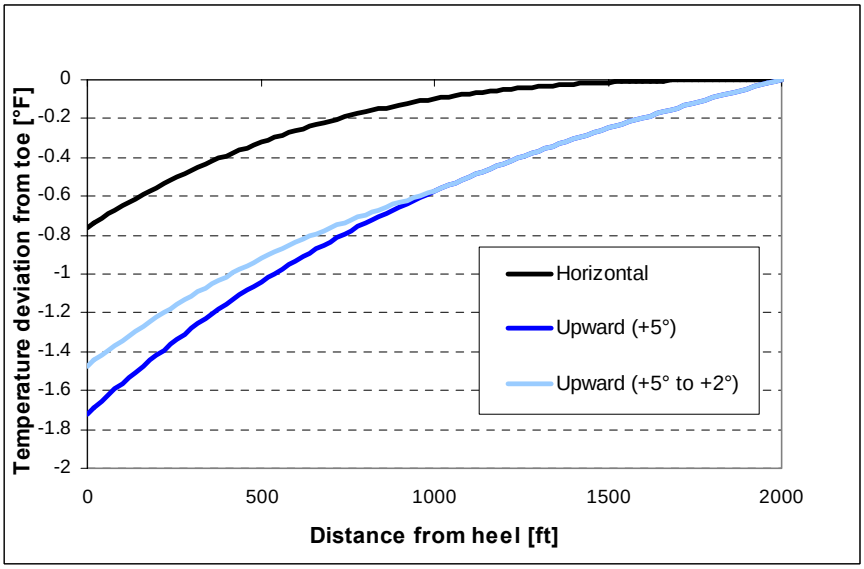

Fig. 5.18 Temperature deviations (gas, upward).

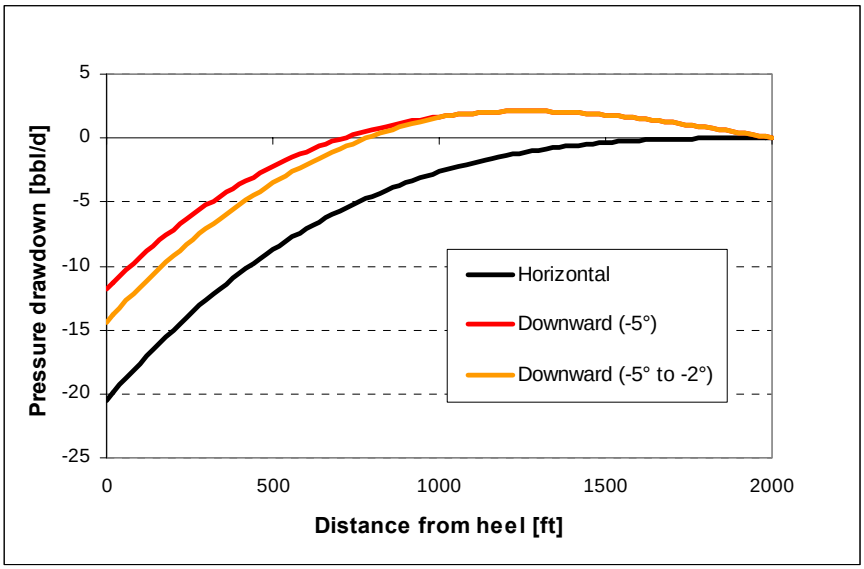

Fig. 5.19 Wellbore pressure drops (gas, downward).

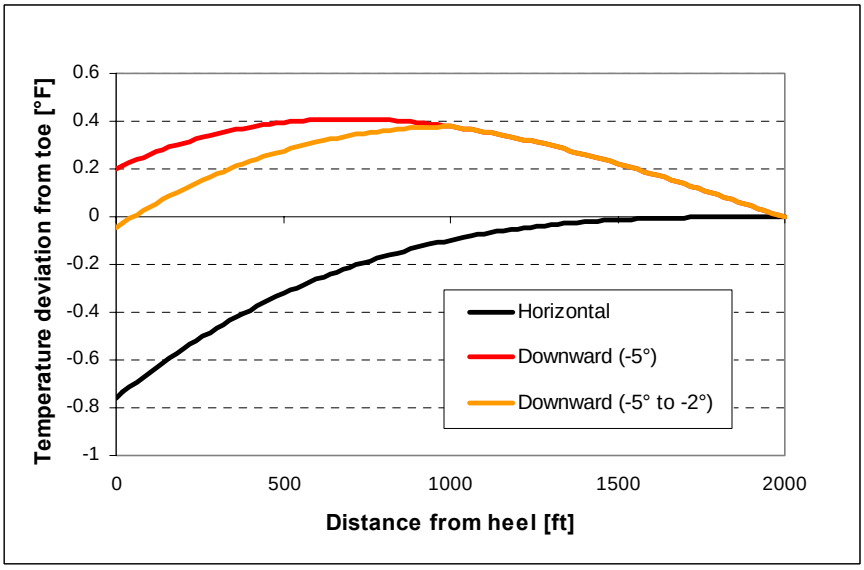

Fig. 5.20 Temperature deviations (gas, downward).

Water and gas production effects

As a last example, we present cases in which gas or water is produced from some zones while oil is produced from others. Figure 5.5 shows that each phase will enter the wellbore with a different temperature. Water enters at a lower temperature than oil

because of its larger heat capacity; gas enters at a lower temperature because of Joule-Thomson cooling.

We first consider water entries from different positions along a horizontal wellbore. The water entry zone is 400 feet long, and the rest of the well has oil inflow with a constant productivity index. For the large diameter well with the wellbore pressure at the heel set at 3300 psia, we examine cases that have water entry at the toe, in the middle, and at the heel of the well. Water holdup profiles (Fig. 5.20) show the water holdup increasing along the water entry zones. Total production for each case is about 10000 bbl/d and water cut is about 0.2. Since the pressure profiles are identical for each case, we only show the temperature deviation (temperature at any location minus the temperature at the toe) profiles (Fig. 5.21). There are clear discontinuities in these profiles; where the water entry starts and ends is readily identifiable. This anomalous temperature behavior is caused primarily by differences in Joule-Thomson effects in the reservoir flow near the well.

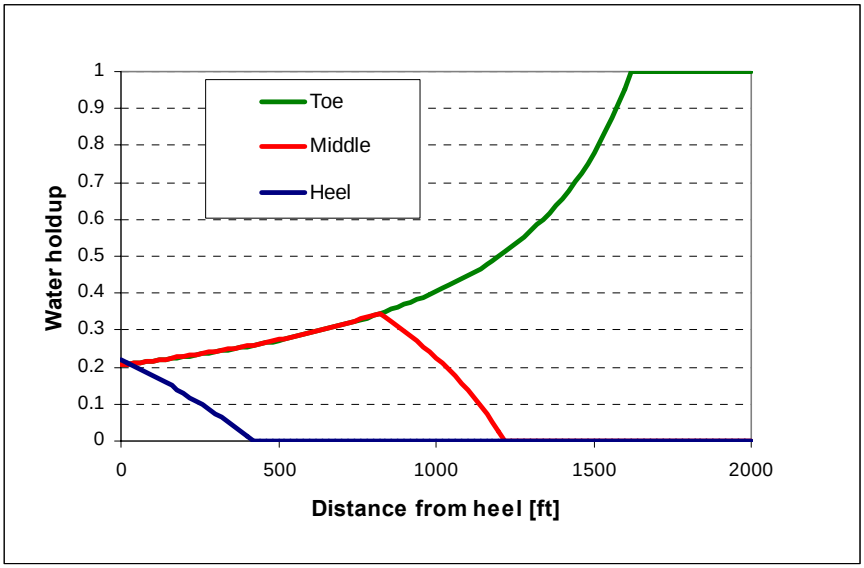

Fig. 5.21 Water holdup profiles (water entry).

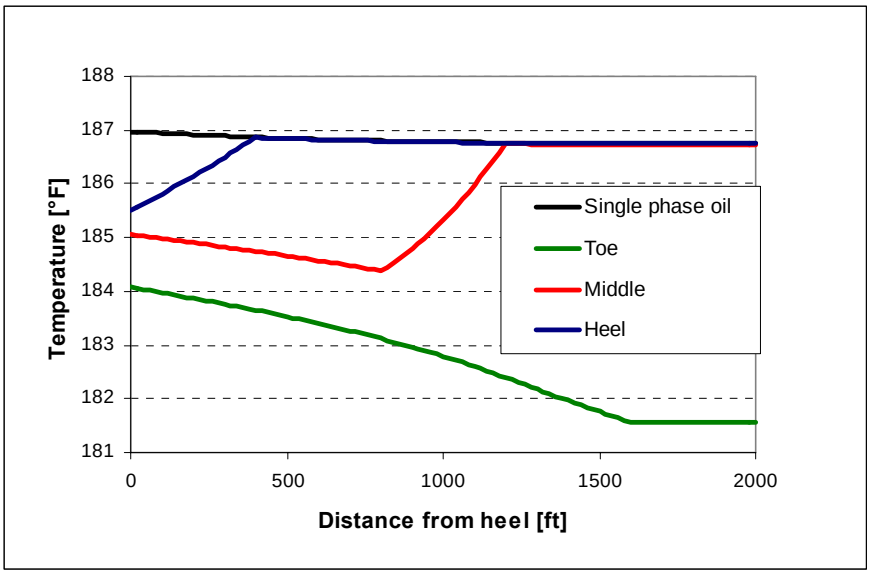

Fig. 5.22 Temperature profiles (water entry).

To explain this complex temperature behavior, consider the case where water is being produced in the middle of the well, from the interval from 800 to 1200 feet from the heel of the well. Beginning at the toe of the well, oil is being produced over the interval from 1200 feet to 2000 feet from the heel. According to Fig. 5.5, with a far field reservoir temperature of 180 ^{o}F, this oil enters the wellbore at a temperature of about 183 ^{o}F. The water being produced experiences less Joule-Thomson heating and arrives at the wellbore at about 181 ^{o}F. Since the inflow and wellbore fluid interact as described in Appendix C, these inflow temperatures will be damped in the calculation. Thus, the temperature in the well begins to drop at the start of the water entry zone and continues to decrease across this entire zone. At the end of the water zone (800 feet from the heel), production into the well of relatively warm oil reverses this trend and the wellbore temperature increases gradually all the way to the heel. Thus, for this scenario, the water zone is clearly identifiable as the region over which the wellbore temperature is decreasing, moving towards the heel. The temperature profiles for the other cases shown in Fig. 5.21 can be interpreted in a similar manner.

For the oil and gas production case, we illustrate the behavior that will occur with gas zones of different lengths. In these cases, the gas zone begins at the heel of the well and extends 400, 1000, or 1600 feet along the wellbore. The remainder of the 2000 ft long well is receiving oil production. The pressure at the heel was set to 3200 psi for this example. The gas holdup and pressure change profiles are shown in Figs. 5.22 and 5.23. Since the pressure drops inside the wellbore are small, oil and gas inflow rates are almost uniform in each fluid production zones. Oil inflow rate is about 5.7 bbl/d/ft and gas is about 6.3 MSCF/d/ft, respectively. Figures. 5.24-5.26 show the wellbore temperature and inflow temperature profiles. Since gas flow results in a lower temperature than geothermal temperature, the difference from oil temperature is

significant. As the gas rate increases, the temperature deviation increases (Fig. 5.25). In the case with gas being produced in the 400 foot interval at the heel of the well, the temperature gain and loss are canceled out and we see small changes (-0.1 ^{o}F). Gas production should decrease the temperature; therefore this type of temperature profile with gas production tells us that gas enters near the heel. In other cases it is obvious where gas production occurs. Temperature deviations are very high.

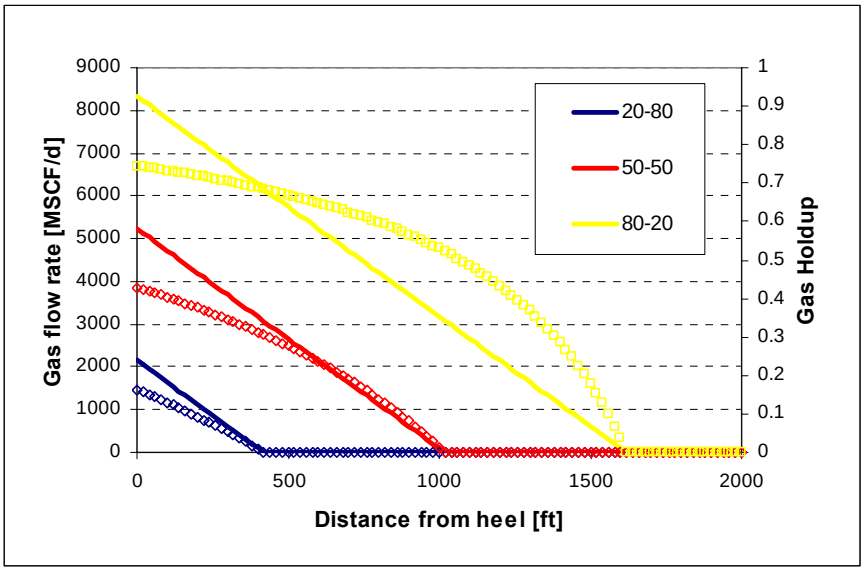

Fig. 5.23 Gas holdup profiles (gas entry).

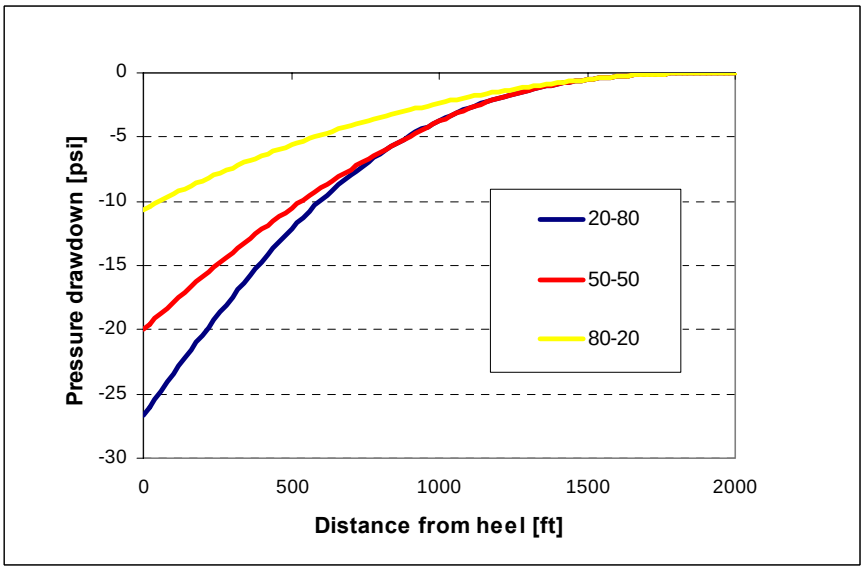

Fig. 5.24 Pressure drawdown profiles (gas entry).

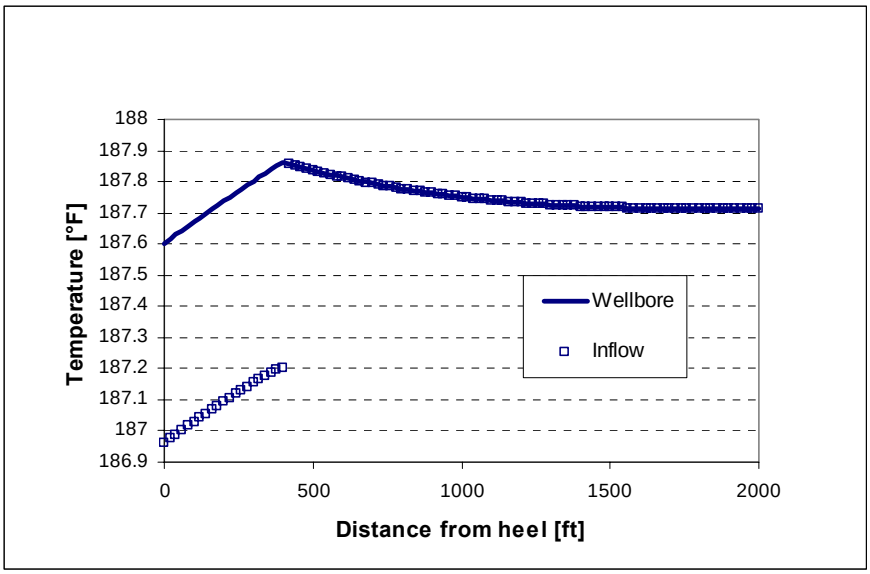

Fig. 5.25 Temperature profiles (400 ft gas).

Fig.5.26 Temperature profiles (1000 ft gas).

Fig. 5.27 Temperature profiles (1600 ft gas).

5.1.4 Summary of analytical coupled model

As observed, if the flow rate is small, temperature profiles show only subtle changes. Also temperature profiles are more sensitive to the well trajectories than that of pressure. Most important finding here is that temperature profiles show anomaly changes when different type of fluid is produced.

5.2 Numerical coupled model

The iteratively coupled reservoir/wellbore model developed is based primarily on the assumptions that flow in reservoir is restricted in the y and z directions (perpendicular to well), and properties of flowing fluid are constant in each reservoir segments. To relax these two assumptions, we numerically solved mass and energy balances using the same reservoir geometry as the model, but fluid properties are a function of reservoir pressure and temperature. The main purpose of this numerical solution is to evaluate how accurate the coupled model is if the assumptions are relaxed.

Before presenting results, we first discuss the mathematical formulation and how to put the set of linear equations into matrix form. The calculation procedure in section 5.2.3 shows how the mass/energy balances and reservoir/wellbore flows are coupled. We also verified the numerical results against the analytical results in section 5.2.4.

5.2.1 Reservoir and wellbore geometry

A box-shaped reservoir geometry is perfectly horizontal with a horizontal well in the center of reservoir. A block-centered grid is used in the finite-difference formulation. Figure 5.27 shows grid blocks. The x- and y-direction are used as areal coordinates and reservoir thickness is uniform. For the grid block numbering, the x-direction (parallel to

wellbore) is the faster-moving grid, while the y-direction is the slower. The following parameters are used unless noted otherwise.

Table 5.5 Parameters for numerical model

Well length (ft)	2000
Reservoir width (ft)	3000
Reservoir thickness (ft)	100
Permeability (md)	50
Porosity	0.2

Grid blocks

Maximum number of grid in x direction, I_{max}=10 Δx = 200 ft

Maximum number of grid in y direction, J_{max}=61 Δy =50 ft

Boundary Conditions

Temperature of fluid entering at reservoir boundaries, T_o=180 ^oF

Pressure at external boundaries, p_e=4000 psi

$T_{inflow}=T_{wellbore}$ at the toe block

p_{wf} is pressure at the heel (must be specified)

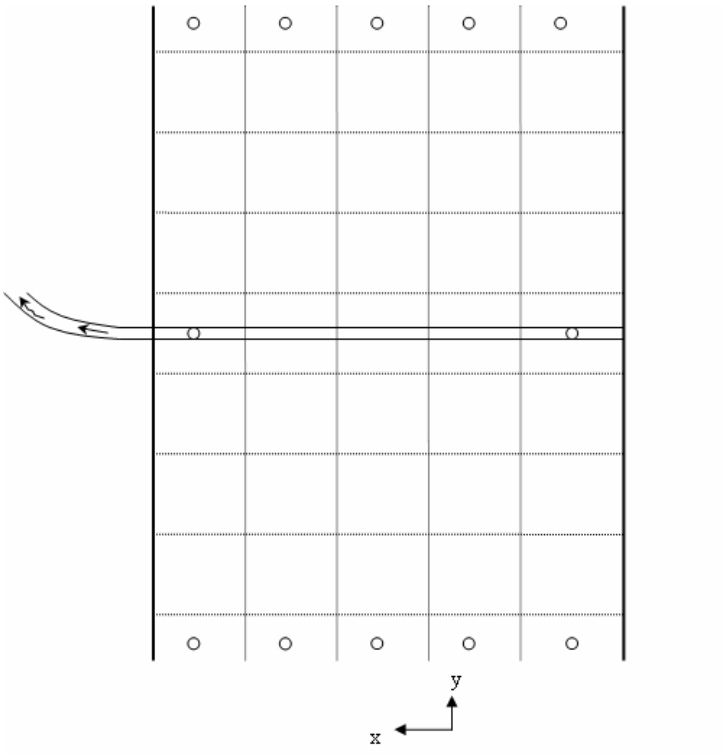

Fig. 5.28 Grid blocks.

5.2.2 Mathematical formulation

The mathematical equations that describe non-isothermal flow are mass and energy balances. For single-phase flow under steady-state condition, the differential form of equations can be written as follows.
The mass balance is

$$\vec{\nabla} \cdot (\rho \vec{\mathbf{u}}) = 0 \tag{4.1}$$

and the energy balance is

$$\rho C_p \vec{\mathbf{u}} \cdot \vec{\nabla} T + \vec{\mathbf{u}} \cdot \vec{\nabla} p - \beta T \vec{\mathbf{u}} \cdot \vec{\nabla} p - \vec{\nabla} \cdot K_T \vec{\nabla} T = 0 \tag{4.6}$$

When we substitute Darcy velocity into mass balance, the equation is expressed in terms of pressure. For energy balance, we have already derived the equation in terms of pressure and temperature.

Mass balance in finite-difference form

Mass balance is discretized using central finite differencing. The subscript i, j indicate the spatial location. The subscript j indicates reservoir blocks containing a well. The finite-difference form is a balance of mass rate, which expresses in a unit of kilogram per second (in SI unit). The final forms of mass balance for reservoir blocks, reservoir blocks containing a well, and wellbore flow are follows;
For reservoir blocks,

$$A_{ij} p_{i+1,j} + B_{ij} p_{i-1,j} + C_{ij} p_{i,j+1} + D_{ij} p_{i,j-1} + G_{ij} p_{ij} = 0 \tag{5.15}$$

where

$$A_{ij} = \left(\frac{k\rho}{\mu} \right)_{ij} \frac{\Delta y \Delta z}{\Delta x} \tag{5.16}$$

$$B_{ij} = \left(\frac{k\rho}{\mu} \right)_{i-1,j} \frac{\Delta y \Delta z}{\Delta x} \tag{5.17}$$

$$C_{ij} = \left(\frac{k\rho}{\mu} \right)_{ij} \frac{\Delta x \Delta z}{\Delta y} \tag{5.18}$$

$$D_{ij} = \left(\frac{k\rho}{\mu} \right)_{i,j-1} \frac{\Delta x \Delta z}{\Delta y} \tag{5.19}$$

$$G_{ij} = -A_{ij} - B_{ij} - C_{ij} - D_{ij} \tag{5.20}$$

For reservoir blocks containing a horizontal well

$$A_{iJ} p_{i+1,J} + B_{iJ} p_{i-1,J} + C_{iJ} p_{i,J+1} + D_{iJ} p_{i,J-1} + G_{iJ} p_{iJ} + q_i \rho_i = 0 \tag{5.21}$$

where

$$q_i = PI_i\left(p_{iJ} - p_{wi}\right) \tag{5.22}$$

$$PI_i = 2\pi \frac{k}{\mu_{iJ}} \frac{\Delta x_i}{\left(\ln \frac{r_o}{r_w} + s\right)} \tag{5.23}$$

$$r_o = \sqrt{\frac{\Delta y \Delta z}{\pi}}$$

The wellbore pressure drop is given by

$$p_{wi} - p_{w,i-1} = \Delta x\left(-\frac{\rho_i v_i^2 f_i}{r_w} - \rho_i g \sin\theta\right) - \left[\rho_i v_i^2 - \rho_{i-1} v_{i-1}^2\right] \tag{5.24}$$

where

$$v_I = \frac{PI\left(p_{iJ} - p_{wi}\right)}{2\pi\, r_w \Delta x\, \phi} \tag{5.25}$$

Velocity inside the well is obtained from solving mass balance below

$$v_i - \left(\frac{\rho_{i-1}}{\rho_i}\right) v_{i-1} = \left(\frac{\rho_{iJ}}{\pi r_w^2 \rho_i}\right)\left(\frac{PI_i}{\phi}\right)\left(p_{iJ} - p_{wi}\right) \tag{5.26}$$

Energy balance in finite-difference form

For reservoir blocks

$$AE_{ij} T_{i+1,j} + BE_{ij} T_{i-1,j} + CE_{ij} T_{i,j-1} + DE_{ij} T_{i,j-1} + GE_{ij} T_{ij} = RHS_{ij} \tag{5.27}$$

where

$$AE_{ij} = \left(\rho C_p\right)_{ij}\left(\frac{k}{\mu}\right)_{ij}\left(p_{i+1,j} - p_{ij}\right)\frac{\Delta y \Delta z}{\Delta x} + K_{Tt}\frac{\Delta y \Delta z}{\Delta x} \tag{5.28}$$

$$BE_{ij} = K_{Tt}\frac{\Delta y \Delta z}{\Delta x} \tag{5.29}$$

$$CE_{ij} = \left(\rho C_p\right)_{ij}\left(\frac{k}{\mu}\right)_{ij}\left(p_{i,j+1} - p_{ij}\right)\frac{\Delta x \Delta z}{\Delta y} + K_{Tt}\frac{\Delta x \Delta z}{\Delta y} \tag{5.30}$$

$$DE_{ij} = K_{Tt}\frac{\Delta x \Delta z}{\Delta y} \tag{5.31}$$

$$GE_{ij} = -AE_{ij} - BE_{ij} - CE_{ij} - DE_{ij} - \beta_{ij} G1_{ij} - \beta_{ij} G2_{ij} \tag{5.32}$$

$$RHS_{ij} = -G1_{ij} - G2_{ij} \tag{5.33}$$

$$G1_{ij} = \left(\frac{k}{\mu}\right)_{ij} \left(p_{i+1,j} - p_{ij}\right)^2 \frac{\Delta y \Delta z}{\Delta x} \tag{5.34}$$

$$G2_{ij} = \left(\frac{k}{\mu}\right)_{ij} \left(p_{i,j+1} - p_{ij}\right)^2 \frac{\Delta x \Delta z}{\Delta y} \tag{5.35}$$

For reservoir blocks containing a horizontal well;

$$AE_{iJ} T_{i+1,J} + BE_{iJ} T_{i-1,J} + CE_{iJ} T_{i,J-1} + DE_{iJ} T_{i,J-1} + GE_{iJ} T_{iJ} + q_i^{Energy} = RHS_{iJ} \tag{5.36}$$

where

$$q_i^{Energy} = -\left[K_{Tt} \left(\frac{2\pi\Delta x}{\ln \frac{r_o}{r_w}} \right) + uA\rho C_p \right]_i \left(T_{iJ} - T_{wi}\right) \tag{5.37}$$

$$uA = PI_i \left(p_{iJ} - p_{wi}\right) \tag{5.38}$$

Wellbore energy balance can be discretized as

$$E_i T_{wi} - T_{w,i-1} - H_i T_{iJ} = F_i \tag{5.39}$$

where

$$H_i = \Delta x \left(\frac{2}{r_w \rho_i v_i} \right) \left(\rho_{iJ} v_{Ii} + \frac{U}{C_p} \right) \tag{5.40}$$

$$F_i = \Delta x \left\{ K_{JT} \left(\frac{dp}{dx}\right)_i - \frac{g \sin\theta}{C_p} - \frac{v_i}{C_p} \left(\frac{dv}{dx}\right)_i + \frac{\rho_{iJ} v_{Ii}}{r_w \rho_i v_i C_{pi}} \left(v_{Ii}^2 - v_i^2\right) \right\} \tag{5.41}$$

$$E_i = 1 + H_i \tag{5.42}$$

5.2.3 Calculation procedure

The calculation procedure is presented in the flow chart below. We first initially guess pressure and temperature for all grid blocks and inside wellbore. Second we calculate fluid properties, and velocity and friction factor inside wellbore. Then we can solve mass balance for pressure. After the pressure is converged, the pressure is used in solving energy balance for temperature.

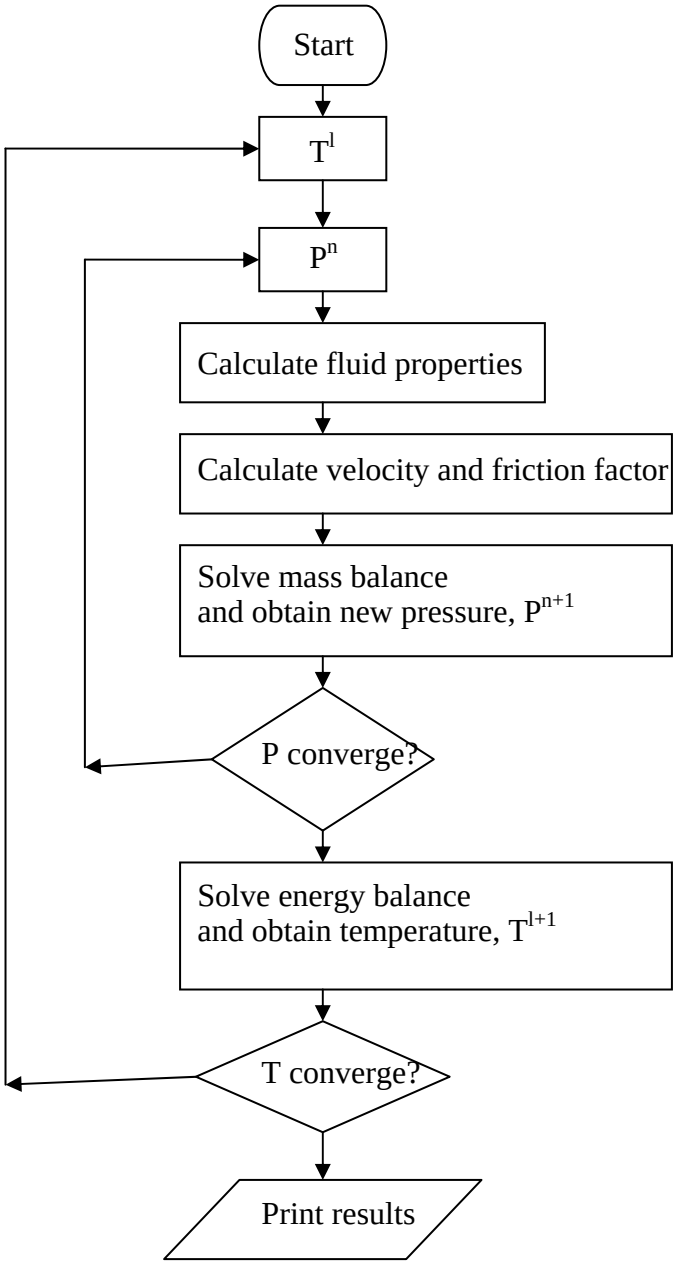

Fig. 5.29 Computation scheme.

In solving mass and energy balances for the next iteration of pressure and temperature, we used Newton-Raphson method. The method is discussed below.

Let $\tilde{x}$ be an unknown column matrix. We are seeking the solution, $\tilde{x}^{n+1}$. We have an equation in the following form.

$$\tilde{A}\tilde{x} = \tilde{b} \tag{5.43}$$

where
$\tilde{A}$; square matrix
$\tilde{x}$; column matrix
$\tilde{b}$; column matrix
We first rearrange the equation and solve for the changes in $\tilde{x}$.

$$\tilde{f} = \tilde{A}\tilde{x} - \tilde{b} = 0 \tag{5.44}$$

The changes in $\tilde{x}$ are obtained from inversing the equation below.

$$\begin{bmatrix} \frac{\partial f_1}{\partial x_1} & \frac{\partial f_1}{\partial x_2} & \cdots & \frac{\partial f_1}{\partial x_{\max}} \\ \frac{\partial f_2}{\partial x_1} & \frac{\partial f_2}{\partial x_2} & \cdots & \frac{\partial f_2}{\partial x_{\max}} \\ \vdots & & & \\ \frac{\partial f_{\max}}{\partial x_1} & \frac{\partial f_{\max}}{\partial x_2} & \cdots & \frac{\partial f_{\max}}{\partial x_{\max}} \end{bmatrix} \begin{bmatrix} \delta x_1 \\ \delta x_2 \\ \vdots \\ \delta x_{\max} \end{bmatrix} = -\begin{bmatrix} f_1(x_1^n) \\ f_2(x_2^n) \\ \vdots \\ f_{\max}(x_{\max}^n) \end{bmatrix} \tag{5.45}$$

The matrix that contains derivatives is called the Jacobian matrix. Instead of taking the derivatives analytically, we numerically calculate each derivative from

$$\frac{\partial f_n}{\partial x_i} = \frac{f_n(x_i + \varepsilon) - f_n(x_i)}{\varepsilon} \tag{5.46}$$

where ε is a small increment = 10^{-3}
Finally, we can obtain $\tilde{x}^{n+1}$ from

$$\tilde{x}^{n+1} = \tilde{x}^n + \delta\,\tilde{x} \tag{5.47}$$

5.2.4 Verification cases with analytical solutions

The numerical results were compared with analytical results for two different p_{wf} (p_{wf} = 3600 psi, and p_{wf} = 3400 psi). In each p_{wf} cases, we also compared results when there is wellbore flow effect and when there is not. Numerical results were set at k_x=0 md and fixed fluid properties at the same conditions as analytical results (4000 psi, 180 ^oF). The main purpose is to verify the mathematical formulations, the numerical solution

procedure, and the program coding. Figures. 5.29 – 5.32 show a good agreement between numerical and analytical solutions.

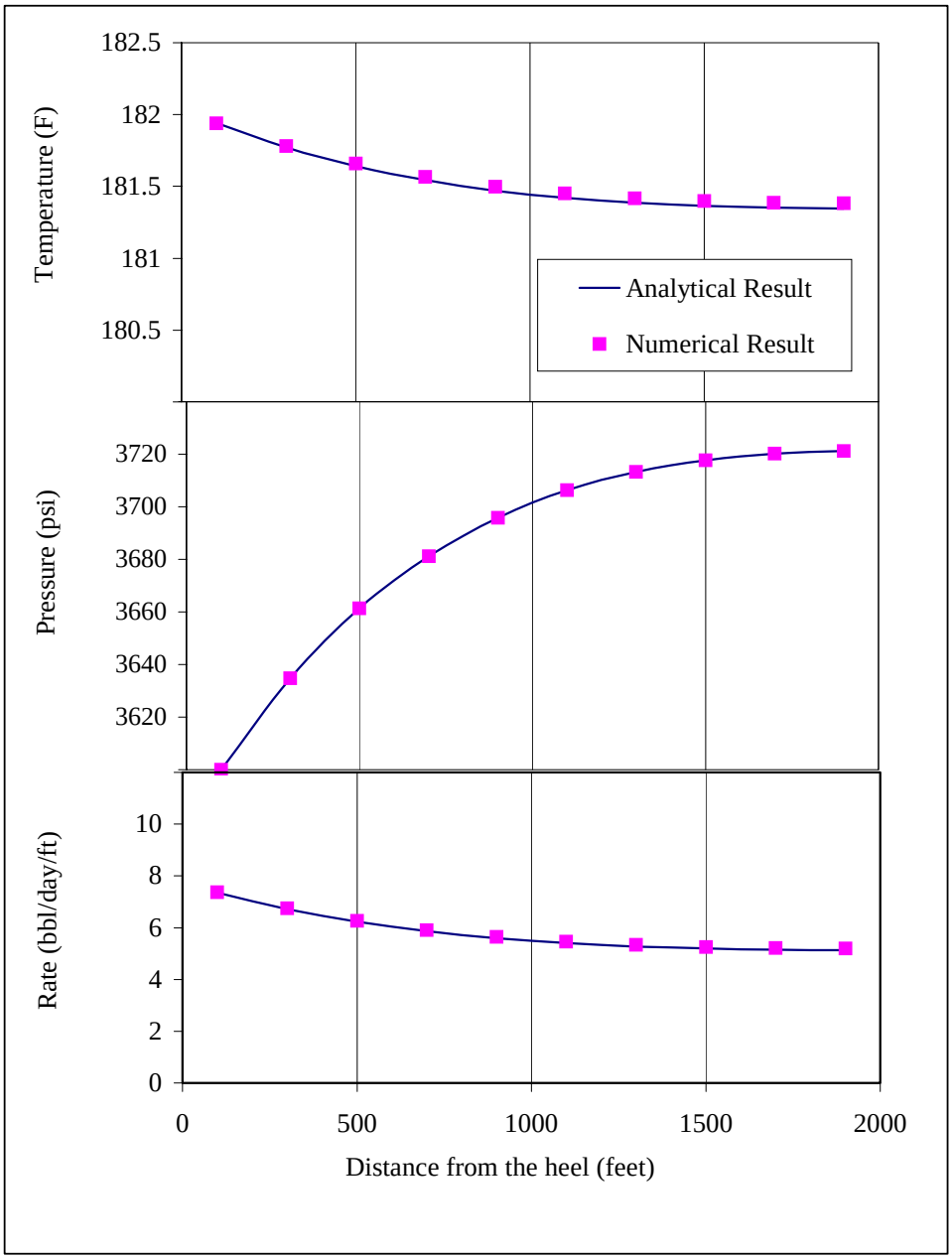

Fig. 5.30 Coupled with wellbore flow (p_{wf}=3600 psi).

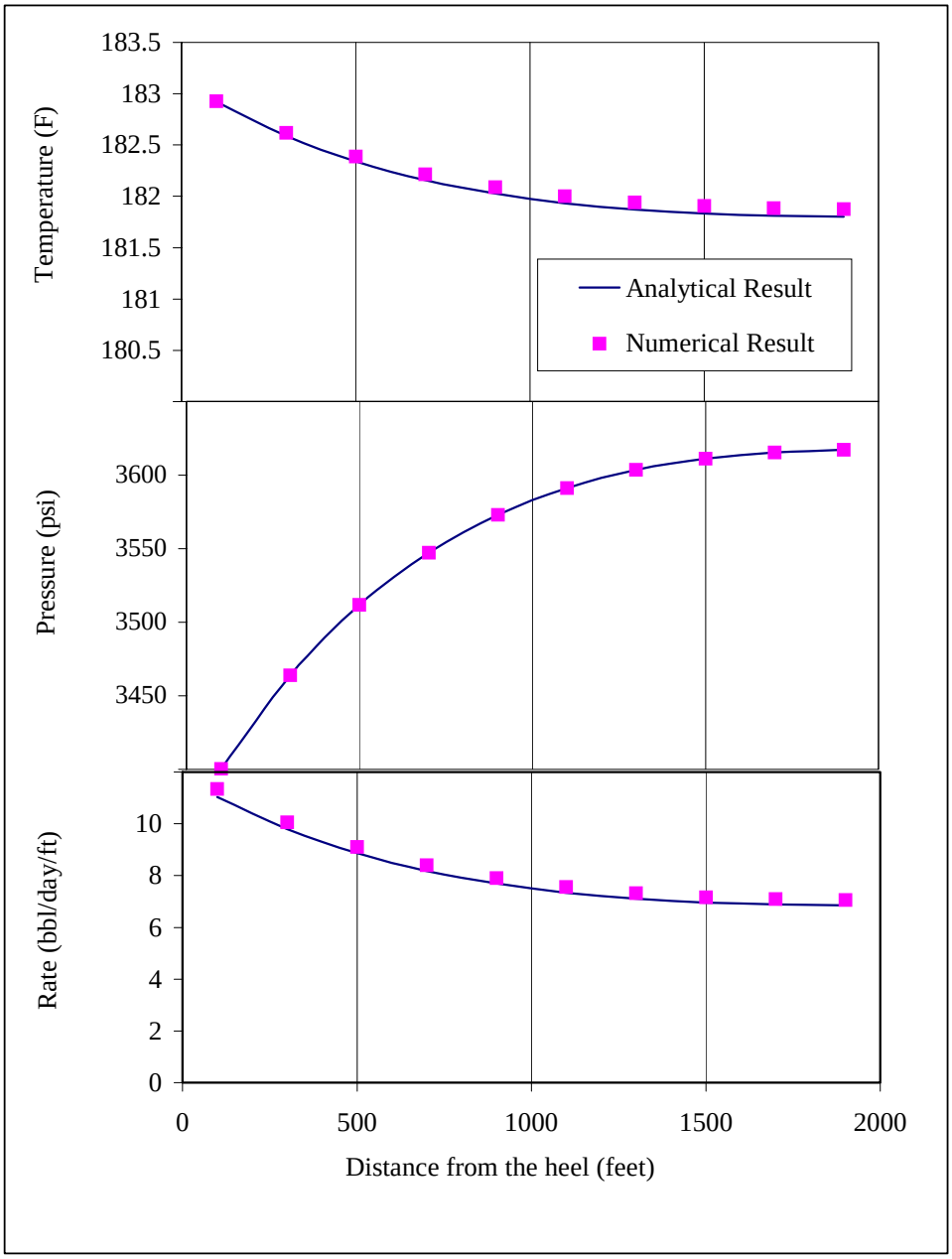

Fig. 5.31 Coupled with wellbore flow (p_{wf}=3400 psi).

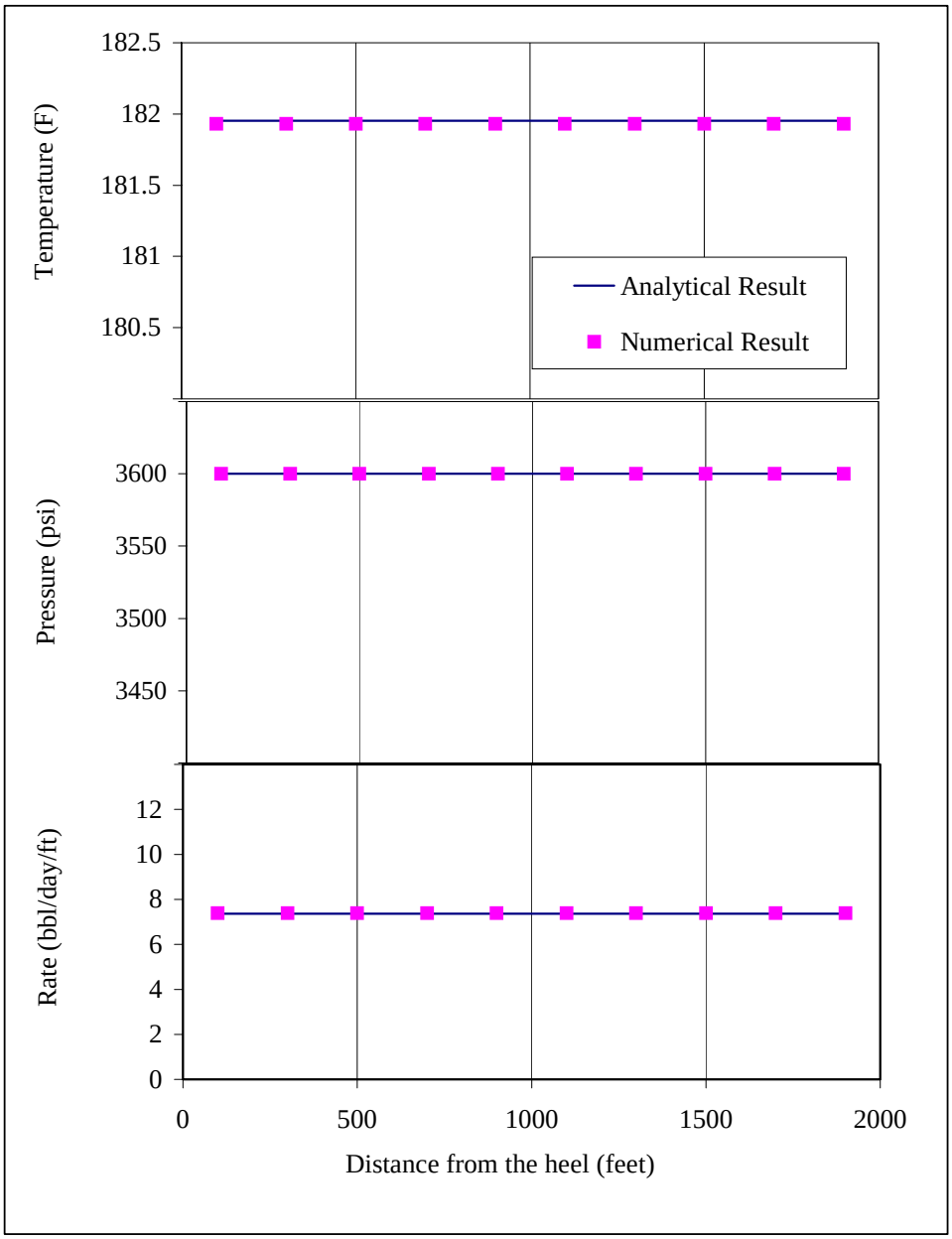

Fig. 5.32 Without wellbore flow effect (p_{wf} = 3600 psi).

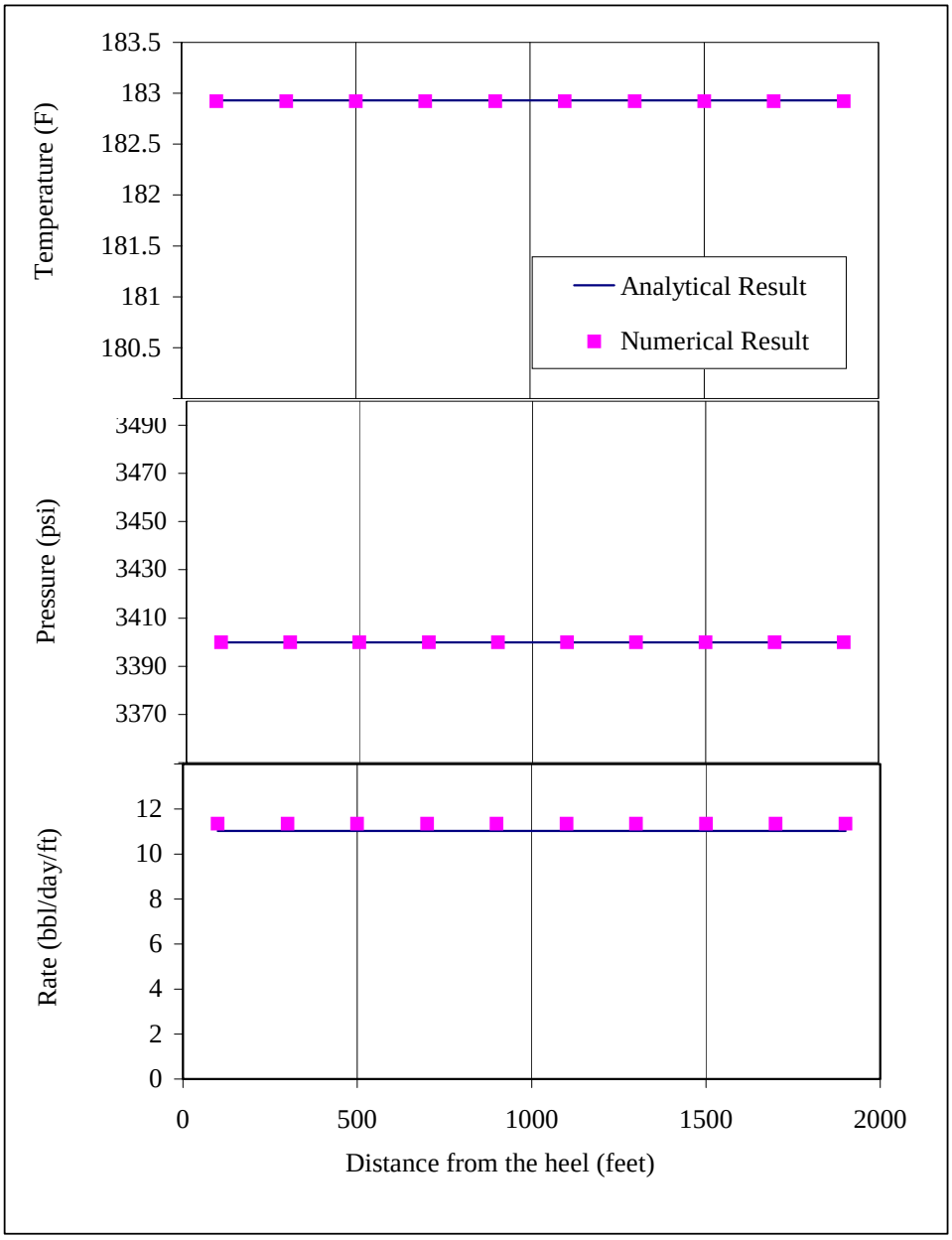

Fig. 5.33 Without wellbore flow effect (p_{wf} = 3f00 psi).

5.2.5 Results

The results presenting below are based on p_{wf} = 3400 psi at the heel of a horizontal well. The pressure and temperature at external reservoir boundary are fixed at 3400 psi and 180 ^{o}F. For numerical solution, fluid properties are a function of temperature and pressure while flowing toward wellbore.

A comparison of numerical solution with analytical coupled model

Figure 5.33 showed how much temperature, pressure and flow rates along wellbore deviated from the analytical coupled model, which means that $k_x = 0$. The numerical model account for reservoir flow in x- direction ($k_x=k_y=k_z$).

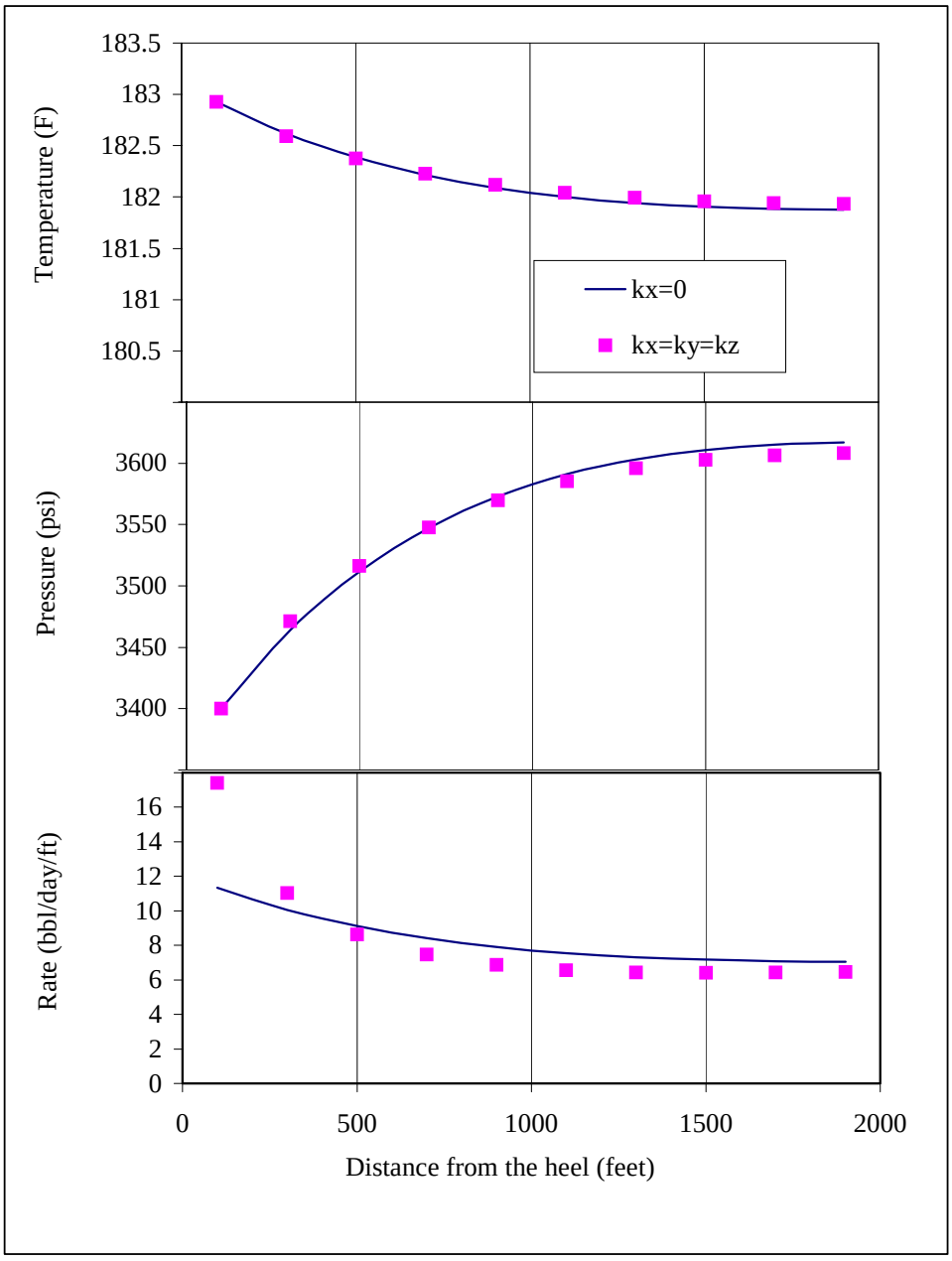

Fig. 5.34 Temperature, pressure, and flow rate profiles along wellbore.

Size of temperature changes in reservoir and wellbore

The following graphs show the size of temperature changes for both reservoir and wellbore flows. Pressure and flow rate are also plotted to show the magnitude of pressure drop that causes temperature change because of the Joule-Thomson effect.

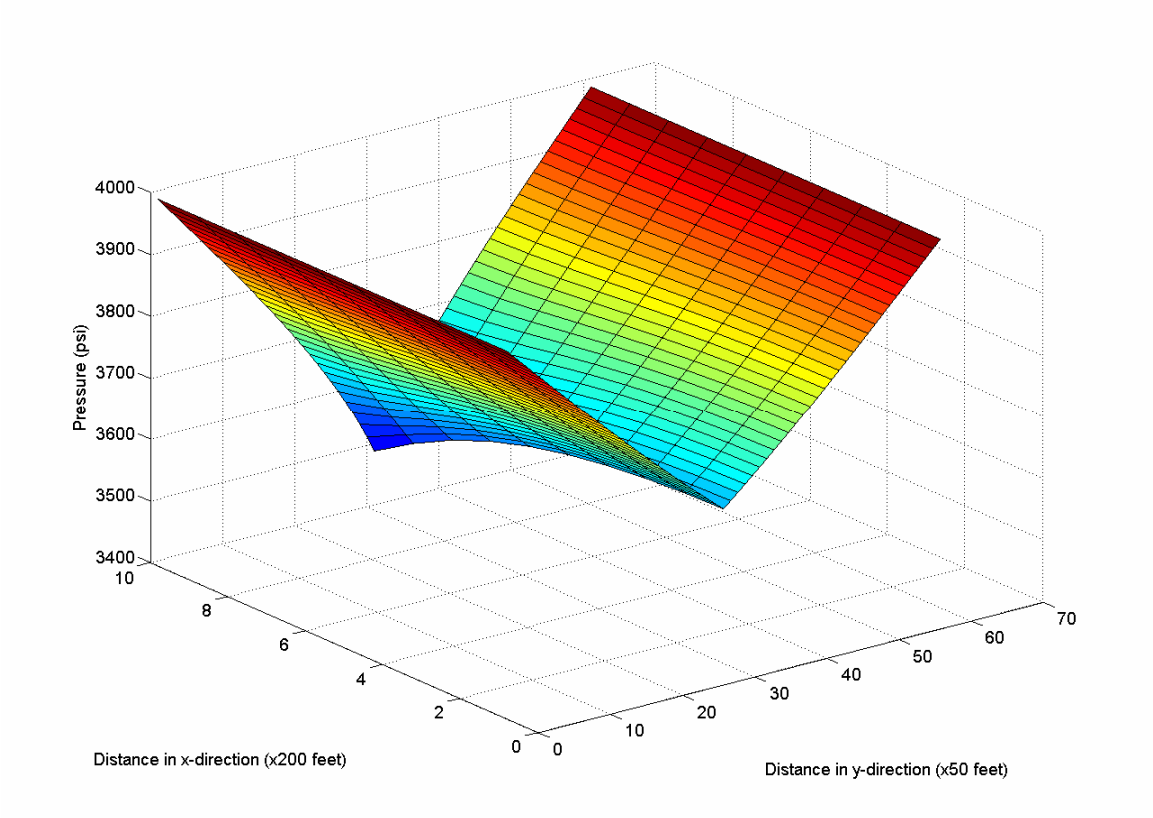

Fig. 5.35 Reservoir pressure distribution for oil flow.

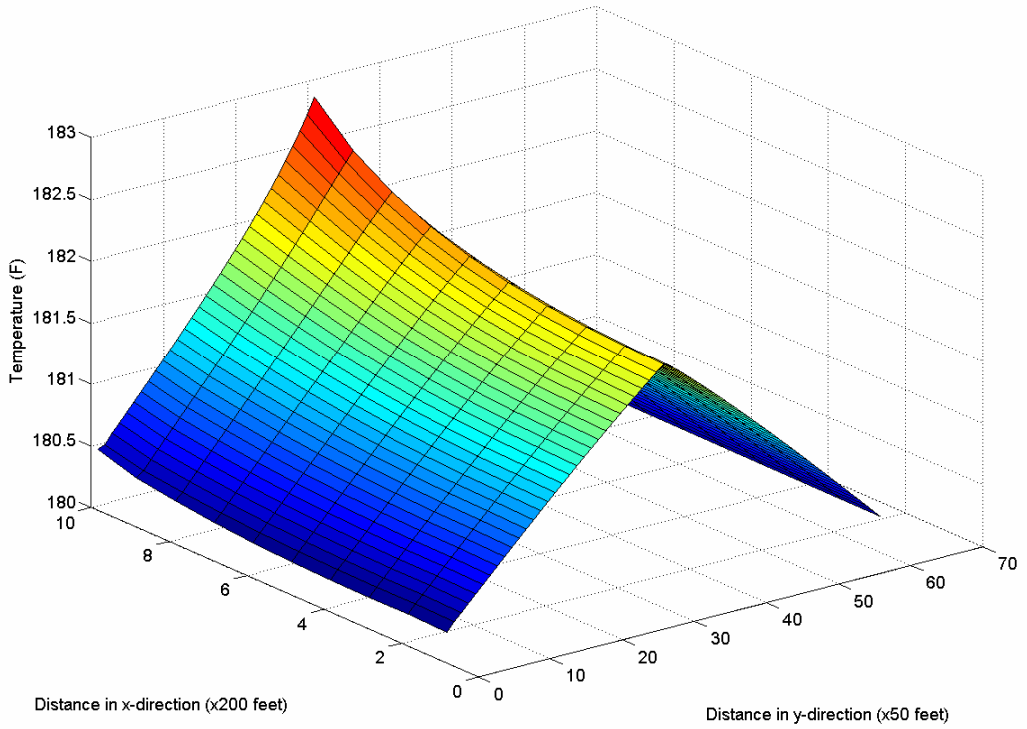

Fig. 5.36 Reservoir temperature distribution for oil flow.

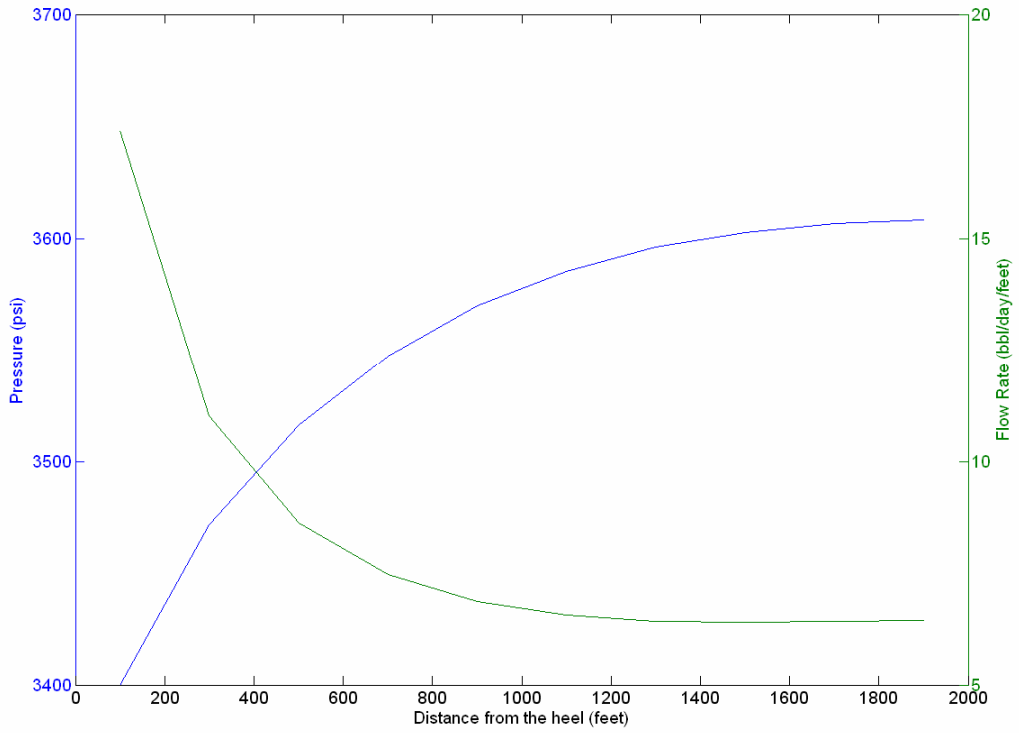

Fig. 5.37 Pressure, and oil flow rate profiles along wellbore.

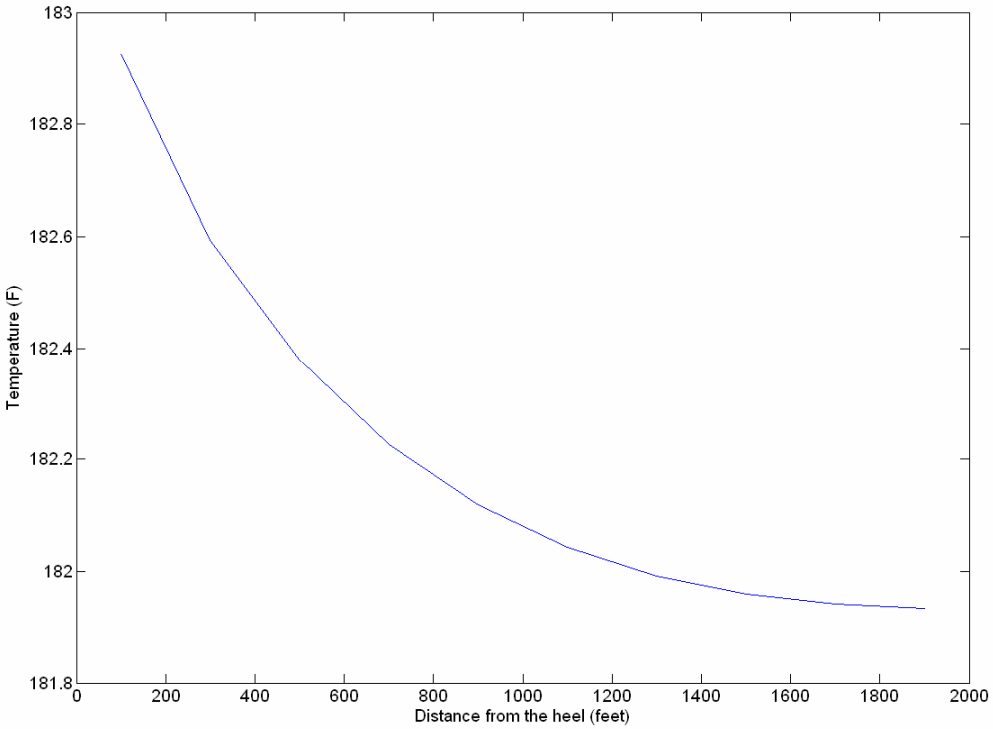

Fig. 5.38 Temperature profile along wellbore.

5.2.6 Summary of numerical coupled model

Numerical results confirmed that the analytical coupled model developed is an accurate prediction model. In other words, the flow in x direction, and temperature and pressure dependency of fluid do not affect significantly on temperature profiles even at large flow rates.

6 BUILD SECTION AND JUNCTION

The *build* section is a section of wellbore that is closed to the formation and that connects the productive lateral to the main wellbore or to another lateral. The temperature and pressure profiles of these build sections are needed to relate the temperature and the pressure at the junction locations to the temperatures and pressures of the source laterals.

6.1 Working equations for build section

To determine the temperature profile of a build section where the well inclination is changing, we extended Ramey's[1] method to this flow geometry.

Applying an energy balance for a segment along the build section as a control volume as shown in Fig. 6.1, yields

$$\frac{dH}{dz}+\frac{g\sin\alpha}{g_c J}+\frac{v}{g_c J}\frac{dv}{dz}=\pm\frac{Q}{w} \tag{6.1}$$

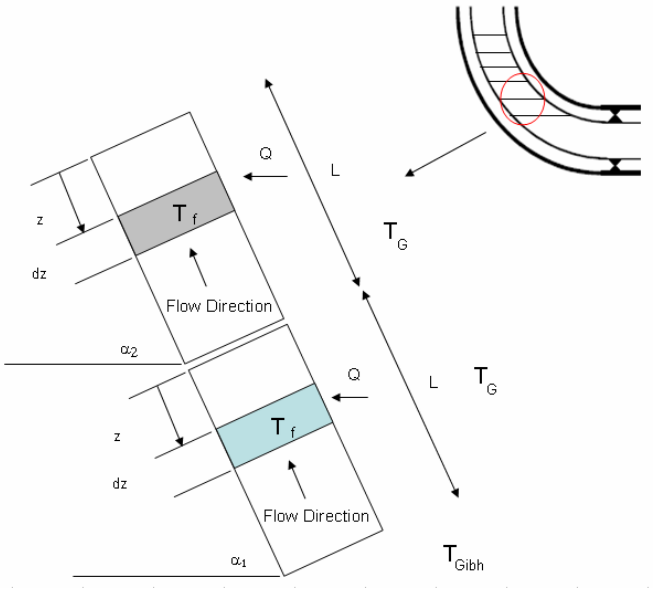

Fig. 6.1 Control volume.

The enthalpy is defined by

$$dH = C_p dT - K_{JT} C_p dp \tag{6.2}$$

By substituting Eq. 6.2 into Eq. 6.1, we get

$$\frac{dT_b}{dz} = K_{JT}\frac{dp}{dz} + \frac{1}{C_p}\left[\frac{Q}{w} - \frac{g\sin\alpha}{Jg_c} - \frac{v}{Jg_c}\frac{dv}{dz}\right] \tag{6.3}$$

The heat flow through the completion can be represented as

$$Q = -2\pi R_{cem}U\left(T_b - T_w\right) \tag{6.4}$$

and the heat loss to the formation as

$$Q = -\frac{2\pi K_T}{f\left(t\right)}\left(T_w - T_{Gi}\right) \tag{6.5}$$

For large t, $f\left(t\right)$ can be approximated

$$f\left(t\right) = -0.272\left(R\right) + 3.53 \tag{6.6}$$

Combining Eq. 6.4 and Eq. 6.5 yields

$$Q = -\frac{wC_p}{A}\left(T_b - T_{Gi}\right) \tag{6.7}$$

where A is defined as

$$A = \left(\left(\frac{2\pi}{wC_p}\right)\left[\frac{R_w U K_T}{K_T + R_w U f\left(t\right)/12}\right]\frac{1}{86400\times 12}\right)^{-1} \tag{6.8}$$

Substituting Eq. 6.7 into Eq. 6.3, the equation becomes

$$\frac{dT_b}{dz} = \frac{\left(T_b - T_{Gi}\right)}{A} - \frac{g\sin\alpha}{C_p Jg_c} - \frac{v}{C_p Jg_c}\frac{dv}{dz} + K_{JT}\frac{dp}{dz} \tag{6.9}$$

6.2 Single phase liquid

The following assumptions were made to develop the equation for single-phase liquid, incompressible fluids, kinetic energy becomes negligible, flowing friction becomes negligible, radiation and convection coefficients are negligible and can be ignored for the calculation of overall heat transfer. Also, because steel has a large thermal conductivity, the thermal resistance of the pipe and casing are negligible as compared to the thermal resistance of the material in the casing.

For single phase liquid flow, the static head loss nearly equals the total pressure gradient.

$$\frac{dp}{dz} = \rho\left(\frac{g}{g_c}\right)\sin\alpha \tag{6.10}$$

Since we assume an incompressible fluid, the Joule-Thomson coefficient can be defined as

$$K_{JT} \equiv \frac{1}{C_p}\left[\frac{\partial H}{\partial p}\right]_T = \frac{V}{C_p} = \frac{1}{\rho C_p} \tag{6.11}$$

and the final energy balance becomes

$$\frac{dT_b}{dz} = \pm\frac{\left(T_b - T_{Gi}\right)}{A} \tag{6.12}$$

Where

$$T_{Gi} = T_{Gibh} - \left(L_w - z\right)g_G \sin\alpha \tag{6.13}$$

Substituting Eq. 6.13 into Eq. 6.12 gives

$$\frac{dT_b}{dz} = \frac{1}{A}\left\{T_b - \left[T_{Gibh} - \left(L_w - z\right)g_G \sin\alpha\right]\right\} \tag{6.14}$$

Solving the first-order linear differential equation with the integration factor method yields

$$T_b = T_{Gi} + Ag_G \sin\alpha + C_1 \exp\frac{\left(z - L_w\right)}{A} \tag{6.15}$$

$$T_b = T_{Gibh} - \left(L_w - z\right)g_G \sin\alpha + Ag_G \sin\alpha + C_I \exp\frac{\left(z - L_w\right)}{A} \tag{6.16}$$

6.2.1 Boundary conditions for single phase liquid

For fluid coming from the formation at the bottom hole location ($z = L_w$) fluid temperature and geothermal temperature are the same ($T_b = T_{Gibh}$). The integration constant for this boundary condition yields

$$C_I = -Ag_G \sin\alpha \tag{6.17}$$

Substituting Eq. 6.17 into Eq. 6.16 yields

$$T_b = T_{Gibh} - g_G \sin\alpha\left[\left(L_w - z\right) - \left(1 - \exp\left(\frac{\left(z - L_w\right)}{A}\right)\right)A\right] \tag{6.18}$$

For other segments, the initial fluid temperature is equal to the last fluid temperature of the last segment.

$$C_I = T_b - T_{Gi} - Ag_G \sin\alpha \tag{6.19}$$

$$T_b = T_{Gi} + Ag_G \sin\alpha + \left[T_b - T_{Gi} - Ag_G \sin\alpha\right]\exp\frac{\left(z - L_w\right)}{A} \tag{6.20}$$

6.3 Single phase gas

For single phase gas flow the static head loss is not the same as the total pressure gradient, but these two terms together can be neglected for gases at low pressure. Solving the Eq. 6.12 yields

$$T_f = T_{Gi} + A\left(g_G \sin\alpha - \frac{g\sin\alpha}{C_p J g_c} \right) + C_I \exp\left[(z - L_w)/A \right] \tag{6.21}$$

6.3.1 Boundary conditions for single phase gas

For the first segment where fluid is coming from the formation at the bottom of the hole ($z = L_w$), the fluid temperature and the geothermal temperature are the same ($T_b = T_{Gibh}$). The integration constant for this boundary condition is

$$C_I = -A\left(g_G \sin\alpha - \frac{g\sin\alpha}{C_p J g_c} \right) \tag{6.22}$$

Substituting Eq. 6.22 into Eq. 6.21, the equation becomes

$$T_b = T_{Gibh} + \left\{ A - A\left[\exp\left((z - L_w)/A \right) \right] \right\} \left(g_G \sin\alpha - \frac{g\sin\alpha}{C_p J g_c} \right) \tag{6.23}$$

For other segments, the initial fluid temperature is equal to the last fluid temperature of the last segment.

$$C_I = T_b - T_{Gi} + A\left(g_G \sin\alpha - \frac{g\sin\alpha}{C_p J g_c} \right) \tag{6.24}$$

$$\begin{aligned} T_b = T_{Gi} &+ A\left(g_G \sin\alpha - \frac{g\sin\alpha}{C_p J g_c} \right) \\ &+ \exp\left[(z - L_w)/A \right] \left\{ T_b - T_{Gi} + A\left(g_G \sin\alpha - \frac{g\sin\alpha}{C_p J g_c} \right) \right\} \end{aligned} \tag{6.25}$$

6.4 Working equations for wellbore junction

For the case of modeling the wellbore junctions and having commingled fluids with different properties, the mixing method[2] was reviewed. According to this method, an enthalpy balance applied to the mixing of two streams of fluid at different temperatures into one combined stream is used to determine the relative flow rates of those streams.

Applying an energy balance to the wellbore junction system, considering no heat loss and gain during the mixing process, yields

$$w_1 C_{p1}(T_m - T_1) + w_2 C_{p2}(T_m - T_2) = 0 \tag{6.26}$$

And the temperature of a mixture can be defined by

$$T_m = \frac{w_1 C_{p1} T_1 + w_2 C_{p2} T_2}{w_1 C_{p1} + w_2 C_{p2}} \tag{6.27}$$

The following equation is used to calculate the heat capacity of a mixture:

$$C_{pm} = \left(\frac{w_1}{w_1 + w_2} \right) C_{p1} + \left(\frac{w_2}{w_1 + w_2} \right) C_{p2} \tag{6.28}$$

When the two streams commingling at the junction are the same fluid, so that all heat capacities are the same, combining Eq. 6.28 with the mass balance at the junction

$$w_m = w_1 + w_2 \tag{6.29}$$

can be arranged to yield:

$$\frac{w_1}{w_2} = \frac{T_m - T_2}{T_1 - T_2} \tag{6.30}$$

Thus, if there are measurable temperatures differences between T_1, T_2 and T_3, the fraction of the total flow from each lateral can be determined by measuring these temperatures. This describes the mixing method[2] used for temperature log interpretation.

6.5 Sensitivity studies and results

In this chapter, results of temperature profiles along the build section with different trajectories were calculated. First, the temperature profile for the variable angle trajectory was obtained and compared to a temperature profile with a constant angle of 45^o. Additionally, temperature profiles for multilateral wells with two single-phase liquid laterals, and temperature profiles for multilateral wells with two single-phase gas laterals were calculated using the model for single-phase liquid and gas, as well as junction mixing, to determine whether the mixing method[2] used in temperature log interpretation could be used to interpret the relative flow rates from different laterals.

6.5.1 Different trajectories

Temperature profiles for several constant angles (90^o, 45^o, 25^o, and 10.5^o) and variable angles along the build section were calculated for an oil flow rate of 3000 STB/D, as shown in Fig. 6.2, using Eqs. 6.18 and 6.20. Table 6.1 summarizes other important characteristics of the reservoir used. As the well deviation from the vertical increases, the temperature at the top of the build section decreases. This is because of the increased length of the wellbore in the build section as the deviation increases, which in turn increases the length of time for the relatively hot wellbore fluid to be cooled by the surrounding formation.

The temperature profile for the variable angle trajectory was surprisingly close to the profile obtained with a constant angle of 45°. Even though these trajectories are quite different (see Fig. 6.3), the net heat transfer from the wellbore fluid to the formation was similar.

Table 6.1 Main characteristics of the reservoir - build section with different trajectories.

Geothermal gradient	0.0274 °F/ft
Oil heat capacity	0.485 Btu/lbm°F
Wellbore diameter	7.5 in
Outside casing diameter	5.5 in
Inside casing diameter	5.047 in
Thermal conductivity of cement	96.5 Btu/D ft °F
Thermal conductivity of earth	33.6 Btu/D ft °F
°API	35

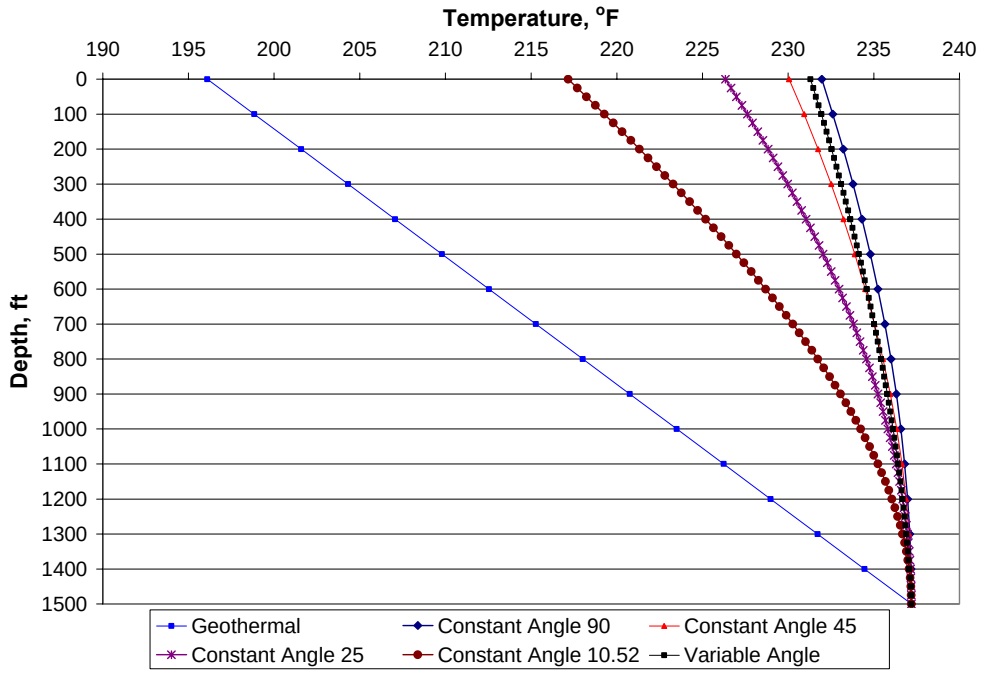

Fig. 6.2 Temperature profiles along the build section (3000 STB/D).

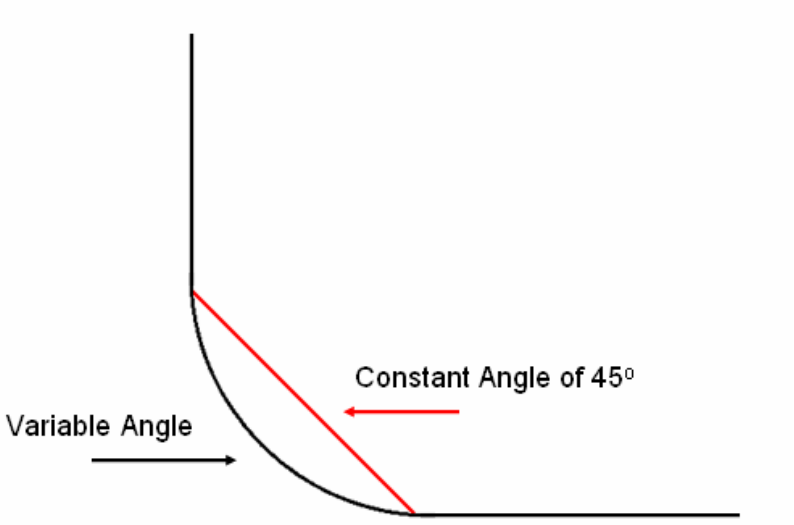

Fig. 6.3 Constant radius of curvature and constant angle trajectory.

At a much smaller flow rate (200 STB/D), the wellbore cools much more (see Fig. 6.4) than at a larger flow rate (3000 STB/D), as shown in Fig. 6.2, because of the increased length of time for the relatively hot wellbore fluid to be cooled by the surrounding formation.

For the vertical case, the temperature at the top of the build section is less than 10 ^{o}F higher than the geothermal temperature; a highly deviated (10.5 ^{o}F from the horizontal), constant angle build section has a temperature at the top of the build section that is only 2 ^{o}F different from the geothermal temperature.

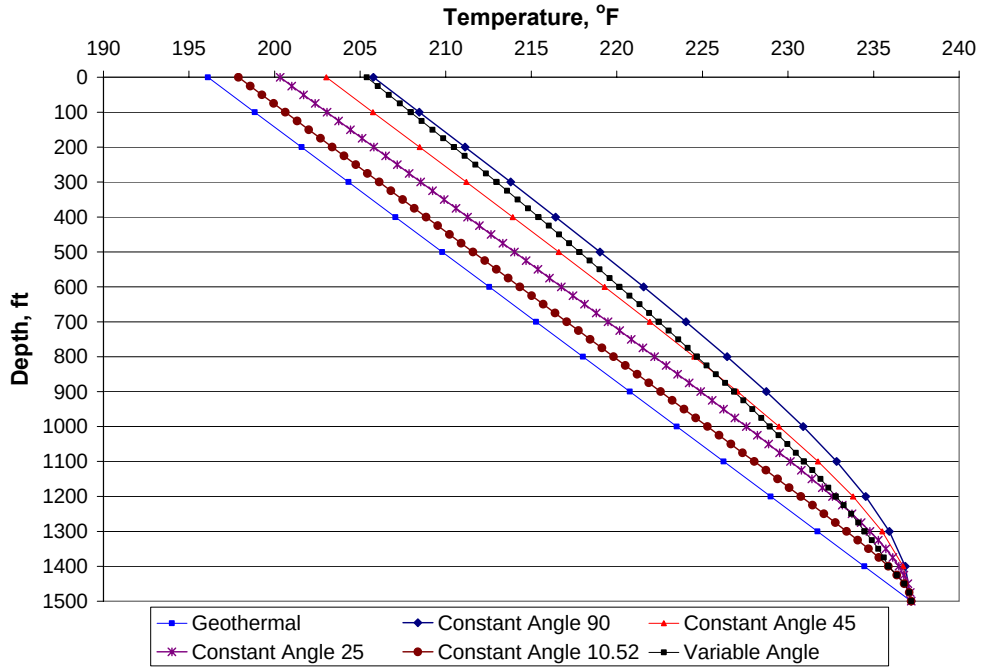

Fig. 6.4 Temperature profiles along the build section (200 STB/D).

6.5.2 Dual-lateral with single phase liquid

Data from Zuata Field in the Orinoco heavy oil belt[20, 21] were used to calculate the temperature profiles for multilateral wells with two single-phase liquid laterals, using the model for single-phase liquid and junction mixing. In this area, dual-laterals are expected to achieve a target oil production rate per single well of approximately 3000 STB/D by increasing the contact area between the wellbore and the reservoir. Because of the depth of the reservoir (1500 ft – 2000 ft), the temperatures were moderately low. Down-hole temperature at the total vertical depth was measured to be approximately 120 ^{o}F, corresponding to an approximate temperature gradient of 0.02 ^{o}F/ft, as can be seen in Table 6.2. For the three cases studied, lateral 1 produced 2000 STB/D and lateral 2 produced 3000 STB/D, with an oil gravity of 10^{o} API for both laterals.

To determine whether the mixing method[2] used in the temperature log interpretation could be used to interpret the relative flow rates from different laterals, we simulated dual laterals produced from different depths as shown in Fig. 6.5. The mixing method depends on the fact that fluids entering a well at different depths have different temperatures because of the geothermal gradient. Similarly, if fluids from two branches of a multilateral have different temperatures before commingling at a junction, the resulting intermediate temperature of the mixed stream should be proportional to the rates from each lateral.

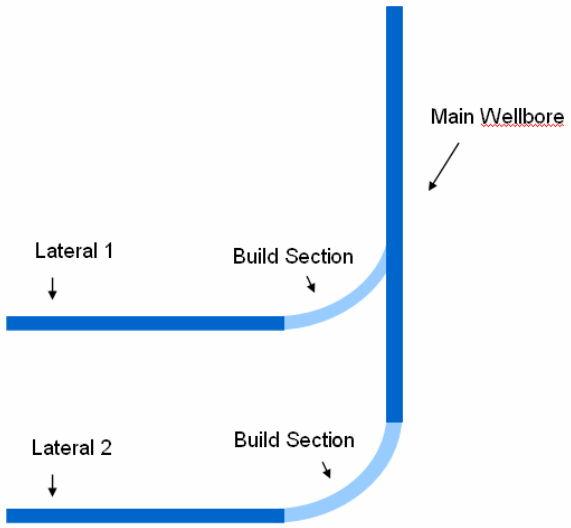

Fig. 6.5 Dual lateral geometry for examples.

Figures. 6.6 – 6.8 show the predicted temperature profiles for laterals completed at the same depth, laterals completed 500 vertical feet apart, and laterals completed 1000 vertical feet apart. For laterals completed at the same depth (see Fig. 6.6), the streams from the two laterals arrive at the junction at slightly different temperatures because of the different flow rates in each lateral. However, the difference is so small (about 0.5 ^{o}F) that interpretation of the junction mixing is probably impossible. When the two laterals are spaced at a significant distance (see Figs. 6.7 and 6.8), the difference in the temperatures of the fluid from the two laterals is significant enough that the mixing method can be applied. The mixing temperature in these cases is different enough from the temperature of the lateral (1 ^{o}F or more) to be readily measured with current distributed temperature sensor devices.

Table 6.2 Main characteristics of the reservoir - temperature profiles for multilaterals: Dual-lateral with single-phase liquid.

Geothermal gradient	0.02 ^{o}F/ft	0.02 ^{o}F/ft
Oil heat capacity	0.485 Btu/lbm^{o}F	0.485 Btu/lbm^{o}F
Wellbore diameter	7.5 in	7.5 in
Outside casing diameter	5.5 in	5.5 in
Inside casing diameter	5.047 in	5.047 in
Thermal conductivity of cement	96.5 Btu/D ft ^{o}F	96.5 Btu/D ft ^{o}F
Thermal conductivity of earth	33.6 Btu/D ft ^{o}F	33.6 Btu/D ft ^{o}F
^{o}API	10	10

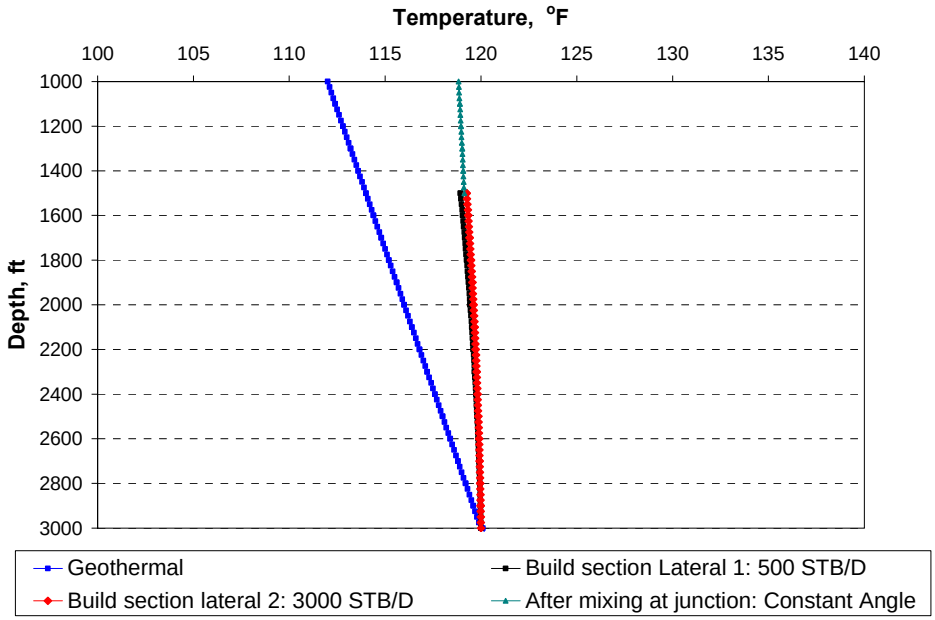

Fig. 6.6 Build section temperature profiles with liquid production at the same depth.

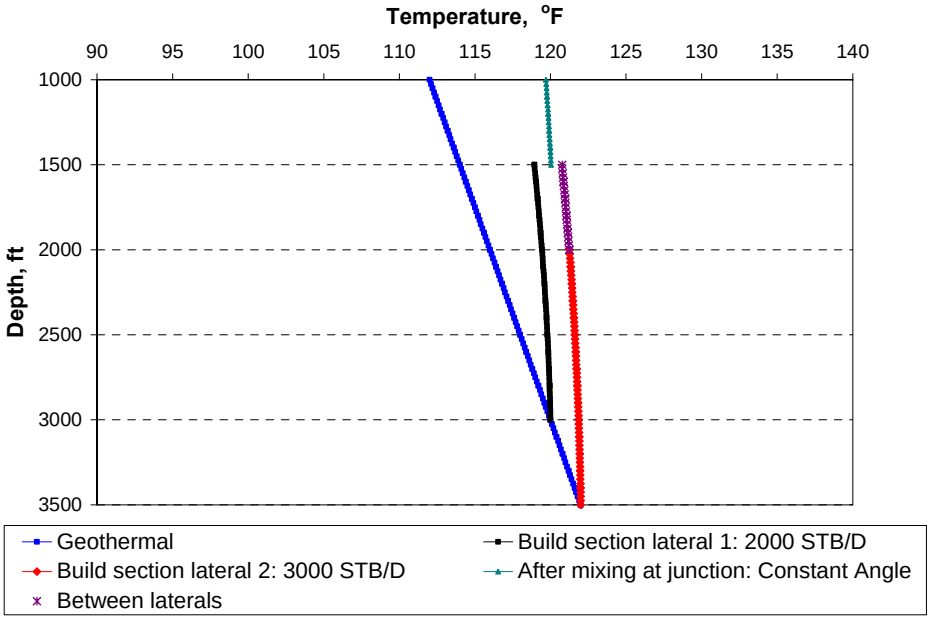

Fig. 6.7 Build section temperature profiles with liquid production at depths spaced 500 ft apart.

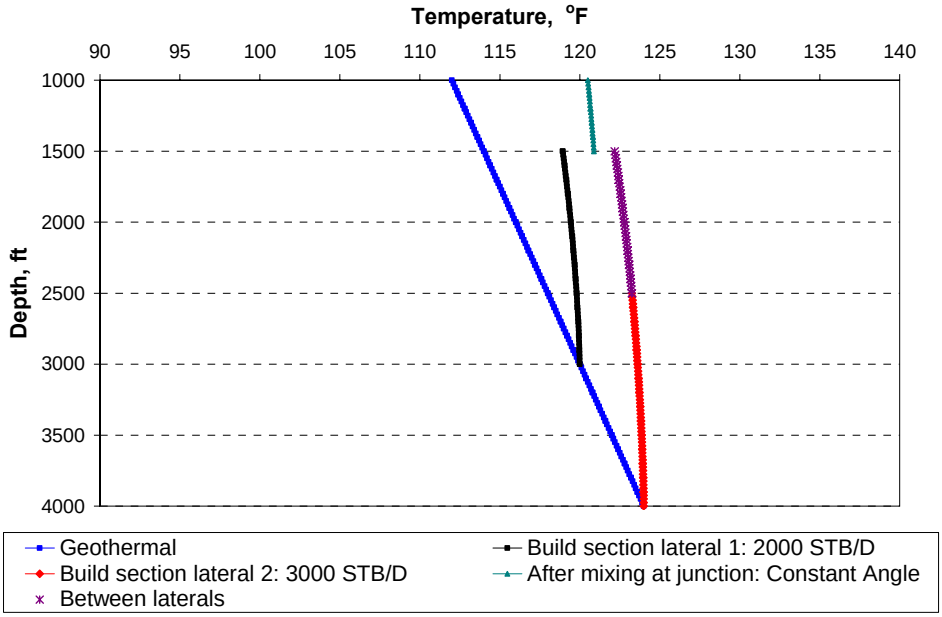

Fig. 6.8 Build section temperature profiles with liquid production at depths spaced 1000 ft apart.

When one lateral is producing at a much smaller rate than the other, a sizable temperature difference at the junction may occur during production from the same depth at both laterals. Figure 6.9 shows the temperature profiles for production rates of 500 STB/D for lateral 1, and 3000 STB/D for lateral 2, both produced at the same depth. The difference in the temperatures of the streams arriving at the junction is significantly greater than the case with similar rates shown in Figure 6.6.

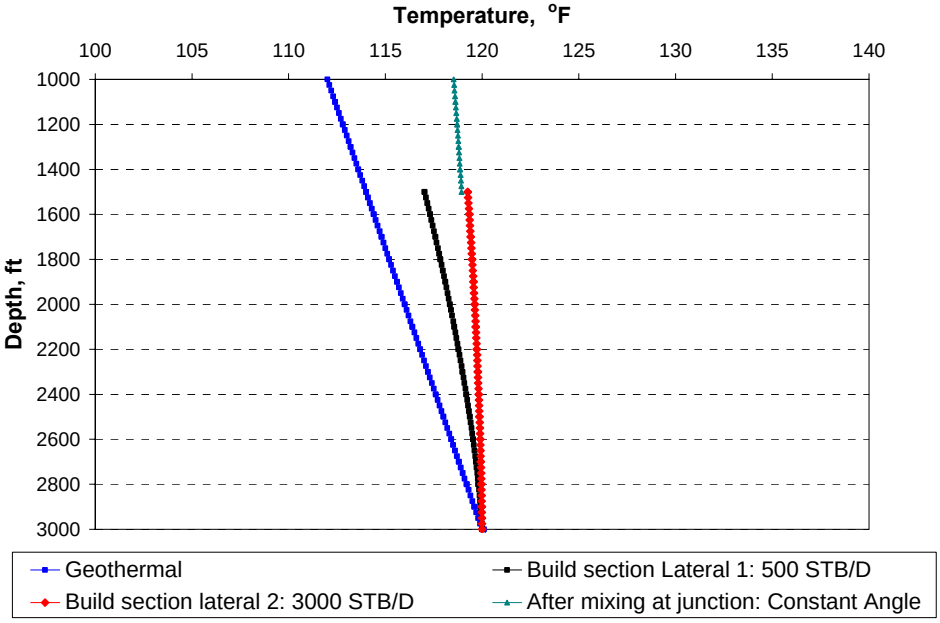

Fig. 6.9 Build section temperature profiles with different rates of 3000 STB/D and 500 STB/D.

6.5.3 Different fractions of total production

Several cases were used for calculations for different fractions of the total production from each lateral, for example if the total production of the well was 5000 STB/D, 20% - 80% means, lateral 1 is producing 1000 STB/D and lateral 2 is producing 4000 STB/D. In these examples, lateral 1 was always kept at the same level, and lateral 2 had a changing depth (0 ft, 500 ft, and 1000 ft) from lateral 1, and the difference of temperature is calculated at the junction.

The difference in temperature at the junction was calculated in the following fashion: lateral 2 minus lateral 1. Therefore, when the difference is positive it is because lateral 2 has a higher temperature than lateral 1. The total flow rate was kept constant and the fraction flow rate of each lateral changed, and calculations were made for different total flow rates.

When there is a difference in lateral production, we can see that the difference in temperature between the laterals increases as the total flow rate increases, as is illustrated in Figs. 6.10 – 6.12, but there is one point when this difference starts decreasing as the flow rate increases. All the differences in depth between the laterals are 0 ft, 500 ft and 1000 ft. This is because of the fact that after certain flow rates (especially high flow rates), the lateral which is producing less increases temperature in a more rapid manner than the lateral which is producing more. This effect is delayed when there is a

difference in depth between the laterals. Even though lateral 1 increases rapidly temperature, lateral 2 also increases because it is deeper than lateral 1. However, eventually the difference in temperature will decrease, even for very high flow rate. For very high flow rate the difference in temperature between the laterals at the junction would have a small value, but for those cases where there is a difference in depth, the resulting effect would be delayed.

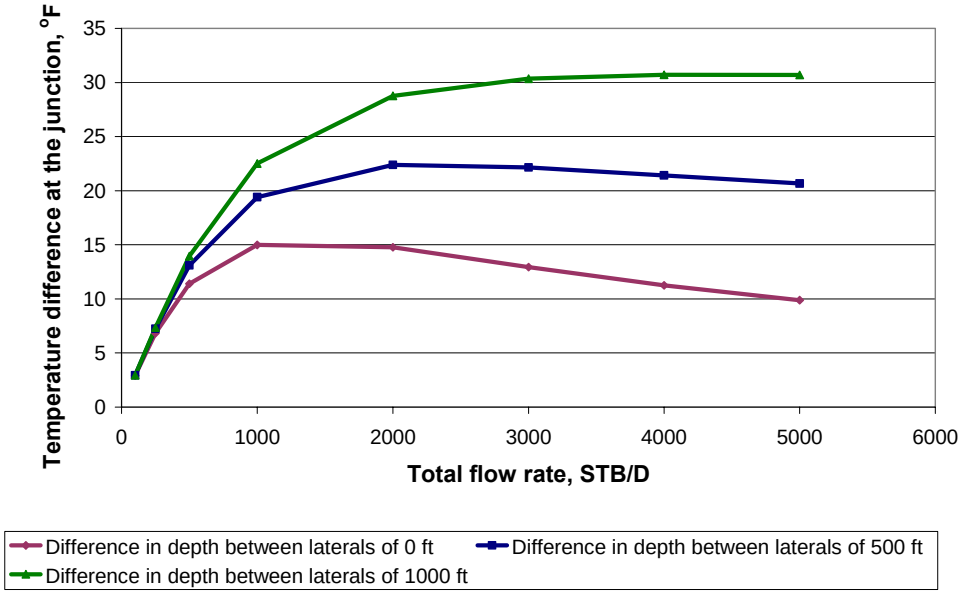

Fig. 6.10 Fraction of total production from each lateral: 20% - 80%.

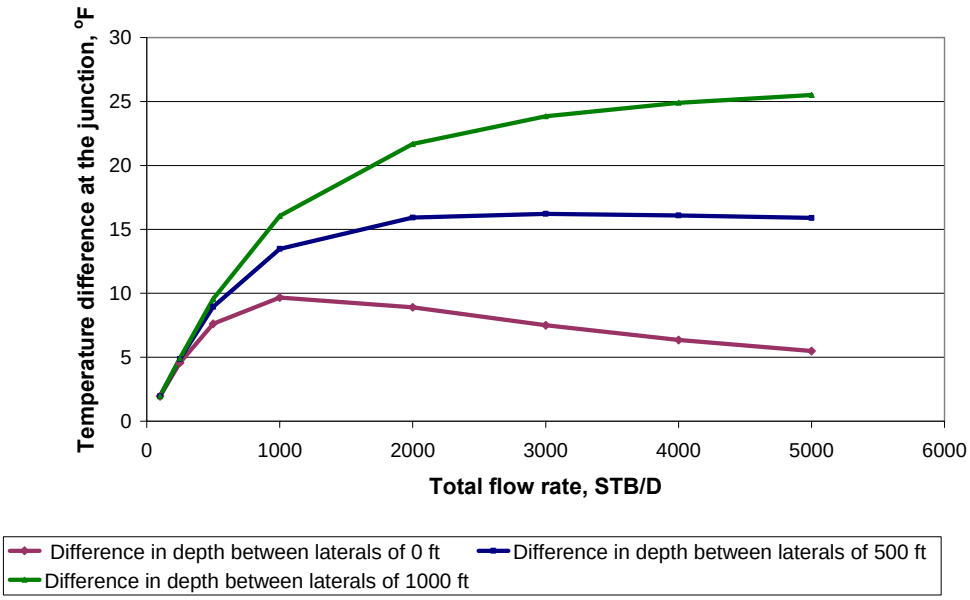

Fig. 6.11 Fraction of total production from each lateral: 30% - 70%.

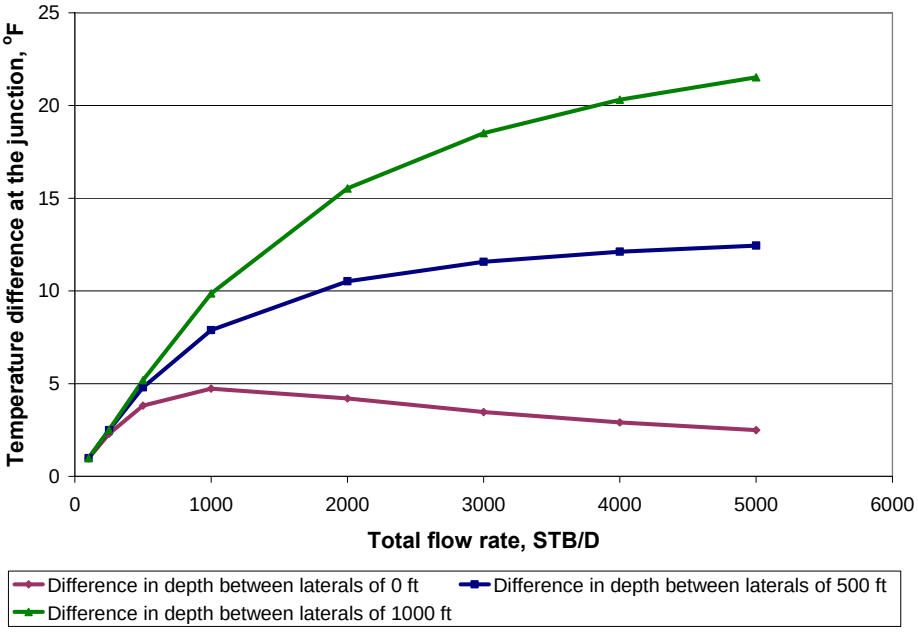

Fig. 6.12 Fraction of total production from each lateral: 40% - 60%.

When the two laterals produce the same flow rate and are at the same level, there is not difference in temperatures at the junction. Therefore, the mixing method can not be applied (as can be seen in Fig. 6.13). The mixing method can be applied when there is a difference in depth between the laterals, and the total flow rate is large enough to have an appreciable temperature difference at the junction measurable by a sensor.

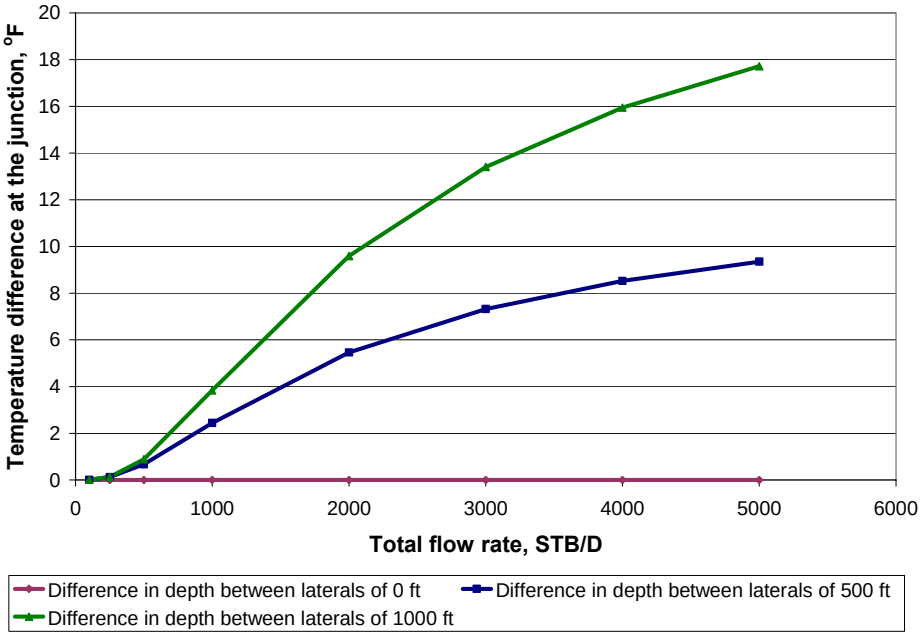

Fig. 6.13 Fraction of total production from each lateral: 50% - 50%.

When a lateral which is producing more is kept at the same level while the other lateral which is producing less is moved to changing depths, there is one instant when there is no difference in temperature at the junction (as shown in Figs. 6.14 – 6.16). This level is reached when the effect of having a high flow rate from lateral 1 has the same effect as having a difference in depth from lateral 2, which has a lower flow rate. If the laterals have a significant difference in flow rate, this effect will not be visible.

From Figures 6.14 – 6.16 we see that the absolute difference in temperature at the junction for different total flow rates can be seen to be smaller for all cases, because the effect of having a higher flow rate is larger than having depth differences between the laterals. Also, in this case lateral 1 will always have a higher temperature than lateral 2, because of its higher flow rate. However, when the total flow rate increases, there is a point where lateral 2 has a higher temperature than lateral 1.

When there is a difference in the lateral's production, it can be seen that the difference in temperature between the laterals usually decreases as the total flow rate increases. However, there is one point where this difference begins to increase as the

flow rate increases for all the differences in depth. These differences between the laterals are 0 feet, 500 feet and 1000 feet as shown in Figs. 6.14 – 6.16. This is because of the fact that above certain flow rates (high flow rates), the lateral producing less increases in temperature in a more rapidly manner than the lateral producing more. When there is a difference in depth between the laterals, the lateral which has less production but a changing depth will increase in temperature even more rapidly than if the laterals are at the same level. Also, when both laterals are at the same level, the difference in temperature decreases for high flow rates. Therefore, for high flow rates and laterals at the same level, the difference in temperature at the junction has a low value.

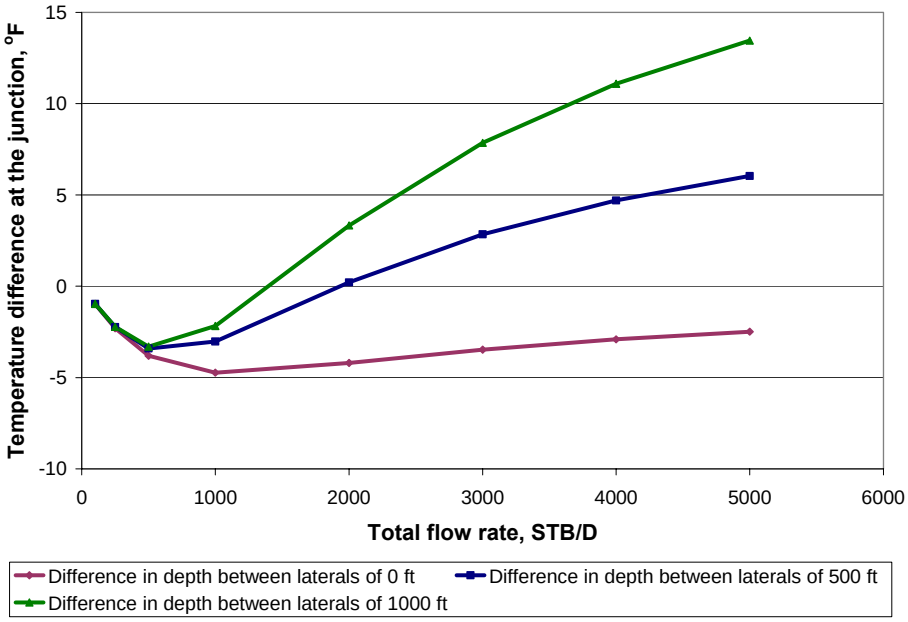

Fig. 6.14 Fraction of total production from each lateral: 60% - 40%.

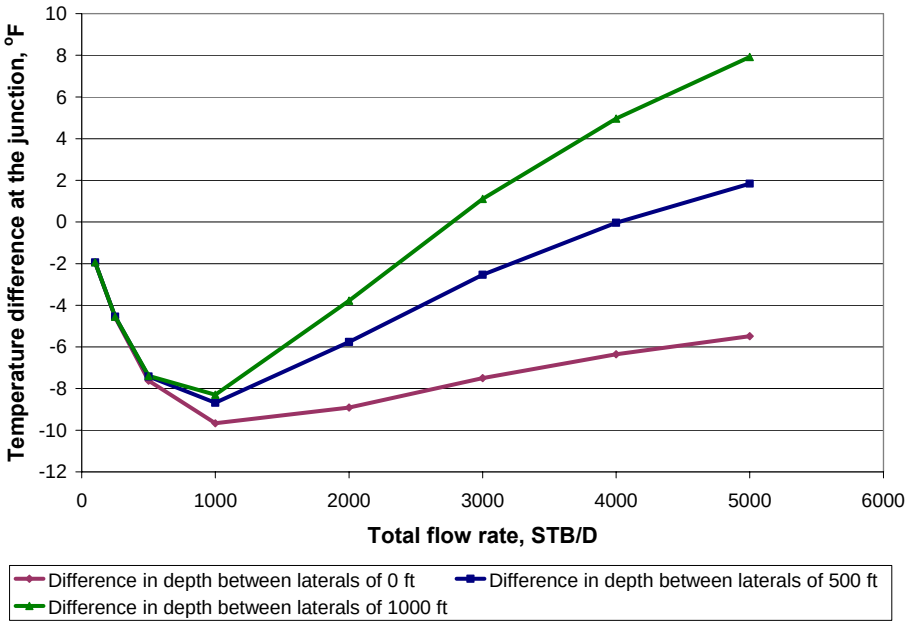

Fig. 6.15 Fraction of total production from each lateral: 70% - 30%.

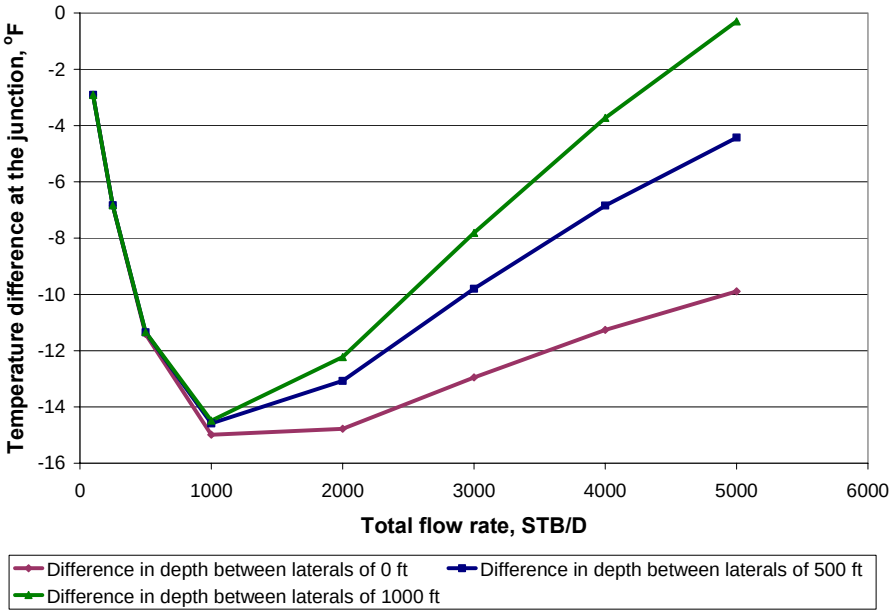

Fig. 6.16 Fraction of total production from each lateral: 80% - 20%.

6.5.4 Dual-lateral with single phase gas

Typical data from the Parks Field Unit in west Texas[22] shown in Table 6.3 were used to calculate the temperature profiles for multilateral wells with two single-phase gas laterals, using the model for single-phase gas in the build section and mixing at the junction. Wells are design to produce gas from the upper and lower porosity lenses of geologically constrained Devonian limestone. The results from temperature profiles for this case are shown in Figs. 6.17 – 6.19, where lateral 1 produces 700 Mscf/D and lateral 2 produces 1.7 MMscf/D. The geothermal temperature gradient used was 0.016^{o}F/ ft.

Table 6.3 Main Characteristics of the Reservoir - Temperature Profiles for Multilaterals: Dual-Lateral with Single-Phase Gas.

Geothermal gradient	0.016 ^{o}F/ft	0.016 ^{o}F/ft
Oil heat capacity	0.3 Btu/lbm^{o}F	0.3 Btu/lbm^{o}F
Wellbore diameter	7.5 in	7.5 in
Outside casing diameter	5.5 in	5.5 in
Inside casing diameter	5.047 in	5.047 in
Thermal conductivity of cement	96.5 Btu/D ft ^{o}F	96.5 Btu/D ft ^{o}F
Thermal conductivity of earth	33.6 Btu/D ft ^{o}F	33.6 Btu/D ft ^{o}F
Gas gravity	1.04	1.04

The results for these gas production cases are similar to those for an oil producing dual lateral. The larger the vertical separation between the laterals, the bigger the temperature difference between the produced streams arriving at the junction. For a vertical spacing of 500 or 1000 feet, the temperature difference between the streams is easily discernible, allowing the application of the mixing method to interpret the relative flow rates from the laterals.

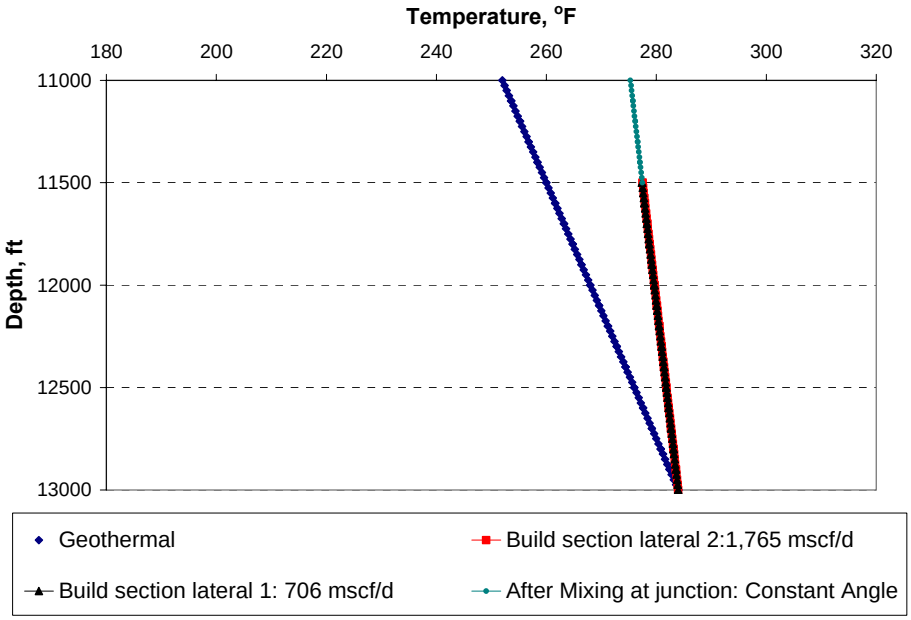

Fig. 6.17 Build section temperature profiles with gas production at the same depth.

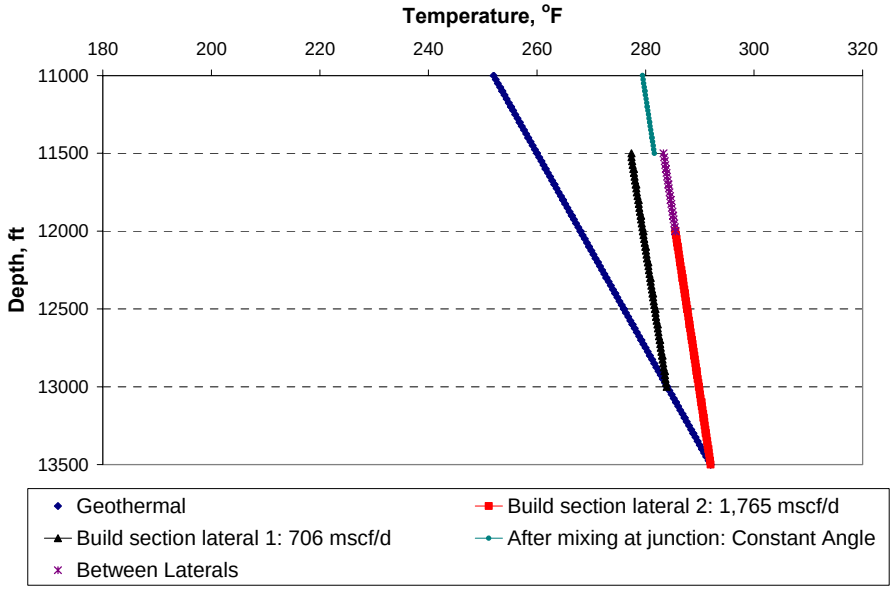

Fig. 6.18 Build section temperature profiles with gas production at depths spaced 500 ft apart.

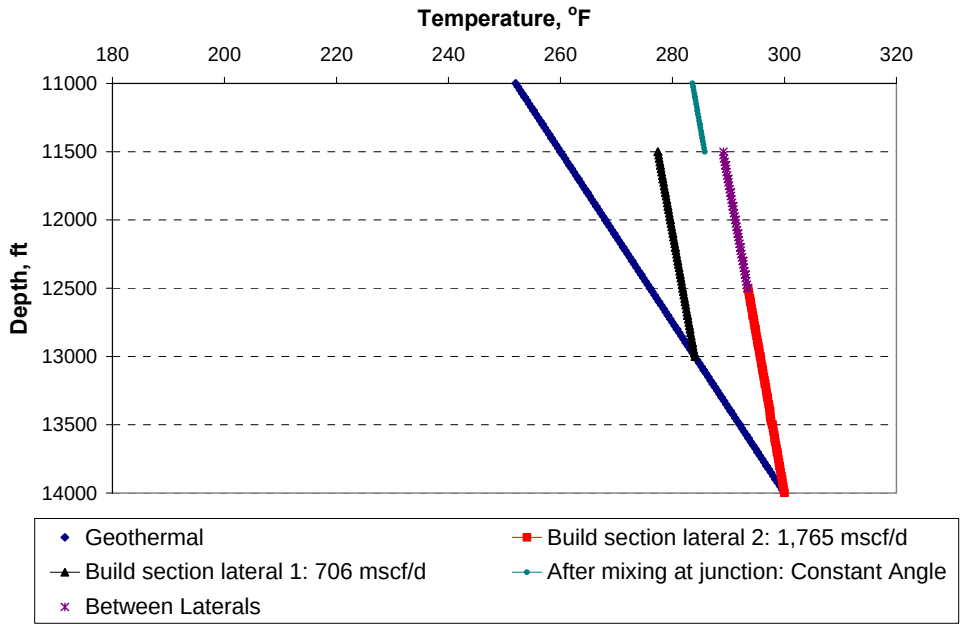

Fig. 6.19 Build section temperature profiles with gas production at depths spaced 1000 ft apart.

6.6 Summary of build section and junction

Based on the results and sensitivities cases studied, several interesting observations follow:

(1) when we consider the effect of variable angles on the build section, we were able to calculate different temperature profiles for variable angles and different constant angles to compare the effects.

(2) From the model for single-phase liquid and gas and junction mixing, the temperature profiles for multilateral wells with two single-phase liquid laterals and two single-phase gases were analyzed in this research. As a result, we were able to obtain different temperature profiles for different depths and flow rates between the laterals. This means that the effect of different depths and flow rates are significant and need to be taken into account.

Also, these results helped to determine whether the mixing method[1] used in temperature log interpretation could also be used to interpret the relative flow rates from different laterals.

7 SYUMMARY AND CONCLUSIONS

7.1 Conclusions of coupled model of reservoir and wellbore

We have derived the governing equations that describe reservoir fluid flow and heat transfer, and solved them analytically in one-dimensional (1D) flow. Results from the 1D analytical reservoir solution indicate that the inflow temperature can change from the geothermal temperature by a few degrees. The size of this change depends on the types of fluids flowing and especially on the well's producing rate. Inasmuch as we must account for the heat transfer from wellbore to formation, we have coupled wellbore and reservoir equations and solved them numerically.

Based on the coupled model's predictions, we see little change on the temperature profiles if the liquid flow rate is quite small or if the pressure drop along the well is small for gas production. We found that temperature and pressure profiles are sensitive to the well trajectories, meaning that an accurate well survey is needed to interpret temperature and pressure profiles when significant elevation changes occur. Perhaps most significantly, the temperature profile shows strong discontinuity in its slope when passing between zones that are producing different fluids. Where the production of one fluid starts and another ends is clearly observed.

The originally stated goal of this work was to find the conditions under which continuous temperature measurements in a horizontal well can be used to quantitatively infer fluid inflow. Our results suggest that this approach will be most successful (that is, temperature changes will be detectable) in oil wells flowing at a high rate, in gas wells, or in wells with a small diameter. The effect of an inclined wellbore can cause the temperature change to be larger (compared to a horizontal well) if the well is inclined downward. Inclination upward can also suppress the temperature change. Perhaps the most significant finding is that readily detectable discontinuities in the slope of a temperature profile appear to clearly indicate where the entry of one fluid begins and another ends.

7.2 Conclusions of build section and junction

We have developed a model to predict temperature profiles in the variable angle build sections of a multilateral well by applying the method developed by Ramey to this geometry. In addition, we have applied an energy balance to a multilateral junction where two flow streams are commingled. From these models of temperature behavior in multilaterals we find:

(1) The temperature of the fluids produced from two laterals will differ significantly at the junction when the streams are commingled if the laterals are producing from reservoirs at different depths. This is because the fluids produced have different temperatures, because of the geothermal gradient.

(2) A significant temperature difference between the two streams can also occur when the flow rates from the two laterals differ greatly.

(3) When measurable differences between the temperatures just below a junction occur, the mixing method of production log interpretation can be used to estimate the fraction of flow produced from each lateral.

8 NOMENCLATURE

A	area of phase
C_I	integration constant
C_p	specific heat capacity
D	pipe diameter
e	total energy flux
f	fanning friction factor with radial influx/outflux
f_0	fanning friction factor without radial influx/outflux
$f(t)$	time function, dimensionless
g	gravity acceleration
g_c	conversion factor, 32.17 lbm-ft/lbf-s^2
g_G	geothermal gradient
h	reservoir thickness
$\hat{H}$	enthalply per unit mass
J	mechanical equivalent of heat
k	permeability
K	thermal conductivity
K_T	total thermal conductivity of rock and fluid
K_{JT}	Joule-Thomson coefficient
L	length of well
L_w	total measure of well depth, ft
M	mass
N_{Re}	Reynolds number
$N_{\mathrm{Re},w}$	wall Reynolds number
p	pressure
PI	productivity index
Pr	Prandtl number
p_R	reservoir pressure
q	heat flux
Q	heat transfer rate per unit length of wellbore
R	inner wellbore radius
r_w	wellbore radius in well cell
s	skin factor
T	temperature
T_{Gi}	formation temperature at initial condition
T_{Gibh}	static formation temperature at the bottom hole

T_I	inflow temperature of fluid entering a wellbore
T_o	temperature at external boundary of reservoir
$\mathbf{u}$	Darcy velocity vector
$\hat{U}$	internal energy
U	overall heat transfer coefficient
$\mathbf{v}$	velocity
v_{sl}	superficial velocity of liquid
v_{sg}	superficial velocity of gas
V	volume
w	mass flow rate
Y	length of reservoir
z	variable well depth from surface
α	heat transfer coefficient
α	wellbore inclination with horizontal
β	thermal expansion coefficient
ε	relative pipe roughness
γ	pipe opened ratio
μ	viscosity
ρ	density
ϕ	porosity
$\mathbf{\Phi}$	combined momentum tensor
θ	angle from horizontal
$\boldsymbol{\tau}$	stress shear tensor

Subscripts

a	air
b	bulk
c	casing
d	dry rock
cem	cement
fl	fluid
g	gas
I	inflow
i	phase
l	liquid
m	phase mixture
o	oil
s	solid part of rock
T	phase total
w	wall

9 REFERENCE:

1. Ramey, H.J., Jr.: "Wellbore Heat Transmission," Journal of Petroleum Technology, Trans. AIME volume 225, pp. 427-435, April 1962.
2. Hill, A.D.; *Production Logging-Theoretical and Interpretive Elements*, Society of Petroleum Engineers Inc., Richardson, TX, 1990.
3. Brown, G., Storer, D., McAllister, K., Al-Asimi, M., and Raghavan, K. : "Monitoring Horizontal Producers and Injectors During Cleanup and Production Using Fiber-Optic-Distributed Temperature Measurements," paper SPE 84379 presented at the SPE Annual Technical Conference and Exhibition, Denver, CO, 5-8 October, 2003.
4. Bird, R. B., Stewart, W.E., and Lightfoot, E.N.; *Transport Phenomena*, second edition, John Wiley and Sons, New York, NY, 2002.
5. Tolan, M., Boyle, M., and Williams, G. : "The Use of Fiber-Optic Distributed Temperature Sensing and Remote Hydraulically Operated Interval Control Valves for the Management of Water Production in the Douglas Field," paper SPE 71676 presented at the 2001 SPE Annual Technical Conference and Exhibition, New Orleans, LA, 30 September-3 October, 2001.
6. Ouyang, L.B., Arbabi, S., and Aziz, K.: "A Single-Phase Wellbore-Flow Model for Horizontal, Vertical, and Slanted Wells", SPE Journal, (1998) 124-133.
7. Ouyang, L.-B. and Aziz, K.: "A Homogeneous Model for Gas-Liquid Flow in Horizontal Wells," Journal of Petroleum Science and Engineering (2000) 119-128.
8. Shi, H., Holmes, J.A., Diaz, L.R. and Aziz, K.: "Drift-Flux Parameters for Three-Phase Steady-State Flow in Wellbores," paper SPE 89836 presented at the SPE Annual Technical Conference and Exhibition, Houston, TX, 2004.
9. Brinkman, H. C.: "The Viscosity of Concentrated Suspensions and Solutions," J. Chem. Hydrodynamics (1952) 571.
10. Decarre, S. and Fabre, J.: "Phase Inversion Prediction Study," Jounal of L'Institut Francais du Petrole (1997) 415-424.
11. Duns, H. Jr. and Ros, N. C. J. "Vertical Flow of Gas and Liquid Mixtures in Wells," paper 22 presented at the 6th World Petroleum Congress, Frankfurt, Germany, 1963.
12. Ouyang, L.-B. and Aziz, K.: "A Mechanistic Model for Gas-Liquid Flow in Pipes with Radial Influx or Outflux," paper SPE 56525 presented at the SPE Annual Technical Conference and Exibition, Houston, TX, 3-6 October, 1999.
13. Yoshioka, K., Zhu, D., Hill, A. D. and Lake, Larry W.: "Interpretation of Temperature and Pressure Profiles Measured in Multilateral Wells Equipped with Intelligent Completion," paper SPE 94097 presented at the 14th Europec Biennial Conference, Madrid, Spain, 13-16 June, 2005.
14. Maubeuge, F., Didek, M., Beardsell, M.B., Arquis, E., Bertrand, O., and Caltagirone, J.P.: "MOTHER: A Model for Interpreting Thermometrics," paper

SPE 28588 presented at the Society of Petroleum Engineers 69th Annual Technical Conference and Exhibition, New Orleans, LA, 25-28 September, 1994.
15. Lake, L. W.: *Enhanced Oil Recovery*, Prentice Hall, Saddle River, NJ, 1989.
16. Ingham, D.B., Pop, I., and Cheng, P.: "Combined Free and Forced Convection in a Porous Medium Between Two Vertical Walls with Viscous Dissipation," Transport in Porous Media, (1990) 381-398.
17. Al-Hadhrami, A.K., Elliott, L., and Ingham, D.B.,: "A New Model for Viscous Dissipation in Porous Media Across a Range of Permeability Values," Transport in Porous Media, (2003) 117-122.
18. Furui, K., Zhu, D., and Hill, A.D.: "A Rigorous Formation Damage Skin Factor and Reservoir Inflow Model for a Horizontal Well," SPE Production and Facilities, (2003) 151-157.
19. McCain, W. D., Jr.: *The Properties of Petroleum Fluids*, second edition, PennWell Publishing Company, Tulsa, Oklahoma, 1990.
20. Ramirez, R., Fernandez, V., and Barrios J.: "Multilateral Field Experience in Developing an Extra Heavy Crude-Oil Reservoir," paper SPE 86947 presented at the 2004 SPE International Thermal Operations and Heavy Oil Symposium and Western Regional Meeting held in Bakersfield, CA, USA, 16-18 March.
21. Robles, Jorge: "Application of Advanced Heavy-Oil-Production Technologies in the Orinoco Heavy-Oil-Belt, Venezuela," paper SPE 69848 presented at the 2001 International Thermal Operations and Heavy Oil Symposium held in Margarita Island, Venezuela, 12-14 March.
22. Owodunni, A., Travis, T., and Dunk, G.: "The Use of Multilateral Technology to Arrest Production Decline in a West-Texas Gas Field," paper SPE 84029 presented at the 2003 SPE Annual Technical Conference and Exhibition held in Denver, Colorado, USA, 5-8 October.
23. Mills, A. F.: *Heat Transfer*, second edition, Prentice Hall, Saddle River, NJ, 1999
24. Kim, D., and Ghajar, A. J.: "Heat transfer measurements and correlations for air-water flow of different flow patterns in a horizontal pipe," *Experimental Thermal and Fluid Science* (2002) 659-676.
25. Economides, M.J., Hill, A.D., and Ehilig- Economides, C.*; "Petroleum Production Systems"*, Prentice Hall Inc., New Jersey, 1994

Appendix A Overall Heat Transfer Coefficient

The object of this Appendix is to derive the overall heat transfer coefficient used in this study. For a cased and cemented wellbore, the temperature profile near the wellbore will look like that shown in Fig. A.1.

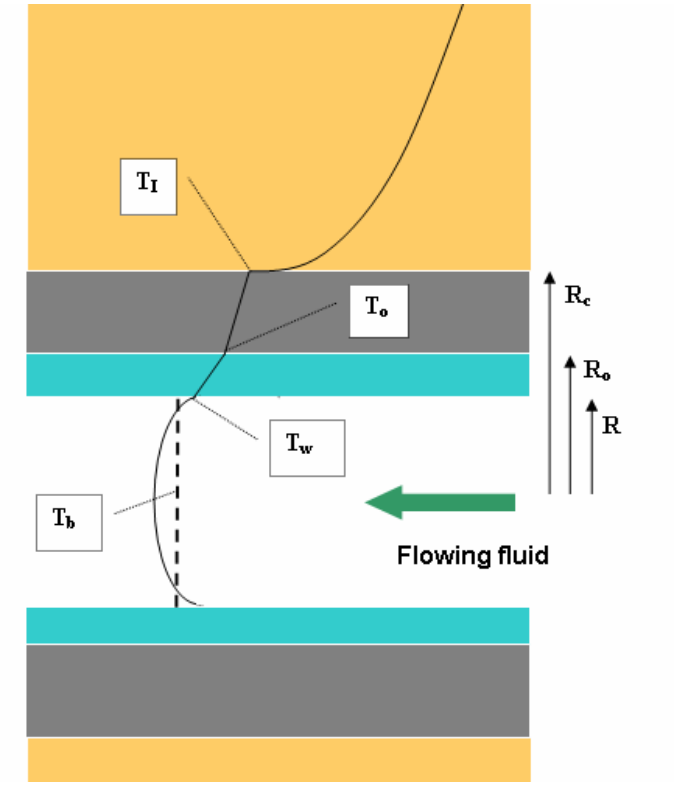

Fig. A.1

The wellbore is surrounded by casing material and cement. Fluid enters with temperature, T_I. At the inside of the cement, temperature is T_{cem} and the temperature is T_c at the inside of casing. The bulk average temperature inside the well is given as T_b. For steady state with constant thermal conductivity, the temperature distribution is given as

$$\frac{1}{r}\frac{d}{dr}\left(r\frac{dT}{dr}\right)=0 \tag{A.1}$$

Solving this differential equation for the casing yields

$$T=T_{cem}+\frac{T_c-T_{cem}}{\ln\left(R/R_c\right)}\ln\left(r/R_c\right) \tag{A.2}$$

For the cement,

$$T = T_I + \frac{T_{cem} - T_I}{\ln\left(R_c / R_{cem}\right)} \ln\left(r / R_{cem}\right) \tag{A.3}$$

Heat flows are

$$Q_c = -2\pi R(1-\gamma)K_c \left.\frac{dT}{dr}\right|_{r=R} = 2\pi(1-\gamma)K_c \frac{T_c - T_{cem}}{\ln\left(R_c / R\right)} \tag{A.4}$$

$$Q_{cem} = -2\pi R_c(1-\gamma)K_{cem} \left.\frac{dT}{dr}\right|_{r=R_c} = 2\pi(1-\gamma)K_{cem} \frac{T_{cem} - T_I}{\ln\left(R_{cem} / R_c\right)} \tag{A.5}$$

Heat flow from wall to flowing fluid is given by

$$Q_{fl} = -2\pi R(1-\gamma)\alpha(T_c - T_b) \tag{A.6}$$

where α is a heat transfer coefficient and would be determined experimentally. From boundary layer analysis with constant wall temperature, laminar flow heat transfer coefficient is

$$\alpha = 3.656 \frac{K_{fl}}{2R} \tag{A.7}$$

For turbulent flow, Gnielinski's formula[24] is widely used. The Nusselt number is given as

$$\alpha = \frac{\left(f/2\right)(\mathrm{Re}-1000)\,\mathrm{Pr}}{1+12.7\left(f/2\right)^{0.5}\left(\mathrm{Pr}^{2/3}-1\right)} \frac{K_{fl}}{2R} \tag{A.8}$$

When liquid-gas two phase flow occurs, heat transfer coefficient will become flow regime dependent. Kim and Ghajar[25] presented a simple flow regime dependent correlation as

$$\alpha_{TP} = (1-y_g)\alpha_l \left[1 + C\left(\frac{x}{1-x}\right)^m \left(\frac{y_g}{1-y_g}\right)^n \left(\frac{\mathrm{Pr}_g}{\mathrm{Pr}_l}\right)^p \left(\frac{\mu_g}{\mu_l}\right)^q\right] \tag{A.9}$$

where

$$x = \frac{\rho_g q_g}{\rho_g q_g + \rho_l q_l} \tag{A.10}$$

α_l is the liquid heat transfer coefficient and is based on the in-situ Reynolds number. The constants are given in the table below.

Table B.1 Parameter values for different flow regimes.

	C	*m*	*n*	*p*	*q*
Slug and Bubbly	2.86	0.42	0.35	0.66	-0.72
Annular	1.58	1.4	0.54	-1.93	-0.09
Stratified	27.89	3.1	-4.44	-9.65	1.56

At steady state, heat flows are equal. Then, we have

$$Q_c = Q_{cem} = Q_{fl} \equiv Q \tag{A.11}$$

Summation of the relationships gives

$$T_b - T_I = \frac{Q}{2\pi(1-\gamma)}\left[\frac{\ln\left(R_c/R\right)}{K_c} + \frac{\ln\left(R_{cem}/R_c\right)}{K_{cem}} + \frac{1}{R\alpha}\right] \tag{A.12}$$

Therefore, the overall heat transfer coefficient for the wellbore is

$$U = \frac{Q}{(T_I - T_b)2\pi R(1-\gamma)} = \left[\frac{R\ln\left(R_c/R\right)}{K_c} + \frac{R\ln\left(R_{cem}/R_c\right)}{K_{cem}} + \frac{1}{R\alpha}\right]^{-1} \tag{A.13}$$

Considering a partly opened well, the total energy entering the wellbore is then

$$\begin{aligned} -e_I 2\pi R_{cem} &= \left(\rho_I \hat{H}_I v_I\right)2\pi R_{cem}\gamma - q_I 2\pi R_{cem}(1-\gamma) \\ &= w\hat{H}_I + K_T \left.\frac{dT}{dr}\right|_{r=R_{cem}} 2\pi R_{cem}(1-\gamma) \end{aligned} \tag{A.14}$$

where w is a mass flow rate per length. Equating with the total energy from the formation is

$$-e_I 2\pi R = wH_I\big|_{r=R} + 2\pi R(1-\gamma)U(T_I - T_b) \tag{A.15}$$

Equating Eqs. B-14 and B-15 and considering the difference of convection term $\left(wH_I\big|_{r=R} - wH_I\big|_{r=R_{cem}}\right)$ is negligible yields

$$K_T \left.\frac{dT}{dr}\right|_{r=R_{cem}} = \frac{R}{R_{cem}} U\left(T_I - T_b\right) \tag{A.16}$$

This is the fourth boundary condition of the reservoir solution for the open hole case $\left(R/R_{cem}\ U = U\right)$.

Appendix B: Inflow temperature model for slightly compressible fluid

The object of this Appendix is to derive and solve analytically the equations for reservoir flow. The pressure relationship is described by Darcy's law as:

$$u_y = -\frac{k}{\mu}\frac{dp}{dy} \tag{B.1}$$

In terms of the volumetric flow rate this becomes.

$$\frac{q}{2Lh} = -\frac{k}{\mu}\frac{dp}{dy} \tag{B.2}$$

In a one-dimensional Cartesian coordinate (y-direction), the energy balance becomes

$$\rho C_p u_y \frac{dT}{dy} - \beta T u_y \frac{dp}{dy} + u_y \frac{dp}{dy} - K_T \frac{d^2T}{dy^2} = 0 \tag{B.3}$$

Substituting Eq. B-2 into Eq.B-3 and rearranging give

$$\frac{d^2T}{dy^2} - \frac{\rho C_p}{K_T}\left(\frac{q}{2hL}\right)\frac{dT}{dy} - \frac{\beta\mu}{kK_T}\left(\frac{q}{2hL}\right)^2 T + \frac{\mu}{kK_T}\left(\frac{q}{2hL}\right)^2 = 0 \tag{B.4}$$

Solving the second order ordinary differential equation gives

$$T = L_1 e^{m_+ y} + L_2 e^{m_- y} + \frac{1}{\beta} \tag{B.5}$$

where

$$m_\pm = \frac{q}{4hL}\left[\frac{\rho C_p}{K_T} \pm \sqrt{\left(\frac{\rho C_p}{K_T}\right)^2 + \frac{4\beta\mu}{kK_T}}\right] \tag{B.6}$$

L_1 and L_2 are integration constants to be determined by boundary conditions.

For the radial flow portion consider a steady-state radial flow in a homogeneous reservoir with length, L, and outer radius of $h/2$. Similarly, from Darcy's Law

$$\frac{q}{2\pi rL} = -\frac{k}{\mu}\frac{dp}{dr} \tag{B.7}$$

In radial coordinates the energy balance becomes

$$\rho C_p\, u_r \frac{dT}{dr} - \beta T\, u_r \frac{dp}{dr} + u_r \frac{dp}{dr} - K_T \frac{1}{r}\frac{d}{dr}\left(r\frac{dT}{dr}\right) = 0 \tag{B.8}$$

Substituting Eq. B.7 into Eq. B.8 gives

$$-\frac{2\pi L\,K_{Tt}}{q}\,r^2\,\frac{d^2T}{dr^2}+\left(\rho C_p-\frac{2\pi L\,K_T}{q}\right)r\frac{dT}{dr}+\frac{\mu q\beta T}{2\pi kL}-\frac{\mu q}{2\pi kL}=0 \tag{B.9}$$

Solution to this second order differential equation is given by

$$T=R_1 r^{n_+}+R_2 r^{n_-}+\frac{1}{\beta} \tag{B.10}$$

where

$$n_\pm=\frac{q}{4\pi L}\left[\frac{\rho C_p}{K_T}\pm\sqrt{\left(\frac{\rho C_p}{K_T}\right)^2+\frac{4\mu\beta}{kK_T}}\right] \tag{B.11}$$

R_1 and R_2 are integration constants. The boundary conditions are:
At the external reservoir boundary, temperature is known (geothermal temperature)

$$T\big|_{y=\frac{Y}{2}}=T_0 \tag{B.12}$$

Temperature and heat flux is continuous at the boundary between radial and linear elements

$$T\big|_{r=\frac{h}{2}}=T\big|_{y=\frac{h}{2}} \tag{B.13}$$

$$\left.\frac{dT}{dr}\right|_{r=\frac{h}{2}}=\left.\frac{dT}{dy}\right|_{y=\frac{h}{2}} \tag{B.14}$$

Heat flux is continuous at the wellbore. See Appendix A.

$$K_T\left.\frac{dT}{dr}\right|_{r=R}=U\left(T\big|_{r=R}-T_b\right) \tag{B.15}$$

This boundary condition makes the inflow temperature dependent on the wellbore temperature and the overall heat transfer coefficient between reservoir and wellbore. From the BCs, finally we have

$$L_1=\frac{l_1+l_2}{\psi_++\psi_-} \tag{B.16}$$

$$L_2=\frac{l_3+l_4}{\psi_++\psi_-} \tag{B.17}$$

$$R_1=\frac{\theta_1+\theta_2}{\psi_++\psi_-} \tag{B.18}$$

$$R_2 = \frac{\theta_3 + \theta_4}{\psi_+ + \psi_-} \tag{B.19}$$

where

$$l_1 = R^{n_-} e^{\frac{h}{2}m_-} \left(-K_T n_- + UR\right) \times \left(\beta T_o - 1\right) \left(\frac{h}{2}\right)^{n_+} \left(\frac{h}{2}m_- - n_+\right) \tag{B.20}$$

$$\begin{aligned} l_2 = \left(\frac{h}{2}\right)^{n_-} \Bigg[& e^{\frac{h}{2}m_-} R^{n_+} \left(-\frac{h}{2}m_- + n_-\right) \left(-K_T n_+ + UR\right)\left(\beta T_o - 1\right) \\ & + e^{\frac{Y}{2}m_-} UR \left(\frac{h}{2}\right)^{n_+} \left(\beta T_b - 1\right)\left(n_+ - n_-\right) \Bigg] \end{aligned} \tag{B.21}$$

$$l_3 = R^{n_{+3}} e^{\frac{h}{2}m_-} \left(K_T n_- - UR\right) \times \left(\beta T_o - 1\right) \left(\frac{h}{2}\right)^{n_+} \left(\frac{h}{2}m_+ + n_+\right) \tag{B.22}$$

$$\begin{aligned} l_4 = \left(\frac{h}{2}\right)^{n_-} \Bigg[& e^{\frac{h}{2}m_+} R^{n_+} \left(\frac{h}{2}m_+ - n_-\right) \left(-K_T n_+ + UR\right)\left(\beta T_o - 1\right) \\ & - e^{\frac{Y}{2}m_+} UR \left(\frac{h}{2}\right)^{n_+} \left(\beta T_b - 1\right)\left(n_+ - n_-\right) \Bigg] \end{aligned} \tag{B.23}$$

$$\theta_1 = e^{\frac{h}{2}(m_+ + m_-)} \frac{h}{2} R^{n_-} \left(m_+ - m_-\right)\left(K_T n_- - UR\right)\left(\beta T_o - 1\right) \tag{B.24}$$

$$\begin{aligned} \theta_2 = & \left(\frac{h}{2}\right)^{n_-} \left(\beta T_b - 1\right) UR \\ & \times \left[e^{\frac{h}{2}m_+ + \frac{Y}{2}m_-} \left(\frac{h}{2}m_+ - n_-\right) + e^{\frac{Y}{2}m_+ + \frac{h}{2}m_-} \left(-\frac{h}{2}m_- + n_-\right) \right] \end{aligned} \tag{B.25}$$

$$\theta_3 = e^{\frac{h}{2}(m_+ + m_-)} \frac{h}{2} R^{n_+} \left(m_+ - m_-\right)\left(-K_T n_+ + UR\right)\left(\beta T_o - 1\right) \tag{B.26}$$

$$\begin{aligned} \theta_4 = & \left(\frac{h}{2}\right)^{n_+} \left(\beta T_b - 1\right) UR \\ & \times \left[e^{\frac{h}{2}m_- + \frac{Y}{2}m_+} \left(\frac{h}{2}m_- - n_+\right) + e^{\frac{Y}{2}m_- + \frac{h}{2}m_+} \left(-\frac{h}{2}m_+ + n_+\right) \right] \end{aligned} \tag{B.27}$$

$$\psi_{\pm} = \beta R^{n_{\pm}} \left(\frac{h}{2}\right)^{n_{\mp}} \left(K_{Tt} n_{\pm} - UR\right) \times \left[e^{\frac{Y}{2} m_{\pm} + \frac{h}{2} m_{\mp}} \left(\frac{h}{2} m_{\mp} - n_{\mp}\right) + e^{\frac{h}{2} m_{\pm} + \frac{Y}{2} m_{\mp}} \left(-\frac{h}{2} m_{\pm} + n_{\mp}\right) \right] \tag{B.28}$$